Funded by
the European Union

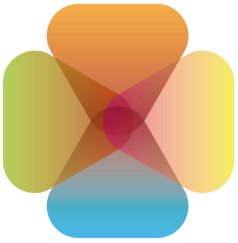

ACCREU
Assessing
Climate Change
Risk in EUrope

Impacts of Extremes, Catastrophic Events, and Supply Chains

GA number: 101081358; Funding type: HORIZON-CL5-2022-D1-07-two-stage

Deliverable number (relative in WP)	D2.5
Deliverable name:	Impacts of extremes, catastrophic events, and supply chains
WP / WP number:	WP2
Delivery due date:	Project month 29 (October 2025)
Actual date of submission:	28/10/2025
Dissemination level:	Public
Lead beneficiary:	PIK
Responsible scientist/administrator:	Christian Otto (PIK)
Contributor(s):	**VU**: Michiel W. Ingels, Max Tesselaar, Jan Brusselaers **Deltares**: Kees van Ginkel **PIK:** Jan Hassel, Christian Otto **UNIGRAZ:** Birgit Bednar-Friedl, Alexander Marbler **DTU**: Martin Drews, Jorge Soto Martin, Ophélie Meuriot
Internal reviewer:	Enrica De Cian

Funded by the European Union. Views and opinions expressed are however those of the author(s) only and do not necessarily reflect those of the European Union. Neither the European Union nor the granting authority can be held responsible for them.

Changes with respect to the DoA

There are no changes with respect to the description of work outlined in Task 2.5 of the ACCREU Grant Agreement.

Dissemination and uptake

The findings and methodologies from this deliverable can directly inform adaptation strategies within ACCREU's WP3, in particular case study 5.2 on the 'stimulation of private sector adaptation through insurance arrangements', and provide critical damage estimates for WP4 macroeconomic models, thereby creating an integrated assessment framework across work packages.

Beyond the project, our results offer valuable evidence for EU- and national-level adaptation planning and risk assessments, including initiatives such as the European Climate Risk Assessments.

Furthermore, our novel modeling approaches and economic damage estimates will benefit researchers across disciplines, including climate impact scientists, environmental economists, and government agencies responsible for implementing climate adaptation policies.

Short summary of results

An executive summary can be found on pages 6-10.

Evidence of accomplishment

Published Manuscripts

- ACCREU Milestone 2.2 - Flood Damage
- Caloia, F. G., van Ginkel, K. C. H. and Jansen, D. (2023). Floods and financial stability: Scenario-based evidence from below sea level. DNB Working Paper No. 796. *(Under review)*
- Hassel, J., Vogt, T., Frieler, K., & Otto, C. (2024). Poor and unequal U.S. counties are more vulnerable to tropical cyclone damage. Available at SSRN 5067633 https://doi.org/10.2139/ssrn.5067633
- Marbler, A. (2025). When Supply Chains Run Dry: Spillovers Intensify the Economic Impact of Water Scarcity. *Available at SSRN 5354158*. https://dx.doi.org/10.2139/ssrn.5354158 [Received the *Young Economists Award* 2025 by the Austrian Economic Association (NOeG); Presented at: 40th *Annual Conference of the European Economic Association* (EEA 2025), Bordeaux, France; 30th *Annual Conference of the European Association of Environmental and Resource Economists* (EAERE 2025), Bergen, Norway; *Annual Conference of the Austrian Economic Association* (NOeG 2025), Krems an der Donau, Austria.]
- Otto, C., Schult, C., & Vogt, T. (2025). Climate Change Economics in Vietnam: Redefining Economic Impact. Available at IWH Discussion Papers 15/2025. https://doi.org/10.18717/dpzggv-cs12. *(Under review in Energy Economics)*
- Schötz et al. (2025). Rethinking Climate Econometrics: Data Cleaning, Flexible Trend Controls, and Predictive Validation. Available at arXiv 2505.18033.

https://doi.org/10.48550/arXiv.2505.18033 *(Under review in Environmetrics)*

Published Datasets & Code

- Hassel, J., & Otto, C. (2025). Projection of fluvial flood-induced damages on NUTS1-level GDP per capita for the ACCREU project [Data set]. Zenodo. https://doi.org/10.5281/zenodo.17360324

Manuscripts in Preparation

- Hassel et al. Long-term effects of floods on regional economic growth and their projected impacts under global warming in Europe.
- Huang et al. (2025). Cause specific mortality risks associated with tropical cyclones in multiple countries and territories: two stage, time series study. (Accepted for publication in BMJ)
- Ingels et al. Business-level flood insurance coverage and adaptation under climate change in the Netherlands.
- Meuriot et al. Future wildfire risk in Southern Europe under changing land use and climate: A data-driven approach using ClimEx2.

Other (web links, etc)

- van Ginkel, K., Caloia, F., Jansen, D.J. (2023). Overstromingen en financiële stabiliteit in Nederland: een toelichting voor de watersector. https://www.h2owaternetwerk.nl/h2o-podium/uitgelicht/overstromingen-en-financiele-stabiliteit-in-nederland-een-toelichting-voor-de-watersector
- Five questions about the impact of floods on the financial sector. News article on the website of Deltares and on the website of the Dutch Central bank. https://www.deltares.nl/en/news/five-questions-about-the-impact-of-floods-on-the-financial-sector & https://www.dnb.nl/algemeen-nieuws/achtergrond-2023/vijf-vragen-over-de-gevolgen-van-overstromingen-op-de-financiele-sector/
- Meuriot, O., Martin, J. S., and Drews, M. (2025). Future wildfire risk in Southern Europe under changing land use and climate: A data-driven approach using ClimEx2. Poster presentation, EMS Annual Meeting, 7-12 September 2025, Ljubljana
- Meuriot, O. et al. (2025). Scalable & explainable ML for wildfire risk modelling in Southern Europe: A case-study in Portugal. Conference paper and spotlight talk, NeurIPS 2025, 2-7 December, San Diego

Table of Contents

Executive Summary

Task 2.5 of the ACCREU project addresses how extreme and catastrophic events shape economic risks in Europe, accounting for direct damages as well as indirect damages propagated through supply chains. The work combines event-based assessments with large-scale analyses to capture both local dynamics as well as systemic impacts of extremes and catastrophic events.

The first three chapters of this deliverable assess flood-related risks on different spatial scales and for different sectors. First, the Vrije Universiteit Amsterdam (VU) reports on the impacts of flood risk on the commercial sector (Netherlands) (Chapter 1). This is followed by the work of Deltares on impacts of large-scale floods on financial stability (Netherlands) (Chapter 2). The last flood-related chapter covers the assessment of long-term effects of flood on economic growth by the Potsdam Institute for Climate Impact Research (PIK) (Europe, sub-national) (Chapter 3). The flood analyses are followed by the works of the University of Graz on the role of global supply chains in amplifying the economic impact of local climate anomalies (Chapter 4). Finally, this deliverable concludes with the assessment of the impacts of compound wildfires from the Technical University of Denmark (DTU) (Chapter 5).

Chapter 1: Impacts of flood risk on commercial sector

This task aims to assess the size of the flood insurance protection gap for the private sector in the Netherlands. This is done by estimating the expected annual damage (EAD) resulting from floods on a NUTS3 level. Furthermore, the EAD is disaggregated into direct damage and business interruption damage, and is further disaggregated on a sectoral level. The EAD is then used in an insurance model to simulate the percentage of insurance coverage on a sector basis in each NUTS3 region. Combining the total damage with the percentage of insurance coverage, we calculate the insurance protection gap on a sectoral level. Moreover, the future protection gap on a sectoral level is estimated for 2050 and 2080 using the middle-of-the road Shared Socioeconomic Pathway (SSP2) and the intermediate Representative Concentration Pathway (RCP4.5).

We find that the EAD for both direct flood damage and business interruption shows large differences across areas in the Netherlands. Further, only a part of the total EAD in the Netherlands is considered insurable. The industry sector and the office sector make up the largest part of the insurable EAD. Insurance uptake was shown to differ moderately between NUTS3 regions. We also show that the insurance coverage gap is projected to increase in 2050 and 2080 due to an increase in EAD in combination with a lower uptake of insurance.

The results highlight the growing importance of effective flood risk management and insurance mechanisms in the Netherlands. The increase in EAD in combination with the decline in insurance uptake leads to a widening insurance coverage gap. These findings highlight the need to align flood risk reduction strategies with a well-functioning insurance system to ensure long-term resilience across all sectors of the economy.

Chapter 2: Impacts of large-scale floods on financial stability

This task adopts a bottom-up, local, and event-based perspective to assessing the financial stability impacts of extreme and catastrophic flooding in the Netherlands. This contrasts with the approach taken in Deliverable 2.1: the approach here is local (Netherlands instead of pan-EU), event-based (instead of risk-based), bottom-up (instead of top-down) and focuses on extreme and catastrophic tail risk (instead of annual expected damage). In this deliverable, we describe how we make a selection of scenarios covering both river and coastal floods, and compounding river and coastal flood events. The objective of this selection was to find a subset of events that is representative of extreme, catastrophic flood conditions for the Netherlands. These events are then used to calculate the credit risk impacts for major lenders in the Netherlands, which feeds into a discussion of adaptation in the financial domain in ACCREU's Deliverables 3.2 and 3.3.

We select 32 scenarios for single-dike breaches, focusing on those with the highest real estate damage and ensuring a broad geographical distribution. The total damage in these scenarios range from €5 to 40 billion. The damage to real estate only in these scenarios range from €0.7 to 5 billion. The credit risk impacts caused by these scenarios are in the range of 30–50 basis points. We complemented these single-breach scenarios with the 6 Worst Credible Flood scenarios. The probability of their occurrence is a factor 10 smaller than the protection levels of the dike rings. Hence, these represent very extreme conditions. The Worst Credible Flood scenarios lead to a capital depletion of 50–110 basis points.

This amount of capital depletion will likely not lead to immediate concerns about financial stability of the Netherlands. However, these results should be interpreted with caution, because it only examines one of the several transmission channels through which floods affect the economy and financial stability. Also, we demonstrate that the flood damage calculation is a major source of uncertainty, which may lead to an upward revision of real estate damage by a factor 2–4. An upward revision of real estate damage will likely also have a significant impact on the credit risk calculations.

Chapter 3: Impacts of floods on long-term economic growth

This task employs a top-down climate econometrics approach to estimate the impact of floods on economic growth, accounting for potential long-term impacts. We find that floods have substantial negative impacts on per capita economic growth on the NUTS-levels 3 to 1, which persist for at least a decade.

We then use these empirical estimates to calculate regional (NUTS1) discounted annual damage (DAD) for the middle-of-the road SSP2 and three RCPs: the strong mitigation pathways RCP2.6, and the strong emission pathways RCP7.0 and RCP8.5. The selection of the RCP scenarios is determined by the global flood model simulations available through the Inter-Sectoral Impact Model Intercomparison Project (ISIMIP, www.isimip.org).

We find that in most regions, DAD increases under global warming compared to a reference scenario with a stabilized pre-industrial climate. Largest DADs arise across Central Europe and the

Alpine region, where DAD range between 0.5% - 2% of 2025 GDP per capita. By contrast, DAD decreases for several Mediterranean and North-Eastern European regions. These large scale patterns are robust across the different RCPs, with the damage trends (positive as well as negative) most pronounced under the strong emission scenario RCP8.5. Further, the projected trends in DAD correspond well to observed trends in flood risk (Blöschl et al. 2019).

Our analyses allow several key conclusions. First, comprehensive estimates of flood damage should account not only for the direct impacts of these disasters but also for their long-term consequences. Our assessments provide top-down estimates that can be compared with bottom-up modeling approaches, such as Computational General Equilibrium (CGE) models. In this context, our study serves as an important test case to better understand the discrepancies between top-down and bottom-up damage estimates, as highlighted in Working Group II's contribution to the Sixth Assessment Report of the Intergovernmental Panel on Climate Change (IPCC) (O'Neill et al. 2022). We find substantial regional heterogeneity in flood damage, emphasizing the importance of subnational-level analyses. Our estimates indicate significant climate-change risks from river floods across many European regions. By revealing considerable adaptation needs, these findings provide crucial guidance for decision-making at European, national, and regional levels.

Chapter 4: Supply Chain Spillovers Intensify the Economic Impact of Local Climate Anomalies

This task explores the role of global supply chains in amplifying the macroeconomic losses from local climate shocks. By integrating global multi-regional input-output tables with high-resolution water availability data, a novel metric to quantify water availability shocks transmitted across global supply chains is created. Combining this metric with subnational gross value added (GVA) data for Europe's NUTS-3 regions, an econometric analysis is conducted to estimate the dynamic causal effect of water scarcity shocks on subnational GVA, explicitly accounting for global supply chain spillovers.

The results reveal that global supply chain spillover effects significantly amplify regional GVA losses, and neglecting these spillovers leads to a substantial underestimation of climate-induced economic damage. The adverse effects on subnational GVA are persistent over time and are accompanied by declines in employment, labor productivity, and investment. Crucially, regions already experiencing water stress are the most vulnerable to water scarcity shocks.

A counterfactual analysis over the period 2000-2019 reveals that cumulative GVA losses across Europe attributable to global water scarcity shocks transmitted through supply chains amount to €12.3 trillion. When supply chain spillover effects are not accounted for, only a third (€3.9 trillion) of these losses are captured. This highlights the importance of incorporating supply chain spillover effects into climate impact assessments and the urgent need for adaptation measures aimed at strengthening supply chain resilience under future climate change.

Chapter 5: Impacts of compound wildfires

This task investigates the growing threat of compound wildfires in Southern Europe, driven by the compoundness of climate extremes, land use changes, and human activity. Using a combination of machine learning and regional climate modeling, we identify key wildfire drivers and investigate future risks under various climate projections and land use scenarios. Wildfires are increasingly recognized as compound climate events, where multiple factors — such as heatwaves, droughts, low humidity, strong winds, and human activities — interact to amplify fire risk and arguably their impacts. Human activity alone is related to approximately 90% of wildfire ignitions in Southern Europe. Climate change is intensifying fire weather conditions, leading to longer fire seasons and more extreme fire behavior.

To this end, a data-driven wildfire risk model was developed using 25 predictors, including climate variables, land cover, topography, and human infrastructure. Among four machine learning models tested, XGBoost performs the best, achieving high accuracy and interpretability. The ensuing analysis revealed that soil moisture, precipitation, relative humidity, vegetation type, slope, and population density are the most influential drivers of compound wildfire risk.

Future projections using the ClimEx-II regional climate model ensemble (Asselin et al. (2024)) show that climate and land use scenarios can play an important role for wildfire risk estimates. While the risk of wildfire increases significantly under high warming scenarios, our results show that also land use change, e.g., afforestation, can exacerbate these risks. This compound characteristic of wildfire risk is confirmed by a case study in the Campania region of Italy, exhibiting a marked increase in extreme wildfire seasons under future climate scenarios.

Our findings underscore the need for high-resolution modeling, dynamic land surface representation, improved wildfire risk management and climate change adaptation approaches to cope effectively with wildfire risks in a changing climate. For example, while increasing forest cover is a key goal of the EU Forest Strategy, this must be balanced with robust local adaptation and forest management to mitigate unintended consequences.

1 Impacts of flood risk on commercial sector

1.1 Introduction

Floods have substantial direct and indirect impacts on businesses that suffer damages. Insurance is an important economic tool for firms to financially protect against such impacts. However, insurance uptake by firms may be limited due to economic or behavioral constraints. Limited societal insurance coverage means that there is an insurance coverage gap, which may have considerable macroeconomic implications after devastating flood events (Von Peter et al., 2024). Here, we aim to assess the size of the flood insurance protection gap for the private sector in the Netherlands, and project how this may develop in the future due to climate change.

The goal of this subtask within the deliverable is to estimate the expected annual damage (EAD) for the private sector in the Netherlands, and use that to estimate flood insurance premiums and uptake of coverage by the Dutch private sector. We do this explicitly taking the part of the risk that is covered by insurance into account and providing a sectoral disaggregation of these damages for both direct damage and business interruption damage.

The private sector EAD is estimated using inundation maps from the National Water & Flooding Information System in the Netherlands (LIWO, 2024) in combination with the Slachtoffer en Schade Module (SSM) (Slager & Wagenaar, 2017). For the insurance uptake, the Dynamic Integrated Flood Insurance (DIFI) model (Hudson et al., 2019; Tesselaar et al. 2020) will be extended with a module to simulate private sector insurance uptake.

This EAD is subdivided into different economic sectors to attain a better understanding of the sectoral impact of flood risk. Furthermore, future trajectories of the flood risk and insurance uptake is estimated using the GLOFRIS model (Ward et al., 2017; Winsemius et al., 2016). The EAD estimates and insurance penetration rates are also used in the case studies of WP3.

1.2 Methods

1.2.1 Risk

Flood risk is defined as the product of hazard, exposure, and vulnerability. Hazard is operationalized via inundation maps. These maps denote inundation levels with a certain probability, referred to as return-periods, on a grid-basis. When a certain inundation level has a return-period of 1/100, this means that this inundation level occurs approximately once every 100 years. The second component of risk, exposure, is operationalized via an exposure layer. This exposure layer denotes the total value of assets in a certain area. The third component of risk, vulnerability, is operationalized via vulnerability curves. These curves can be attached to a certain asset class and denotes the relationship between inundation depth and percentage of value lost. By combining these three elements, it is possible to calculate the damage of an inundation event with an accompanying probability. By running a Monte Carlo simulation on the return periods the expected annual damage (EAD) can be estimated.

In this deliverable, two models are used to calculate the EAD: SSM or is used to compute the current EAD (decomposed by sector) and GLOFRIS is used to provide an estimate for the future EAD.

The SSM model is capable of estimating flood risk for direct damage as well as flood risk for business interruption damage. Furthermore, the model decomposes these damages into 7 different sectors: hospitality, industry, retail, office, healthcare, education, and sport. These sectors are based on the 'Basisregistratie Adressen en Gebouwen' (BAG), which comprises all buildings in the Netherlands and, moreover, registers the intended use of each building.

As input for SSM, inundation maps from LIWO (LIWO, 2024) are used. LIWO has several sets of inundation maps, each with a distinct return period. For the Netherlands and for the insurance analysis, it is important to distinguish the different flood types in the Netherlands. In the Netherlands, floods are differentiated into 4 different types: Type A, Type B, Type C, and Type D. Type A comprises floods that occur outside of dikes, Type B comprises floods that occur due to the failure of a primary flood defence (along larger rivers and inundation resulting from the sea), Type C comprises floods that occur due to the failure of secondary flood defences (smaller rivers), Type D comprises floods that occur in unprotected regional water systems. In the current situation only Type C and Type D floods are considered insurable. For this reason, the EAD is calculated separately for all four LIWO flood types.

The LIWO inundation maps depict the maximum inundation levels in the Netherlands for the different flood types and for different flood return periods. The flood return periods range from 1/10 to 1/100,000 years. Table 1 depicts which flood return periods are available for each flood type. In order to obtain localised estimates for the risk and insurance premiums in the Netherlands, the LIWO inundation maps are clipped for the 40 NUTS3 regions in the Netherlands.

Table 1. *Return periods per flood type.*

Flood type	Flood return periods
Type A	1/10, 1/100, 1/1000, 1/10000
Type B	1/100, 1/1000, 1/10000, 1/100000
Type C	1/100, 1/1000
Type D	1/10, 1/100, 1/1000

For businesses, SSM makes use of the BAG2014 ESRI geodatabase to assess the number of companies. This geodatabase also decomposes the businesses into the seven aforementioned sectors. Each sector has an associated maximum damage coming from de Bruijn et al. (2015). The vulnerability curves used in SSM are aggregated to three types: retail, industry, office. The hospitality sector uses the retail curve, healthcare and education uses the office curve, sport uses the industry curve. For business interruption one vulnerability curve is used for all sectors.

Using SSM, the total direct damage and total business interruption damage for each return period of each flood type is calculated. Furthermore these damages can be decomposed based on the aforementioned 7 sectors. For the insurance analysis we need both the EAD and the standard deviation of the damages. It becomes apparent that the number of return periods differs between the flood types, which results in non uniform calculations of the standard deviation between the flood types. In order to harmonize the calculation of the standard deviations, the return periods within each flood type are turned into a piecewise linear system:

$$y(x) = \begin{cases} y_1 + \frac{(x-x_1)(y_2-y_1)}{x_2-x_1}, & \text{if } x_1 \leq x < x_2 \\ y_2 + \frac{(x-x_2)(y_3-y_2)}{x_3-x_2}, & \text{if } x_2 \leq x < x_3 \\ \vdots & \\ y_{n-1} + \frac{(x-x_{n-1})(y_n-y_{n-1})}{x_n-x_{n-1}}, & \text{if } x_{n-1} \leq x \leq x_n \end{cases}, \quad \text{for } x \in [0, \Omega]$$

Where $y(x)$ represents the interpolated return period and Ω stands for the highest return period. The probability of no damage is defined as $1 - \Omega$.

Using this piecewise linear system, the return periods are interpolated, after which a Monte Carlo simulation is applied to obtain the EAD ($\bar{L}$):

$$\bar{L} = E[y(x)] = \frac{1}{N}\sum_{i=1}^{N} y(x_i)$$

And the standard deviation (σ) of the EAD:

$$\sigma = \sqrt{E[(y(x) - E[y(x)])^2]} = \sqrt{\frac{1}{N}\sum_{i=1}^{N}(y(x_i) - \bar{L})^2}$$

To estimate future flood risk for the commercial and industrial sectors, we adjust our detailed baseline EAD-estimates by a factor that represents expected impacts of climate- and socioeconomic change on regional flood risk. This factor is constructed by using current and future flood risk projections obtained from the global flood risk model GLOFRIS (Ward et al., 2017; Winsemius et al., 2016).

GLOFRIS estimates direct flood damages to commercial and industrial properties by combining flood hazard, exposure, and flood vulnerability. Flood hazard is simulated for 9 flood return periods, for 0.5° x 0.5° grid cells, by applying the hydrological and hydrodynamic model PCR-GLOBWB-DynRout (Van Beek & Bierkens, 2009; Van Beek et al., 2011), forced using meteorological data from 1960-1999, obtained from the EU-WATCH project (Weedon et al., 2011) or global climate model output for future projections. Flood hazards for the years 2050, and 2080

are obtained by running the model cascade using 40-year time-slices around the years 2050, and 2080 under RCP4.5

Flood impacts for the 9 return periods are simulated by overlaying flood hazard (inundation) maps with spatial data on urban density and associated economic values of urban areas. Present-day urban density data is obtained from the HYDE database (Klein Goldewijk et al., 2011), and future changes in urban density are obtained from the 2UP-model (Van Huijstee, 2018) for SSP2. The economic value of urban density is assigned based on national GDP per capita, which, for future projections, also changes according to the SSPs. The extent that exposed economic value is damaged by a certain level of inundation is assessed by applying simplified flood depth-damage functions (Huizinga et al., 2017).

EAD is estimated by constructing a flood probability-impact curve using results from the approach described above. For this, regional flood protection standards are obtained from the FLOPROS database (Scussolini et al., 2016). Urban flood risk per grid cell is separated into risk for residential, commercial, and industrial sectors using an assumed ratio (75%, 15%, 10%, respectively) based on observed output from the CORINE land cover map.

The GLOFRIS model is capable of producing future flood risk estimates at NUTS3 level for the commercial sector and the industrial sector. These future estimates are achieved by forcing the model with SSP and RCP scenario combination. To obtain the future estimates for the Netherlands, the difference between the GLOFRIS base level EAD and future estimates is applied to the more detailed current EAD estimates of the Netherlands from the SSM:

$$EAD_{SSM\_industrial,t} = \frac{EAD_{GLOFRIS\_industrial,t}}{EAD_{GLOFRIS\_industrial,baseline}} \times EAD_{SSM\_industrial,baseline}$$

$$EAD_{SSM\_commercial,t} = \frac{EAD_{GLOFRIS\_commercial,t}}{EAD_{GLOFRIS\_commercial,baseline}} \times EAD_{SSM\_commercial,baseline}$$

The future EAD is estimated for t = 2030, 2050, 2080. The distinction between industrial and commercial categories is based on criteria similar to those used for the vulnerability curves in SSM. The industry and sport sectors make use of the industrial GLOFRIS delta. The hospitality, healthcare, office, education, and retail sectors make use of the commercial GLOFRIS delta.

1.2.2 Insurance

Using the EAD and standard deviation of the EAD, the insurance premiums can be calculated. The insurance premiums are calculated based on Hudson et al. (2019) and Tesselaar et al. (2020). They follow a risk-layering approach meaning that the EAD is split into three parts: i) 15% of the risk is covered by the policyholder, ii) 70% of the risk is covered by the primary insurer, and iii) 15% of the risk is covered by a private reinsurer. The primary insurer and the reinsurer both charge operating costs. The reinsurer charges on top of this operating cost, a profit loading factor, as it is assumed that there are not many reinsurers. Whereas the primary insurer is assumed to have a profit loading factor of 0 due to many primary insurers being present in the market.

The insurance system in the Netherlands is voluntary and only Type C and Type D floodings are considered insurable. Moreover, businesses can insure against both direct damage and business interruption damage, but the insurance policies are considered to be separate.

Insurance uptake is simulated on a company basis. For each company, a balance sheet is simulated based on data obtained from the Dutch Chamber of Commerce (KvK). Each company first checks whether insurance is affordable based on their balance sheet and then looks at whether the insurance policy is worth it using a subjective cost-benefit analysis comparing the reduction in EAD with the insurance premium. The system is calibrated on survey data from the Limburg floods in 2021 (Endendijk, 2024), which is used to calibrate the benefit misperception.

1.2.3 Coverage gap

The coverage gap is defined as the difference between the total risk and the part of the risk that is insured. A distinction is made between the coverage gap for total insurable risk (flood Type C and Type D) and the coverage gap for total extended risk (flood Type A,B,C,D). The coverage gap is a key indicator for understanding financial resilience against flood events. A large gap indicates that a significant portion of the population or economy remains unprotected, highlighting the need for policy interventions, improved insurance products, or public-private risk-sharing mechanisms.

1.3 Results & Discussion

Figure 1 shows the total insurable EAD (flood Type C and D), combining direct EAD and business interruption EAD, for each of the 7 SSM sectors across NUTS3 regions in the Netherlands. The figure shows that most of the damage is concentrated in the western part of the Netherlands and that the Industry and Office sectors are most exposed to flood risk. For certain sectors, the EAD ranges over 1 million euros in certain NUTS3 regions.

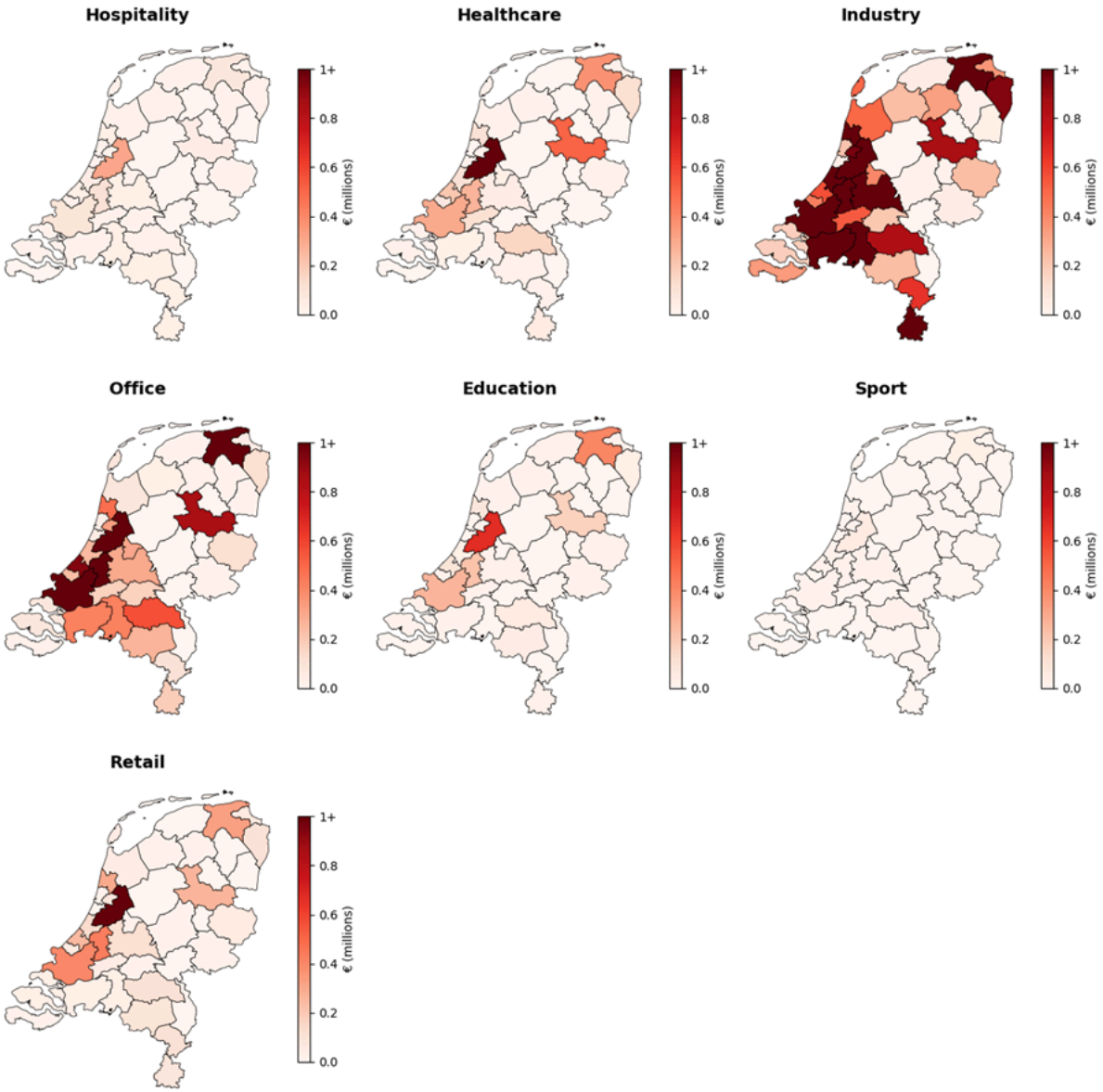

Figure 1. *Total insurable EAD per sector across NUTS3 regions (2011 euros).*

Figure 2 shows the total extended EAD (flood Type A,B,C,D), combining direct EAD and business interruption EAD, per sector across NUTS3 regions in the Netherlands. Comparing Figure 2 with Figure 1, it becomes apparent that the extended EAD is a lot higher than the insurable EAD, with the Industry sector and Office sector having an EAD of over 1 million in the large majority of NUTS3 regions. Furthermore, the extended EAD seems to be more evenly spread out across the Netherlands.

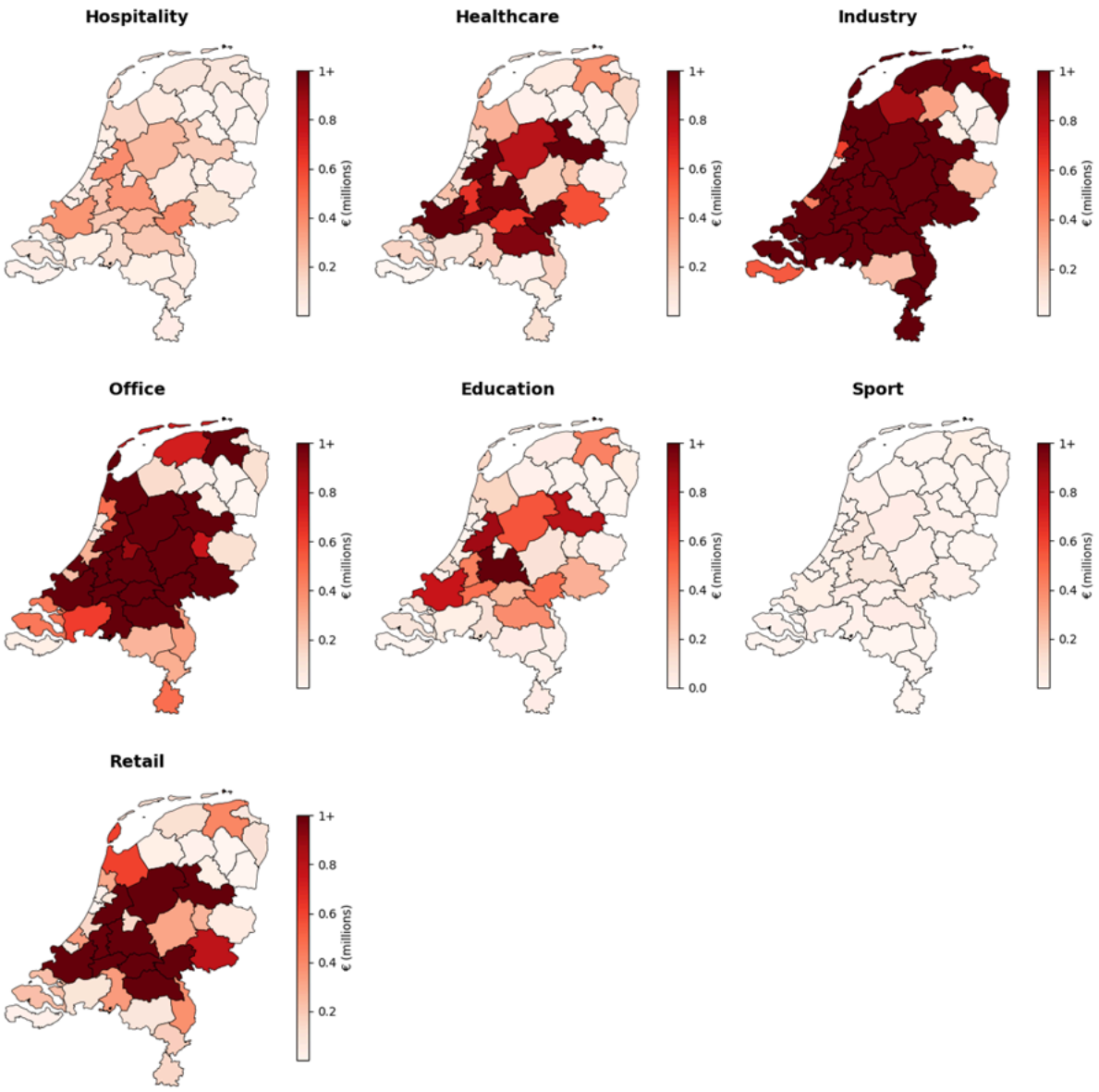

Figure 2. *Total extended EAD per sector across NUTS3 regions (2011 euros).*

Table 2 shows that the total extended direct EAD is about a factor 4 larger than the total insurable direct EAD. Whereas, Table 3 shows that the total extended business interruption EAD is about a factor 3.5 larger than the total insurable business interruption EAD.

Table 2. *Average Insurable direct EAD per company per sector across NUTS3 region in 2011 euros.*

	Mean	Min	Max
Hospitality	24	0	118
Healthcare	352	0	1613
Industry	307	0	2146
Office	543	0	2239
Education	561	0	2970
Sport	27	0	145
Retail	417	0	2064

Table 3. *Average Insurable Business Interruption EAD per company per sector across NUTS3 region in 2011 euros.*

	Mean	Min	Max
Hospitality	21	0	114
Healthcare	416	0	2175
Industry	412	0	2433
Office	1109	0	5929
Education	274	0	1740
Sport	67	0	306
Retail	196	0	855

Comparing the differences between sectors, Table 2 and Table 3 reveal the average insurable direct EAD and average insurable business interruption EAD per company and sector across NUTS3 region in euros. First, it becomes apparent that there is a discrepancy for the height of the average EAD for direct damage and business interruption damage between sectors. For certain sectors, the average direct EAD per company is higher than the average business interruption EAD per company, whereas for other sectors, the average direct EAD per company is lower than the average business interruption EAD per company. In this regard, the retail sector is particularly interesting. Its business interruption EAD (€196) is more than two times lower than the direct EAD (€417). Furthermore, the office sector interestingly has a business interruption EAD (€1109) which is more than two times higher than the direct EAD (€543).

Other sectors demonstrate more balanced exposure patterns. The hospitality sector, for example, has a slightly higher direct EAD (€24) than business interruption EAD (€21), indicating that physical damage plays a marginally more significant role in expected losses than operational downtime. Healthcare and industry sectors, on the other hand, exhibit larger absolute values in both direct and business interruption EADs, reflecting their higher capital intensity and operational scale. The education sector shows a higher direct EAD (€561) compared to business interruption (€274), which may be explained by the value of educational facilities and equipment relative to temporary disruption costs (here we do not take into account the value of lost education). Similarly, the sport sector has relatively low EAD values overall, with a direct EAD of €27 and business interruption EAD of €67, highlighting limited exposure in both dimensions compared to larger sectors such as office, education, and industry.

It is important to note that these tables depict the EAD for companies in a one-in-a-thousand year flood zone. This means that a singular flood event will have a much larger impact. The EAD spreads out the damage over time to obtain an annualized damage figure.

Table 4. *Average Insurance premiums for insurable direct EAD per company per sector across NUTS3 region in 2011 euros.*

	Mean	Min	Max
Hospitality	32	0	164
Healthcare	481	0	2155
Industry	416	0	2824
Office	744	0	3119
Education	767	0	4107
Sport	36	0	200
Retail	572	0	2864

Table 5. *Average Insurance premiums for insurable business interruption per company per sector across NUTS3 region in 2011 euros.*

	Mean	Min	Max
Hospitality	29	0	160
Healthcare	572	0	3045
Industry	561	0	3218
Office	1517	0	8059
Education	373	0	2364
Sport	92	0	419
Retail	268	0	1195

Table 4 and Table 5 present the average insurance premiums for direct EAD and business interruption EAD per company per sector across NUTS3 regions in euros. First, it becomes evident that the premiums generally align with the underlying EAD (Table 2 and Table 3). In other words, sectors with higher direct or business interruption EAD tend to have higher insurance premiums, reflecting the proportionality between expected losses and the cost of transferring risk to insurers. The insurance premiums again highlight the fact that certain sectors are more exposed to direct damage, such as the retail sector, whereas other sectors are more exposed to business interruption damage such as the office sector.

Table 6. *Average percentage of companies purchasing direct damage insurance across NUTS3 region.*

	Mean	Min	Max
Hospitality	39.37	0	43.18
Healthcare	39.06	0	50.00
Industry	34.58	0	40.77
Office	35.76	0	45.55
Education	32.24	0	39.75
Sport	33.76	0	51.24
Retail	30.70	0	40.15

Table 7. *Average percentage of companies purchasing business interruption insurance across NUTS3 region.*

	Mean	Min	Max
Hospitality	38.39	0	43.19
Healthcare	37.25	0	46.71
Industry	33.66	0	40.25
Office	32.43	0	43.36
Education	33.87	0	41.86
Sport	36.09	0	49.59
Retail	32.08	0	42.38

Table 6 and Table 7 present the average percentage of companies per sector purchasing direct damage insurance and business interruption insurance across NUTS3 regions. Insurance penetration varies only moderately across sectors and the maximum insurance penetration rate does not exceed 51.24% for direct damage insurance and 49.59% for business interruption damage insurance in all NUTS3 regions. The minimum penetration rate is 0% for all sectors, this is due to some NUTS3 regions being not exposed to flood risk. For direct damage insurance, the hospitality and healthcare sectors exhibit the highest average uptake, at approximately 39% each. This suggests that insurance for companies in these sectors is more often (subjectively) cost-effective compared to other sectors. The retail sector, in contrast, exhibits a slightly lower average uptake of 30.70%, which may indicate that direct damage insurance in this sector is generally less cost-effective. When looking at the business interruption insurance penetration rates, the hospitality sector again has a high average insurance uptake of 38.39%. In contrast, the office sector exhibits a lower uptake for business interruption insurance (32.43%), despite the earlier results showing that companies in the office sector face substantial business interruption damage. A potential explanation for this may be the relatively high insurance premiums for the office sector.

Table 8. *Average future direct EAD and insurance premium in 2011 euros, and insurance uptake per company per sector across NUTS3 region.*

	EAD 2050	EAD 2080	Premium 2050	Premium 2080	Uptake 2050	Uptake 2080
Hospitality	48	82	65	112	20.89	9.74
Healthcare	707	1121	968	1656	21.84	10.11
Industry	616	1055	837	1432	19.38	9.23
Office	1091	1867	1496	2560	20.81	10.44
Education	1128	1930	1542	2639	14.86	6.22
Sport	53	92	73	125	17.98	8.65
Retail	838	1434	1149	1966	19.95	9.16

Table 9. *Average future (based on RCP4.5) business interruption EAD and insurance premium in 2011 euros, and insurance uptake per company per sector across NUTS3 region.*

	EAD 2050 (€)	EAD 2080 (€)	Premium 2050 (€)	Premium 2080 (€)	Uptake 2050 (%)	Uptake 2080 (%)
Hospitality	42	73	59	100	25.26	13.53
Healthcare	837	1432	1151	1969	20.79	10.83
Industry	828	1416	1127	1929	12.90	5.29
Office	2229	3815	3048	5217	11.95	5.97
Education	551	943	751	1284	34.51	22.14
Sport	134	230	184	316	6.16	2.12
Retail	393	673	538	921	33.86	24.73

Table 8 and Table 9 show the average projected future EAD in euros, insurance premium in euros and insurance uptake in percentages per company per sector across NUTS3 region for both direct damage and business interruption damage. The average EAD is obtained using the GLOFRIS factors under SSP2-RCP4.5.

The projected EAD increases significantly in 2050 and 2080 compared to the baseline, highlighting growing risk. For all sectors, the EAD more than triples in 2080, this is also reflected in higher insurance premiums. Due to the fact that the insurance premiums are calculated taking the standard deviation into account and a percentual operating and profit margin, the premiums are projected to rise even more strongly than the EAD

The uptake columns show that the high increase in insurance premiums lead to a fall in the insurance penetration rates. In 2080, the industry sector, the office sector and the sport sector are projected to fall below 6% insurance penetration rate. This is especially striking due to the industry and office sector having the highest absolute risk (Figure 1). The decline in insurance uptake by businesses is due to premiums rising more rapidly than the ability or willingness to pay for insurance coverage. The fall in insurance penetration rates means that the coverage gap will widen over time. This is further exacerbated by the fact that the sectors that have the lowest penetration rate are also the sectors that are most exposed in terms of absolute risk.

Table 10. *Total coverage gap (direct EAD and business interruption EAD combined) in 2011 euros.*

	Coverage gap current (€)	Coverage gap 2050 (€)	Coverage gap 2080 (€)
Hospitality	640,999	1,624,882	3,193,216
Healthcare	2,737,950	6,995,681	13,606,909
Industry	25,664,443	65,950,368	124,524,661
Office	11,441,603	29,467,304	54,802,991
Education	1,508,038	3,551,098	6,837,576
Sport	116,147	325,546	592,368
Retail	3,269,592	7,223,737	14,040,415

Table 10 shows the total coverage gap by combining the direct EAD and business interruption EAD. It becomes evident that with the increase in EAD and decrease in insurance penetration rate over time, the coverage gap will widen in 2050 and 2080. Furthermore, the industry and office sector account for over 80% of the coverage gap across all three time periods. The industry sector accounts for more than half of the coverage gap in 2080 with an estimated uninsured EAD of nearly €125 million. The main driver for this is the sharp decline in insurance coverage for these sectors relative to the other sectors, as is visible in Table 8 and Table 9.

Over time, the coverage gap doubles or triples for all sectors from now until 2050, and approximately doubles again from 2050 to 2080, leading to an overall increase of the coverage gap of nearly 380% by 2080. As a result, the total coverage gap in 2080 is €217.6 million. It is important to note that this is the yearly uninsured EAD, meaning that on a yearly basis, damages worth €217.6 million are not paid out by insurers and need to be financed by other means. Moreover, this is only the uninsured part of the damage that is considered insurable, meaning that the total yearly flood EAD (including flood Type A and Type B) is estimated to be much larger.

1.4 Conclusion/Key takeaways

This analysis provides an estimation of the Expected Annual Damage (EAD) for both direct flood damage and business interruption flood damage in the Netherlands. Furthermore, the EAD is disaggregated based on 7 economic sectors, and projections for 2050 and 2080 are made. The estimated EAD is used to calculate risk-based insurance premiums, which are applied in a firm-level cost-benefit analysis to estimate the sectoral insurance uptake for both direct damage insurance and business interruption insurance. Using the insurance uptake, the sectoral coverage gap is calculated, and it is shown how this coverage gap increases due to climate change.

First, the estimated EAD shows large differences across areas in the Netherlands. The difference is made between insurable EAD and uninsurable EAD. It is shown that the insurable EAD is only a part of the total EAD in the Netherlands. Moreover, the industry sector and the office sector make up the largest part of the insurable EAD. Furthermore, the EAD divided by the exposed companies shows large differences between sectors. The hospitality and sport sector particularly stand out by having a low average EAD, whereas the office sector has relatively high EAD. It is important to note here that the reported EADs are averages across NUTS3 regions and across companies in these NUTS3 regions. Within the simulation, the building-size of each company is used to scale the EAD and hence influences the size of the premium. This makes the actual EAD used in the simulation different for each company.

Second, the premiums reflect the underlying risk. It is important to note here that the increase in risk over time leads to a higher increase in premium due to the increasing uncertainty (standard deviation) of risk, which is operationalized into a higher premium surcharge.

The uptake differed only moderately among the different sectors. With the uptake not being higher than 51.24% in any NUTS3 region. Furthermore, for every sector, there is at least one NUTS3 region in which flood insurance is not relevant.

The coverage gap is estimated to increase over time due to an increase in EAD in combination with a decline in insurance uptake. Especially the industry and office sectors are expected to be hit hard, with the industry sector accounting for over 50% of the total coverage gap in 2080. It is important to note that this concerns only the part of the flood EAD that is currently considered insurable. The total flood risk in the Netherlands (including flood type A and type B) is estimated to be much larger. Moreover, although expressing the insurance coverage gap in terms of EAD may be useful for budgetary planning, it is important to note that uninsured damages of a single flood event may be substantially higher. Inadequate preparation for such events may result in sudden public budget deficits, cutting funding from welfare-enhancing objectives, and often delayed reconstruction processes, which may have considerable negative macroeconomic impacts (Von Peter et al., 2024).

Overall, the results highlight the growing importance of effective flood risk management and insurance mechanisms in the Netherlands. While the modelling shows that risk-based premiums can capture the spatial and sectoral variation in expected flood losses, the widening coverage gap over time underscores the need for policy interventions to maintain affordability and uptake. Without targeted measures such as public-private partnerships, risk reduction incentives, or

subsidies for high-risk sectors, the economic burden of flood damage will increasingly shift toward businesses and society at large. These findings therefore emphasize the urgency of integrating climate adaptation strategies with financial risk management to ensure long-term resilience across all sectors of the economy.

2 Impacts of large-scale floods on financial stability

2.1 Introduction

This task complements the top-down pan-European flood risk work in Deliverable 2.1 with a bottom-up, local, event-based assessment of the impacts of extreme flood scenarios in the Netherlands, to inform a credit risk model of the DNB Dutch Central bank (a deep engagement stakeholder of the ACCREU project in the case study 5.1, adaptation options for enhancing financial stability, see D3.2). We include both river and coastal floods, and compounding river and coastal flood events.

The selected events are spatially refined, with a 100 m x 100 m resolution. The models that were used to produce these events have more hydrodynamic and terrain complexity than the pan-European LISFLOOD (Van Der Knijff et al., 2010) and GLOFRIS (Ward et al., 2017; Winsemius et al., 2016) models that have been described in ACCREU Deliverable 2.1.

We made a subselection from a set of more than 1,800 flood events that were produced by local waterboards in the Netherlands. The objective of this selection was to find a subset of events that is representative of extreme, catastrophic flood conditions for the Netherlands. The other selection criteria originated from the financial impact model that was used, which is the financial stability stresstest model by the Dutch Central Bank (DNB). This model is also used in case study CS5.1 on 'adaptation options for enhancing financial stability'. The results of this study were published as a whitepaper by the Dutch Central Bank (Caloia et al., 2023) and in the Dutch Water Magazine (van Ginkel et al., 2023). The case study results are described in ACCREU's Deliverable 3.2, where we also discuss their implications for adaptation in the financial domain. Together with case study CS5.2 on the 'stimulation of private sector adaptation through insurance arrangements', our case informs decision type 5: Financial and private sector adaptation decisions. The results of this decision type are described in ACCREU's Deliverable 3.3

2.2 Methods

2.2.1 Extreme flood scenarios for stress testing financial stability

We first discuss the type of considered floods. We here only focus on flood events that are caused by breaches of the primary flood defenses in the Netherlands. Primary flood defenses are the dikes, storm surge barriers, dunes and other flood defenses that protect against flooding from the sea, the large rivers and the large lakes[1], i.e., we only consider river flooding and coastal flooding, and not pluvial flooding. Further, we do not examine failures of so-called 'secondary' flood defenses, that are the smaller dikes etc. protecting against flooding from the regional water system, such as canals, small rivers and small lakes. Also, we do not examine flooding of areas that are not protected by dikes, i.e., the outerdike areas.

The focus on floods resulting from failure of primary defenses is justified by the fact that the consequences of these floods are much more severe than for the other flood types. Since we are

[1] In the Dutch flood risk management bookkeeping system: only type-B floods.

concentrating on extreme and catastrophic flood events, it is natural to focus on failure of primary defenses because these cause the largest damage and societal disruption. Also, the failure probabilities of these defenses are rather small, making them good examples of tail-risk events we are interested in here. Furthermore, this flood type is currently not insurable in the Netherlands, whereas most other flood types are.

2.2.2 Scenarios for extreme single dike breaches

The LIWO database (http://www.basisinformatie-overstromingen.nl) contains more than 1800 of floods that result from individual breaches of the primary flood defenses in the Netherlands. From these, we selected 32 flood scenarios, which consist of individual flood events that cause large real estate damage. Further, we selected the scenarios such that they have a good geographical spread throughout the Netherlands.

To this end, we first extracted the real estate damage to houses for all 1800 scenarios. Second, for each dike ring area in the Netherlands, we selected the scenario causing the largest real estate damage. A dike ring is a compartment enclosed by a ring of dikes, the Netherlands has more than 50 of such compartments. Some dike rings are very large, spanning multiple big cities with millions of inhabitants and billions Euro worth of exposed real estate, where others are much smaller. Third, we therefore removed all dike rings where the worst flood event caused more than €500 million (2011 price level) damage. This results in 24 scenarios, each in a different dike ring in the Netherlands (Annex B.3).

Fourth, we manually added 8 scenarios to our selection (Annex B.4). We do this because some dike rings are so large that a breach at one side of the dike ring will flood a different part of the dike ring than a breach at the other side. This means that alternative breach locations may affect a different part of the real estate. This is important for our financial stability model, which is not only sensitive to the absolute damage caused by the flood, but also how this relatively relates to the finance structure (mortgage status) of the real estate such that both flood depth and real estate characteristics are relevant for the damage estimate. The final selection of 32 scenarios is shown in the results section (Figure 3). The return periods of these floods range between one-in-a thousand years to one-in-ten-million years (Figure 7). These estimates are conservative in the sense that they do not reflect the effect of the dike strengthening activities that are currently ongoing in the Netherlands.

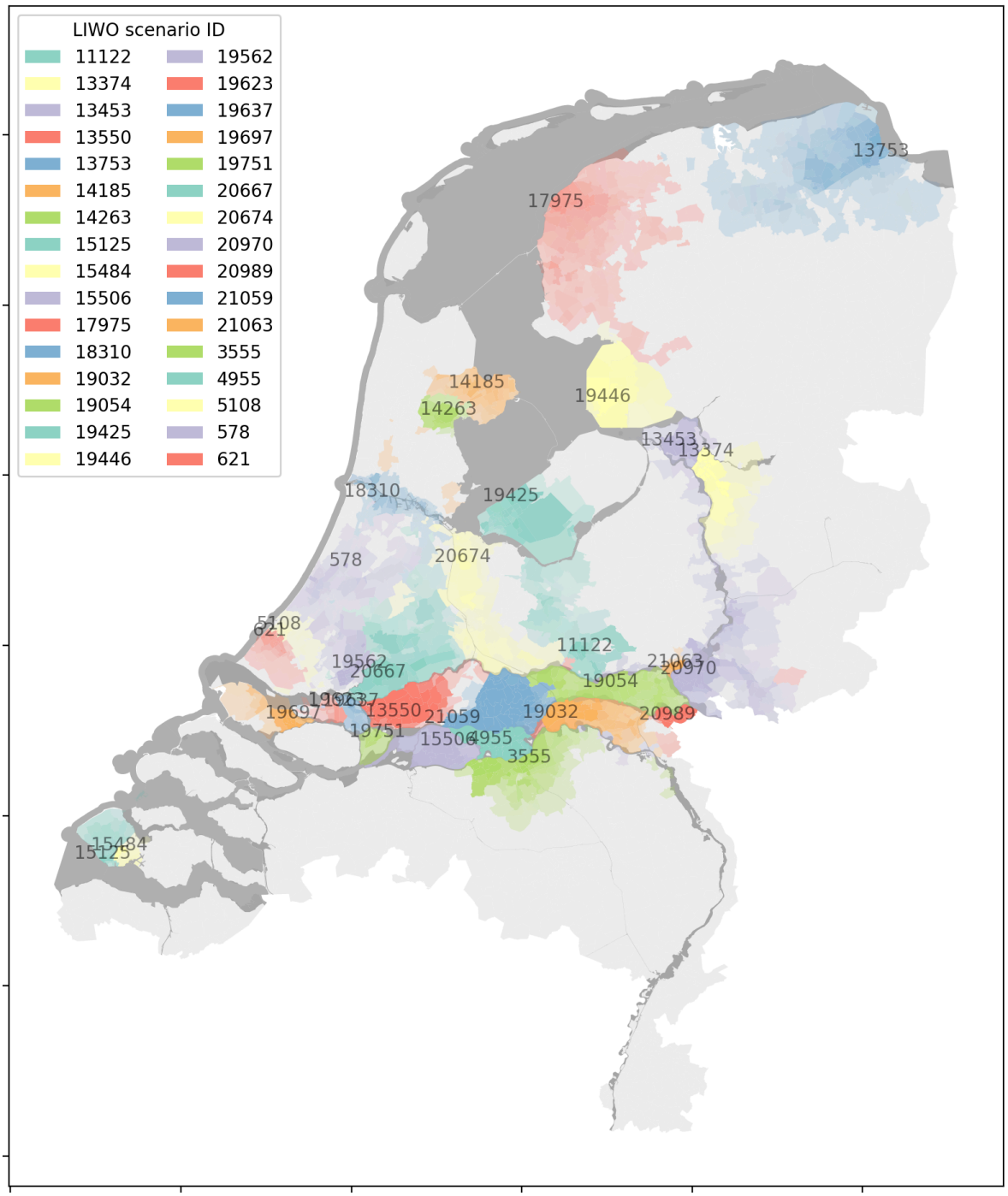

Figure 3. *The 32 extreme flood single dike breach scenarios. IDs refer to the scenario numbers on www.basisinformatie-overstromingen.nl .*

2.2.3 Worst Credible Flood scenarios

Note that in the previous section, we only focused on single dike breaches. In reality, it is very well possible, and even likely, that multiple breaches will happen at the same time. After all, when the weather and hydrological conditions are so extreme that a dike breaches at one location, these conditions are most likely also very extreme at other locations.

To get an impression of what could happen in a very extreme, yet still somewhat realistic, scenario, we used the so-called Worst Credible Flood scenarios. This is a set of 6 scenarios that were developed in 2007 by the consultancy HKV Lijn in Water (ten Brinke et al., 2010). The rationale behind the scenarios is that despite being very extreme and catastrophic, they are still realistic representations of tail risks. Their return periods are estimated at least a factor 10 greater than protection levels of the dike rings, which usually offer protection against floods with return periods of one-in-a-thousand to one-in-ten-thousand years. At the same time, they should not be seen as the upper bound of what is possible; more extreme floods are imaginable, yet their probability is even smaller.

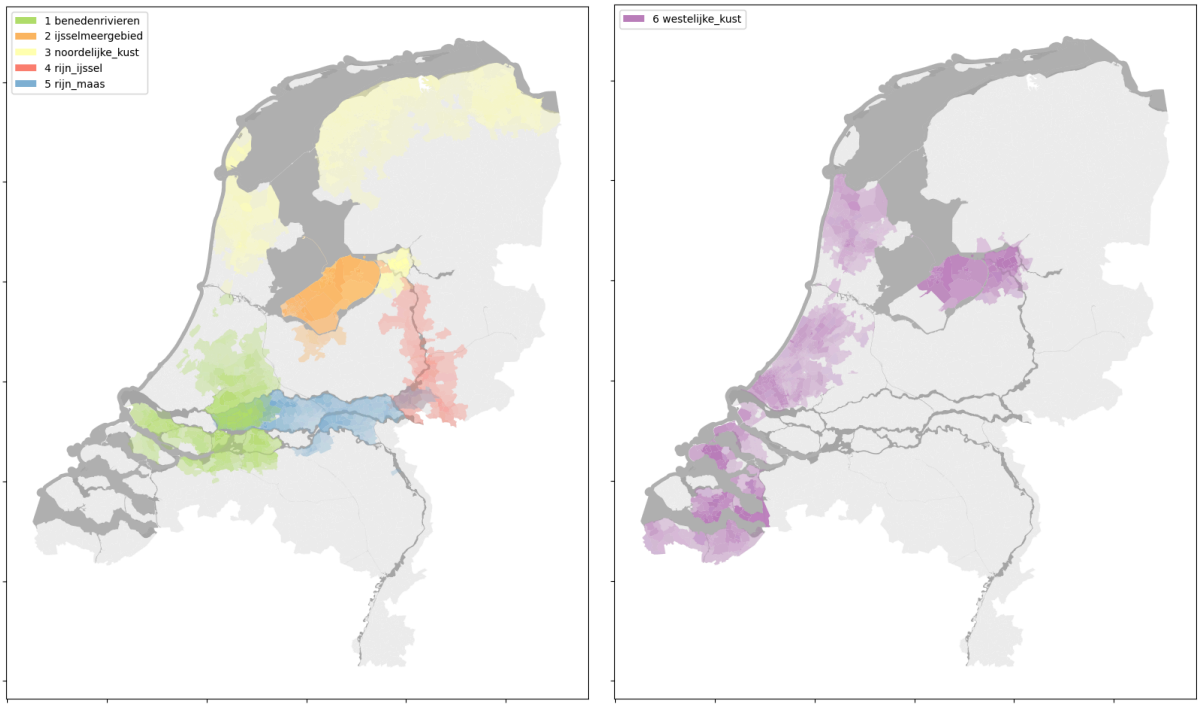

Figure 5. *The 6 Worst Credible Flood events in the Netherlands (ten Brinke et al., 2010). These represent highly unlikely (extreme and catastrophic) but physically plausible events.*

2.2.4 How the extreme flood scenarios relate to ACCREU's scenario selection

According to its scenario framework, ACCREU assesses three future emission scenarios (RCP2.6, RCP4.5 and RCP7.0), and the middle-of-the-road socioeconomic SSP2. Here, we discuss how our scenarios, which do not directly consider climate change impacts through e.g. sea level rise, align with ACCREU's scenario selection. One of the main drivers of flood risk in the Netherlands is sea level rise. Figure 6 shows the observed and projected sea level rise compared to the reference period 1995–2014, for RCP2.6, RCP4.5 and RCP8.5. In addition to the very likely range (5th to 95th percentile confidence interval), also low-probability high impacts scenarios are shown (Van Dorland et al., 2023). These low-probability high-impact scenarios result from climate tipping points on the West-Antarctic and Greenland ice sheet.

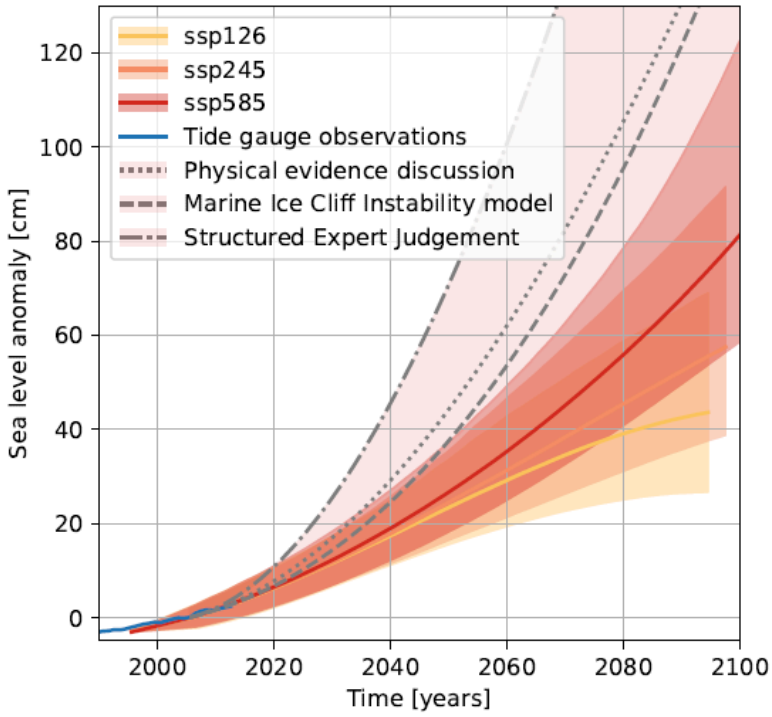

Figure 6. *Sea level rise scenarios at the Dutch Coast (Van Dorland et al., 2023).*

Up to 2050, there is little divergence between different RCP forcing scenarios. After 2050, the scenarios start to diverge more strongly. For the year 2100, the 5th to 95th percentile range is 26–73 cm in RCP2.6, 40-95 cm in RCP4.5 and 59–124 cm in RCP8.5 (Van Dorland et al., 2023). The 95th percentile of RCP7.0 can be assumed to be somewhere in-between 95 cm (RCP4.5) and 124 cm (RCP8.5).

The Dutch government is currently working on a very large national dike strengthening project (called the Hoogwater Beschermingsprogramma) that will run up to the year 2050. In consequence, up to 2050, the national flood risk is expected to decrease rather than to increase, because adaptation will reduce the risk faster than climate change increases it - provided that the

adaptation is successfully and timely implemented. We expect that also in the period 2050–2100, dike reinforcements will be continued, to ensure that the flood protection systems meet the failure probability standards.

The consequence of this flood risk management strategy is that the magnitude of the risk is mainly determined by the failure probability of the installed flood defenses. The failure probabilities assigned to the discussed scenarios are typically very small. Consequently, the risk in terms of expected annual damage is also very low, and if it would increase due to climate change, the flood defense system will likely be reinforced so that the probability is low again and meets the standard.

Because of our focus on extreme and catastrophic events, we have selected scenarios with very small probabilities of occurrence, ranging from one-in-a-hundred years to one-in-ten-million years (Figure 7). We consider these scenarios to be valid up to 2050. They may become slightly more likely due to the effect of sea level rise. However, they could also become less likely when the flood defenses at the dike breach location are strengthened. After 2050, the scenarios still give a reasonably good proxy of the flood severity, but their probability will be even more influenced by the amount of sea level rise or adaptation efforts. However, with very extreme sea level rise (such as the dashed low-probability and high-impact 'tipping point' scenarios under RCP8.5), the validity of the scenarios may decrease, because sea level rise will not only have an impact on the probability of flooding, but will also become a significant factor for the flood severity in terms of water depth. These kinds of tipping-point scenarios are however not part of the default ACCREU scenarios.

The analysis is performed for the present mortgage exposure of major lenders in the Netherlands. Our analysis therefore implicitly assumes that this present distribution of assets over higher and lower risk zones in the Netherlands is also representative for future conditions. This assumption fits well with the 'middle-of-the-road' narrative of SSP2 considered in ACCREU assuming that economic trends further develop along their historical path.

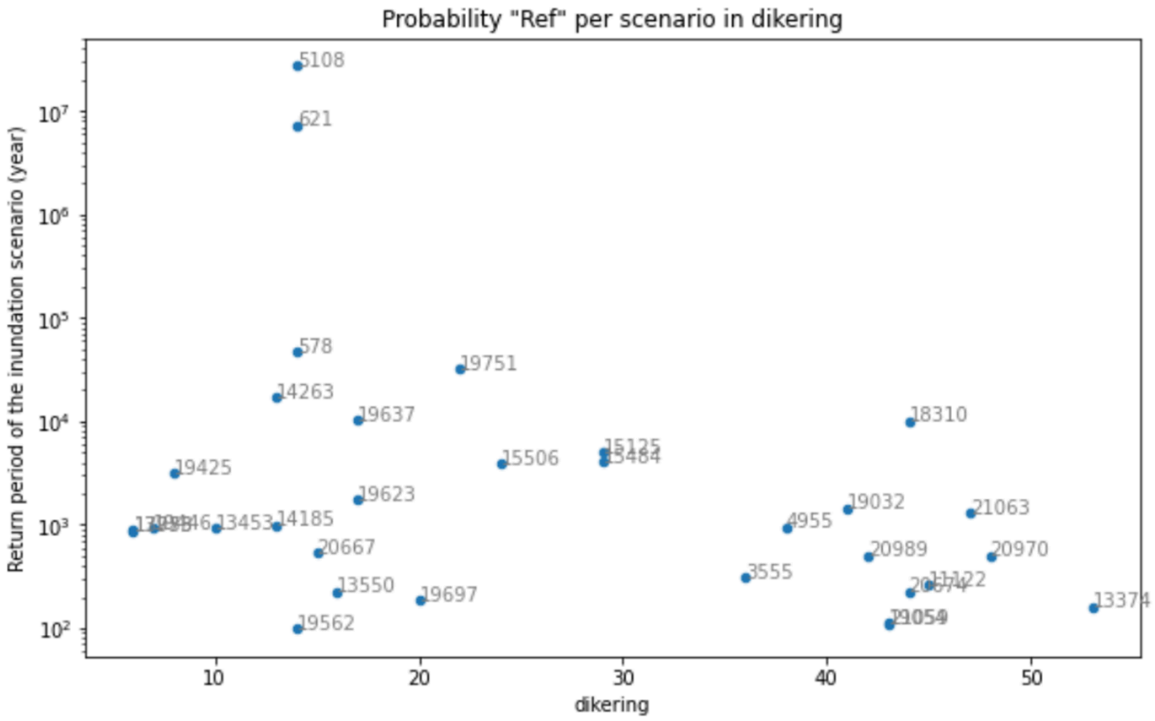

Figure 7. *Indicative probabilities of the scenarios (y-axis), without implementation of the dike strengthening activities that are currently ongoing.*

2.2.5 Damage estimates

For each of the selected scenarios, we calculate the damage with the 2023 version of the Schade- en Slachtoffer Model (SSM), which is a software tool designed to compute flood damage (to buildings, contents, etc.) and estimate victims (i.e. fatalities or injuries) based on the outputs of flood (hydraulic) simulations (Slager and Wagenaar, 2017, De Moel et al., 2025) (cf. Model description in Chapter 1). SSM is the standard tool for calculating flood damage in the Netherlands. The model allows calculating total damage, which includes damage to businesses, infrastructure, houses and other land use categories such as agriculture. It also includes both direct damage and indirect economic losses. Further, we will single out damage to residential real estate Here, we only focus on the structural damage to residential real estate. Note that this does not include all damage to building contents, because these are not part of the collateral of the mortgage of a bank. The calculation uses depth-damage functions, assuming a maximum damage of 1,295 €/m². Hence, a building of 100 m² can have a maximum damage of €129,500. This value is reached when the maximum water depth occurs (5 meter). Further, the model accounts for the size of the building, expressed in terms of 'living area' (m²), which may be distributed over multiple floors. This living area is larger than the building footprint when the building has more than one floor. The real estate damage is calculated by multiplication of the dimensionless damage fraction (from damage function at given water depth) with the maximum damage and the building size. This calculation is

a source of (large) uncertainty, which is quantitatively discussed in Section 2.3.1. Note that for apartments, the calculation procedure is slightly different (see De Moel et al., 2025 for details).

2.3 Results

In Sections 2.3.1 and 2.3.2, we first discuss the damage resulting from the 32 extreme single dike breach scenarios of Section 2.2.2 and the 6 Worst Credible Flood scenarios of Section 2.2.3, respectively, before presenting the credit risk impact of these property damages in Section 2.3.3.

2.3.1 Damage caused by extreme single dike breach scenarios

We first assess the damage caused by the 32 flood events that result from single dike breaches (Figure 3). Figure 7 gives an indication of their corresponding return periods. These probabilities are conservative in the sense that they do not reflect the effect of the dike strengthening activities that are currently ongoing in the Netherlands.

Table B.1 in the Annex provides an overview of the total damage for each flood event. The total damage associated with the 32 flood scenarios ranges from €3.7 to 28.1 billion (2011 prices) for scenario 15484 and 19054, respectively, and the number of casualties ranges from 223 to 10596 for the scenario 17975 and 15484, respectively. The table reports the damage for the land cover in 2014 as well as damage and casualties for the land cover in 2022. The latter are retrieved from De Grave and Juch (2023).

Further, Table B.2 in the Annex provides an overview of the damage to residential real estate only. The damage ranges from €0.7 to 5.0 billion (2011 prices) for the scenario 17975 and 3555, respectively. Notably, these estimates include only the direct damage to the building and exclude damage to the contents of the building, such as furniture.

2.3.2 Damage caused by Worst Credible Flood scenarios

Next, we discuss the damage associated with the Worst Credible Flood scenarios, which are used to study the upper bound of extreme floods that could happen in the Netherlands. This is in line with the rationale of financial stress testing, that focuses on extreme but plausible floods. These cause total damage between €9 to 121 billion (2010 price level) (Table 11), i.e., the most damaging Worst Credible Flood scenario causes about five times more total damage than the most damaging extreme single dike breach scenario.

Table 11. *Total damage as well as casualties caused by the 6 Worst Credible Flood events (ten Brinke et al., 2010).*

Flood event	**Total flood damage** (billion € (2010 prices))	**Casualties**
1. Lower (tidal) river courses	51	3060
2. IJsselmeer lake district	19	950
3. Wadden sea coast	40	3440
4. Rhine (IJssel) with breaches in Germany	9	10
5. Rhine and Meuse in the Netherlands	39	55
6. Southwest and central coast	121	10300

2.3.3 Impacts on credit risk

The selected events have been connected to the financial stress testing model of the DNB Dutch Central bank. The results are reported in a separate whitepaper, published on the website of the central bank (Caloia et al., 2023).

Here, we will briefly summarize the key findings of the stress test. The DNB model calculates the impacts of flooding on banks that occur through a credit risk channel. For each flood event, we calculate the flood damage to residential and commercial real estate. The flood damage reduces the value of the building, i.e. the value of the collateral for the mortgage. In the DNB-model, this leads to an increase of the loan-to-value (LTV) ratio. This also increases the loss-given-default for a bank. Additionally, the probability of a default (PD) on the mortgage increases. Both channels (LTV and PD) lead to a decline of the capital position of a bank. This is measured by the so-called Common Equity Tier 1 (CET-1) indicator.

Figure 8 shows the impact on the CET-1 expressed in basis points (1/100 of a percent point). The single dike breaches lead to a capital depletion of some 30–50 basis points. The worst credible floods lead to a capital depletion of some 40–110 basis points.

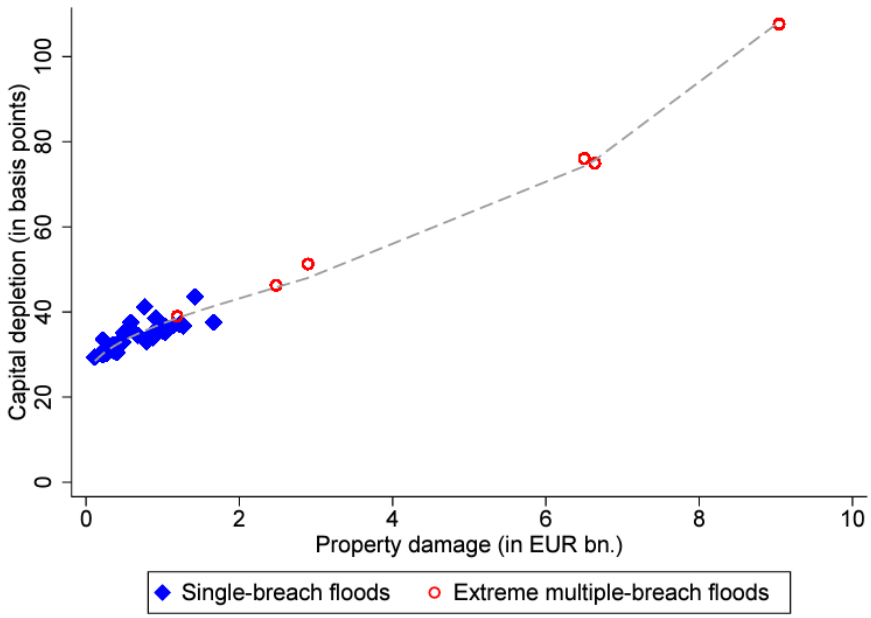

Figure 8. *CET-1 capital depletion of banks due to the 32 extreme single dike breaks (blue dots) and the 6 Worst Credible Floods (red circles) flood scenarios (from Caloia et al., 2023).*

To interpret these results, we need to give some context to the order-of-magnitude of the CET-1 indicator. In a recent bank stresstest by the European Banking Authority (EBA, 2023), the CET-1 starting point was around 15%, on average. After imposing a scenario with a severe economic recession, these CET-1 ratios declined with 459 basis points. This capital decline (from about 15 % to about 10 %) did not lead to immediate concerns about the stability of the banks. In this context, the maximum decline (of 1.1 %), that we find for the Worst Credible Flood, seems manageable and is much smaller than the effect of a severe economic recession.

2.3.4 Implications for adaptation

The implications of these results for adaptation are detailed in case study CS5.1 'adaptation options for enhancing financial stability', which can be found in ACCREU's Deliverable 3.2. It describes three strategic directions that could be followed: (1) full reliance on (physical) flood risk adaptation options; (2) active steering with financial adaptation instruments; and (3) active steering on land use planning to reduce the exposure to flood risk. This case study also quantitatively explores the effectiveness of a reduced lending standard for reducing credit risk. The rather specific Dutch context of flood defenses and floods is put into a broader European context in Deliverable 3.3; in the fifth 'adaptation decision type' we create a broader synthesis of financial adaptation strategies in the European context, where we also incorporate the work on insurance.

2.4 Uncertainties

In our analysis, we account for different dimensions of uncertainty. First, with regard to the credit risk model, we identify two uncertainties. On the one hand, we only looked into one transmission channel (credit risk through real estate damage), whereas several other mechanisms also play a role. For example, a declining demand for real estate in the hazard zone can also devalue the collateral and hence the capital position of a bank. On the other hand, there are several other macroeconomic impacts that may also have an impact on the operations of a bank. For example, a flood event may lead to reduced economic impacts of various commercial sectors, which indirectly may also affect the credit position of the bank.

Second, our analysis also comprises uncertainties resulting from the selection of the extreme and catastrophic floods. We limited our selection to tail risk events in the present climate. Also, we only looked into flooding that results from breaches in the primary flood defenses, and not to flooding resulting from regional water systems, flooding of outerdike areas, or flooding outside the Netherlands. Instead, we limited our selection to single-breach scenarios on the one hand, and extreme multi-breach scenarios (Worst Credible Floods) on the other hand. A recent study by the International Monetary Fund (IMF) confirms however that our approach results in a good sample of extreme and catastrophic events (Lepore and Mok, 2024). The IMF made a broader selection of flood events, that also included flooding in unembanked areas and outside the Netherlands. Moreover, they used a different method proposed by Kolen & Nicolai (Kolen and Nicolai, 2025) to compose scenarios with multiple dike breaches at the time. Nevertheless, the damage found for these scenarios is all well within the range that we have selected in our study (Figure 8). One advantage of the Kolen & Nicolai breach method, however, is that it can give a richer understanding of the event probability and correlation structure (Kolen and Nicolai, 2025).

Third, we account for uncertainty in real estate damage estimates. A recent flood experience in the Netherlands (July 2021) provided new insights into the damage caused by flooding. In August 2025, Deltares, the VU University and Achmea published the report “Calculating Flood Damage to Homes: New Insights for Financial Applications” (de Moel et al., 2025). Based on survey data (Endendijk et al., 2023) and insurance claim data (van Ederen et al., forthcoming) they found strong evidence that SSM2023 underestimates the damage to residential real estate, which is the model used in this analysis An upward revision of the real estate damage numbers would also have an impact on the credit risk calculations presented here, for which the real estate damage is an important input. In the following, we investigate the magnitude to which these inputs may change.

One problem with the data retrieved in July 2021, is that the experienced flooding was relatively ‘shallow’, with a maximum water depth of some 2.2 m. The vulnerability function in the SSM2023 model has a domain from 0 to 5 m. The empirical findings (Endendijk et al., 2023) only covers water depths from 0–2 m, and we therefore have to make an assumption for depths between 2–5 meters. We therefore shift the original SSM function vertically, so that we achieve a continuous function that starts from the empirical findings. This results in a function that gives higher damage across the full 0–5 m range. The maximum damage to a 100 m² single-family home increases from

€129,500 to €177,266. Figure 9 shows the resulting damage function that we used for this uncertainty analysis. We recalculated the flood damage for the 32 scenarios with this new damage curve. Figure 10 shows the extent to which the flood damage increases.

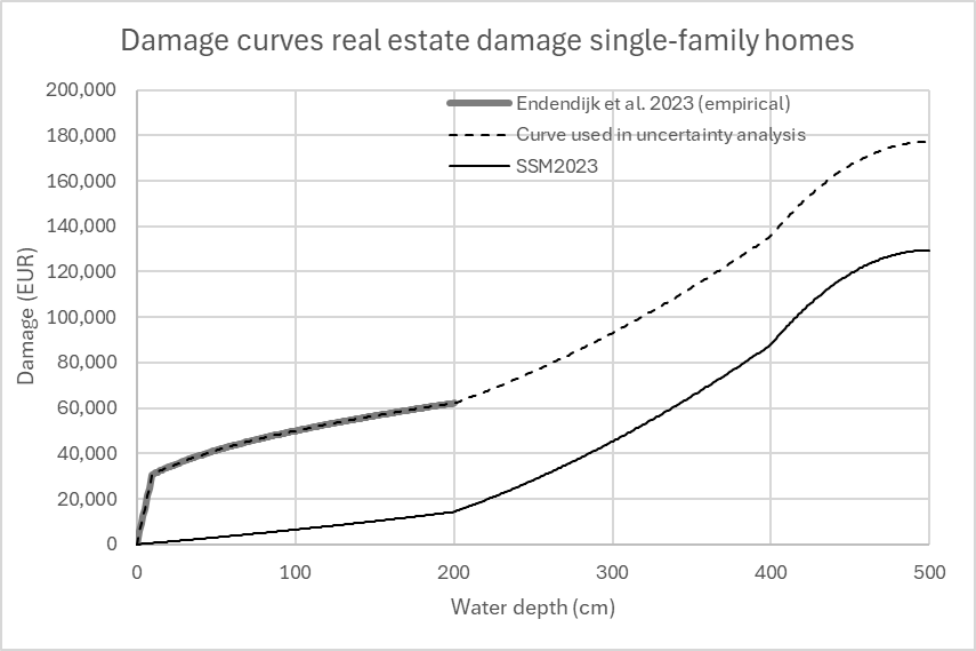

Figure 9. *Damage function used in the uncertainty analysis, after De Moel et al. (2025) and Endendijk et al. (2023).*

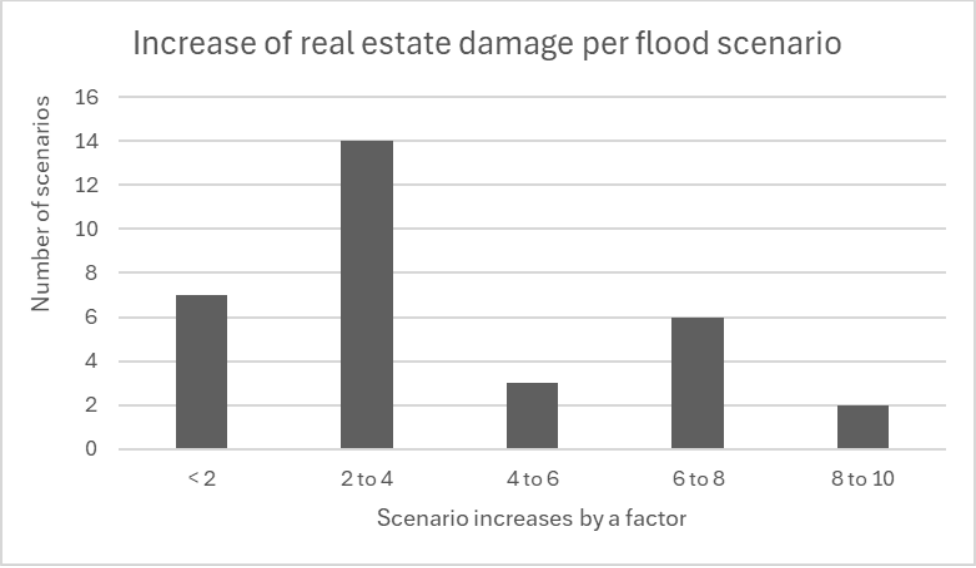

Figure 10. *Increase of real estate damage when using the new damage curve, compared to the curve in SSM2023.*

In 14 of the 32 scenarios, the flood damage increases by a factor 2–4. In 7 scenarios, the increase is less than a factor 2. This is typically the case in areas with large flood depths. In 2 scenarios, the damage increases by a factor 8 to 10. This is typically the case in areas with shallow flood depths. The difference in sensitivity of deep vs. shallow water depth scenarios can be explained from the relative difference between the old and the new damage curve: the difference is the largest at shallow water depths (Figure 5).

This quick exploration shows that the uncertainty in the real estate damage modelling may have a large impact on our results. It could lead to a doubling of the real estate damages, and for exceptional scenarios with relatively shallow water depths it may increase up to a factor 10. Note that the assumptions we have made here are 'pessimistic' and therefore indicative of the upper range of the uncertainty. While both Endendijk et al. and Van Ederen et al. find higher damage than SSM2023, the numbers of Endendijk et al. are the highest, and this is the function we have chosen here. Also, to vertically shift the damage function to create a continuous new function is a somewhat pessimistic assumption that had to be made in the absence of any empirical data for larger water depths. The curve that we constructed must therefore be interpreted as a temporary back-of-the-envelope estimate, that is only meant to give insight into the uncertainty around our analysis.

2.5 Conclusion/Key takeaways

We took a bottom-up, local, and event-based perspective to the financial stability impacts of extreme and catastrophic flooding in the Netherlands. We found that the least favorable instances of a dike breach at one single location could cause a total flood damage of €5 to 40 billion. Damage to real estate would make for €0.7 to 5 billion of the total damage (both 2011 prices). The consequent capital depletion to major lenders in the Netherlands is some 30 to 50 basis points.

In the 6 Worst Credible Flood scenarios, where dikes would breach at multiple locations at the same time, the capital depletion would be substantially higher, up to some 40–110 basis points. This magnitude of capital decline (a maximum of 1.1 % for the most severe flood) would likely not lead to immediate concerns about the stability of the banks. This effect is smaller than the effect of a severe economic recession (which could lead to a capital decline of some 5%).

Our results should be interpreted with caution, because we only looked into one specific transmission channel from flooding to financial stability: credit risk impacts resulting from real estate damage. For instance, we do not account for a risk perception shock on the real estate market, while this could also be a source of reduced real estate values and therefore lead to credit risks for banks. Also, financial stability may be affected by other macroeconomic effects, such as a reduced economic output of affected sectors in the aftermath of a flood event. Finally, we have shown that there is large uncertainty in the real estate damage calculation. Our uncertainty analysis demonstrates that in most scenarios, this could increase the damage by a factor 2–4. An upward revision of the real estate damage will likely also have a significant effect on the credit risk calculations.

3 Impacts of floods on long-term economic growth

3.1 Introduction

We assess the aggregate impacts of floods on economic growth, accounting for potential long-term effects. To this end, we define an econometric model which statistically links GDP & GVA panel data to a flood indicator. The novelty in our approach is the application of so-called impact indicators (e.g. affected areas or people) instead of meteorological indicators (e.g. modelled flood depth or precipitation), as well as the subnational scale of our analysis. We then project future flood impacts based on SSP-RCP scenario-dependent simulations of fluvial floods from the Inter-Sectoral Impact Model Intercomparison Project (ISIMIP, www.isimip.org). While the regression analyses are conducted across different NUTS levels and macroeconomic variables, the projected impacts are assessed based on the model deemed most appropriate, which corresponds to the model which regresses GDP per capita growth on the NUTS1 scale.

3.2 Method

3.2.1 Regressions

First, we calibrate a distributed lag model with three-way fixed effects to estimate the regional growth responses to the share of annually flood-affected populations for different macroeconomic variables and at different NUTS levels

$$g_{i,t} = \sum_{l=0}^{L} \beta_l P_{i,t-l} + \alpha_t + \alpha_{i,0} + \alpha_{i,1} t + \varepsilon_{i,t},$$

where $g_{i,t} \equiv \ln(y_{i,t}) - \ln(y_{i,t-1})$ represents the logarithmic growth rate of a given macroeconomic variable in region i at time t. The sum $\sum_{l=0}^{L} \beta_l P_{i,t-l}$ describes the cumulative growth response of region i to the regional shares of annually flood-affected populations, $P_{i,t-l}$, for the years $t-l$ to L. Further, α_t, $\alpha_{i,0}$, $\alpha_{i,1}$, $\varepsilon_{i,t}$ denote the year-specific fixed effect, the region-specific fixed effect, the region-specific linear time trend and the error term, respectively.

To calibrate each regression model, we use the ordinary least squares method. The above regression equation is identified as the most robust for the purpose of this research.

Macroeconomic data. We use macroeconomic data from the Annual Regional Database of the European Commission (ARDECO) of the European Commission's Joint Research Centre (version 2025.04). The database provides pan-European data for the NUTS-levels 0 to 3.

Table 12. *Applied data from the Annual Regional Database of the European Commission (ARDECO) of the European Commission's Joint Research Centre (version 2025.04).*

Variable	Unit	ARDECO code	Website
GDP at constant prices	2015 EUR	SOVGD	https://territorial.ec.europa.eu/dataset/ARDECO-SOVGD/metadata
GVA at constant prices	2015 EUR	SOVGE	https://territorial.ec.europa.eu/dataset/ARDECO-SOVGE/metadata
GVA at constant prices by industry	2015 EUR	SOVGZ	https://territorial.ec.europa.eu/dataset/ARDECO-SOVGZ/metadata
Average annual population	Persons	SNPTD	https://territorial.ec.europa.eu/dataset/ARDECO-SNPTD/metadata

We aggregate the *GVA data by industry* into three sectors (agriculture, manufacturing and services) in order to reduce the number of GVA variables. We do so based on the mapping used in the DOSE dataset (Wenz et al. 2023). The per capita values of all macroeconomic variables are calculated by dividing the macroeconomic variable by the average annual population. This means we end up with five different macroeconomic variables: GDP per capita, total GVA per capita, Agriculture GVA per capita, Manufacturing GVA per capita and Services GVA per capita.

Flood data. We use the historical flood dataset of Paprotny et al. (2025), which contains impact data (i.e., fatalities, population affected, and economic loss) on 1729 fluvial, coastal, flash and compound flood events in Europe, which were responsible for an estimated 96% of the population affected from flooding in Europe between 1950 and 2020. While the data itself is provided in NUTS3 resolution, we aggregate it to the NUTS levels 2, 1, and 0 for the corresponding analyses. In combination with the study's underlying population data (Paprotny, 2023), we then calculate the shares of annually flood-affected populations per region.

Final regression data. Since much of the subnational macroeconomic data from ARDECO from before the year 2000 is estimated, e.g. by means of interpolation or backcasting, we only apply macroeconomic data from 2000 onwards in the regression analyses. In the chosen, final setup the maximum number of lags L is set to 10, meaning the earliest flood data per region which is applied is from the year 1990. Due to the limitations of the flood data set, the latest observations included in the regressions are from the year 2020.

3.2.2 Projections

We then use our main specification model (GDP per capita, NUTS1-level) as well as projected fluvial flood data to project future GDP per capita growth perturbations for NUTS1 regions under different RCP scenarios,

$$\Delta g_{i,t} = \sum_{l=0}^{L} \hat{\beta}_l P_{i,t-l}^{proj}.$$

Here, $\Delta g_{i,t}$ denotes the projected GDP per capita growth perturbation of region i at time t, and $\hat{\beta}_l$ is the estimated coefficient from the regression model at lag l. Further, $P_{i,t-l}^{proj}$ describes the projected share of annually flood-affected populations in region i at time $t-l$, and L denotes the maximum lag number.

The climate change-perturbed GDP per capita growth rate is then derived by adding the projected baseline growth (SSP-dependent) rate to the projected flood-induced perturbation (RCP-dependent),

$$g_{i,t}^{cc} = g_{i,t}^{bl} + \Delta g_{i,t},$$

where $g_{i,t}^{cc}$ denotes the climate change-perturbed GDP per capita growth rate for region i at time t and $g_{i,t}^{bl}$ the baseline GDP per capita growth rate derived from the SSP.

Based on this climate-change perturbed growth rate, we calculate the perturbed regional GDP per capita pathways as,

$$y_{i,t} = y_{i,t-1} e^{g_{i,t}^{cc}}.$$

Here, we use the year 2024 as the starting point for the projected trajectories.

Finally, we quantify the present value of annual economic damages by means of Discounted Annual Damages (DADs). DAD is defined as the discounted difference between the GDP per capita of the baseline and the perturbed pathway,

$$DAD_{i,t} = \left(y_{i,t}^{bl} - y_{i,t}^{cc}\right) \prod_{\tau=2025}^{t} e^{-r_{i,\tau}^{bl}}.$$

Here $DAD_{i,t}$ represents the discounted annual damage of region i at time t. Further, $y_{i,t}^{bl}$ denotes the baseline GDP per capita for region i at time t and $y_{i,t}^{cc}$ the climate-change perturbed GDP per capita for region i at time t, and $r_{i,\tau}^{bl}$ describes the growth-adjusted discount rate, defined as

$r_{i,\tau}^{bl} = \rho + \eta g_{i,\tau}^{bl}$,

with the rate of time preference ρ, the elasticity of marginal utility of consumption η and the baseline GDP per capita growth rate $g_{i,\tau}^{bl}$ of region i at time τ.

Macroeconomic data. We use projected, gridded GDP and population data from ISIMIP3b (www.data.isimip.org) for the Shared Socioeconomic Pathway 2 (ACCREU's main SSP) to calculate the time series of projected GDP per capita per region. The resulting time series per region is considered the baseline GDP per capita trajectory, which does not include any explicit perturbation (no-flood baseline; black line in Figure 12 of example region AT3 and Annex Figure D.1 for all regions of this assessment). In addition, we derive a perturbed baseline GDP per capita trajectory, which includes the negative effects of floods associated with a pre-industrial control climate on GDP per capita growth (PI-flood baseline; grey line in Figure 12 of example region AT3 and Annex Figure D.1 for all regions of this assessment). This GDP per capita time series is calculated analogously to the climate-change perturbed GDP per capita time series.

Flood data. For the projections, we apply gridded flood data in 0.25 degree resolution from the global projections of fluvial floods within ISIMIP3b (Volkholz et al., 2025). The dataset includes gridded flooded area fractions derived from state-of-the-art climate, hydrological, and hydrodynamic model simulations. It is calculated within the global hydrodynamic model CaMa-Flood (Yamazaki et al., 2011; https://hydro.iis.u-tokyo.ac.jp/~yamadai/cama-flood/) and is based on the ISIMIP3b bias-adjusted atmospheric climate input data (Lange and Büchner, 2021) for the 5 CMIP6 global climate models (GFDL-ESM4, IPSL-CM6A-LR, MPI-ESM1-2-HR, MRI-ESM2-0, UKESM1-0-LL), as well as on the currently available hydrological model WaterGAP2-2e (Schmied et al., 2024). The assumed level of flood protection is taken from Paprotny et al. (2025), specifically the 2020 protection levels for fluvial floods. For coastal regions without available fluvial flood protection data, the coastal flood protection levels are used.

Table 13. *Model ensemble for the projection of fluvial floods.*

Climate Model	**Hydrological Model**	**Hydrodynamical Model**	**Flood protection**
GFDL-ESM4	WaterGAP2-2e	CaMa-Flood	Paprotny et al. (2025)
IPSL-CM6A-LR			
MPI-ESM1-2-HR			
MRI-ESM2-0			
UKESM1-0-LL			

To account for the different flood data sources in the regression and the projection, we bias-correct the projected flood indicators based on a multiplicative, climate model-specific, national bias-factor.

3.3 Results & Discussion

3.3.1 Regressions

The regressions show a significant (90% level) negative long-term effect of floods on GDP per capita growth across the NUTS-levels 3 to 1. The cumulative effect at lag 10 increases from NUTS3 to NUTS1, indicating that the impact of floods is stronger for NUTS1 regions than for NUTS3 regions. The significance of impacts is highest on the NUTS1 level. Meanwhile, the regression on NUTS0 (national) level does not show significant negative effects of floods.

Similarly, the regressions of total GVA per capita show negative effects for NUTS3 to NUTS1, however with a higher uncertainty, leading to an absence of significance in the case of NUTS2. The magnitude of cumulative effects is similar to the GDP per capita regressions, which is due to the similar nature of GDP and total GVA. Again, the NUTS0 regressions do not show significant long-term effects of floods.

The regressions of GVA per capita growth for the sectors Agriculture, Manufacturing and Services have large confidence intervals and therefore do not indicate any significant long-term effects within this regression model specification. However, when excluding the most extreme GVA per capita growth rates from the regression, i.e. the observations associated with lower growth rates than the 1st or higher growth rates than the 99th percentile, the negative long-term effects become statistically significant for the sector Services at the levels NUTS3 to NUTS1 (see Annex Figure D.5).

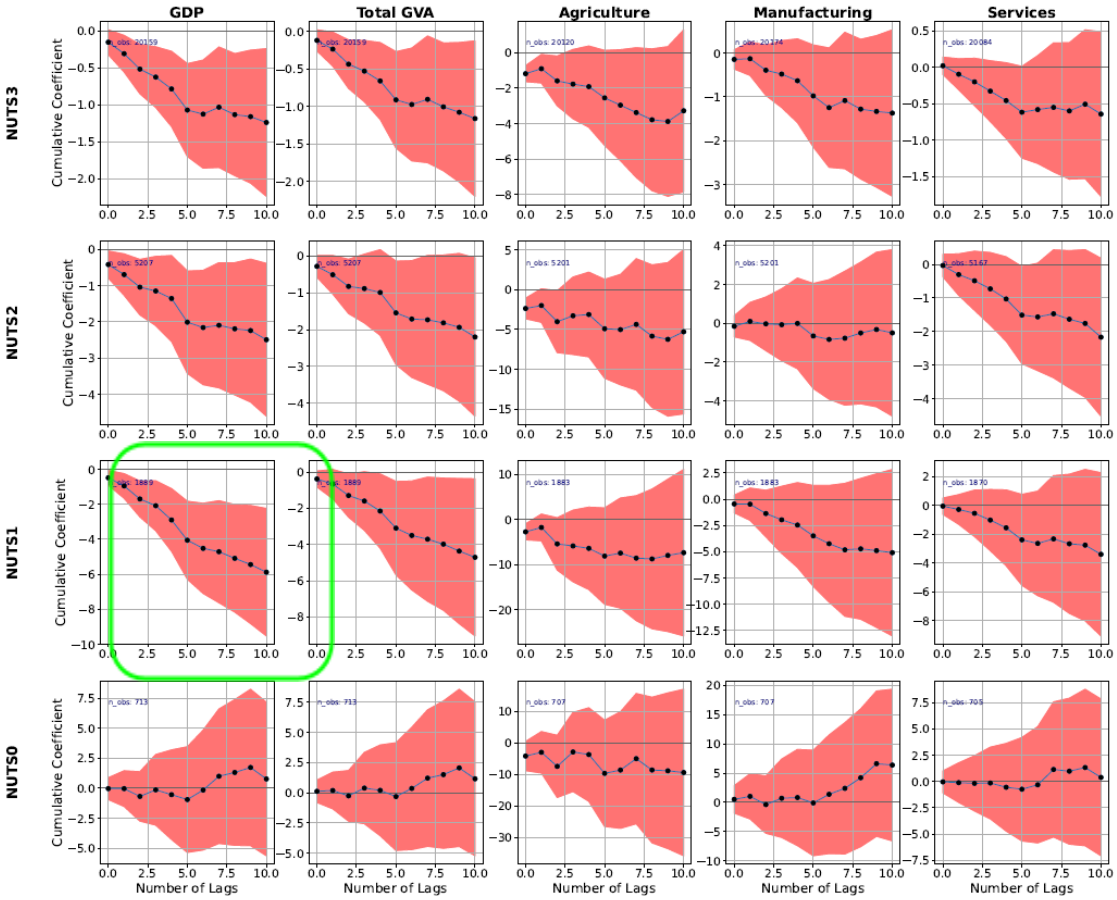

Figure 11. *Cumulative response of GDP, total GVA and sector GVA per capita growth to the population exposed to floods in terms of the cumulative coefficient for different NUTS levels. Shaded areas represent the confidence intervals at the 90% level, with clustered standard errors at the region-year level. The main model choice for the projections is the GDP per capita growth regression at NUTS1 level (green box).*

3.3.2 Projections

First, we assess the projected time series of GDP per capita, which are derived based on the SSP2 GDP and population projections from ISIMIP3b (www.data.isimip.org/). Since the integrated assessment models used to generate the GDP trajectories of the SSPs do not explicitly account for flood impacts, we assume that the SSP scenarios do not account for any flood damage. Therefore, we here follow Krichene et al. (2023) and first calculate the impacts of floods on the SSP growth trajectories in a stable, pre-industrial climate (pre-industrial control (PI)). This yields perturbed baseline trajectories. Growth reductions (or gains) under the different emission scenarios (RCP2.6, RCP7.0, and RCP8.5) are then measured relative to these perturbed baseline trajectories (**Figure 2**). The full picture of all NUTS1 regions' projected GDP per capita highlights the different magnitudes at which European regions are and will be affected by fluvial floods, even on a subnational scale. Some regions barely suffer from any fluvial flood perturbation of the GDP per

capita trajectory, no matter the emission scenario. Others, however, show large perturbations for all scenarios, indicating a generally strong exposure to fluvial floods.

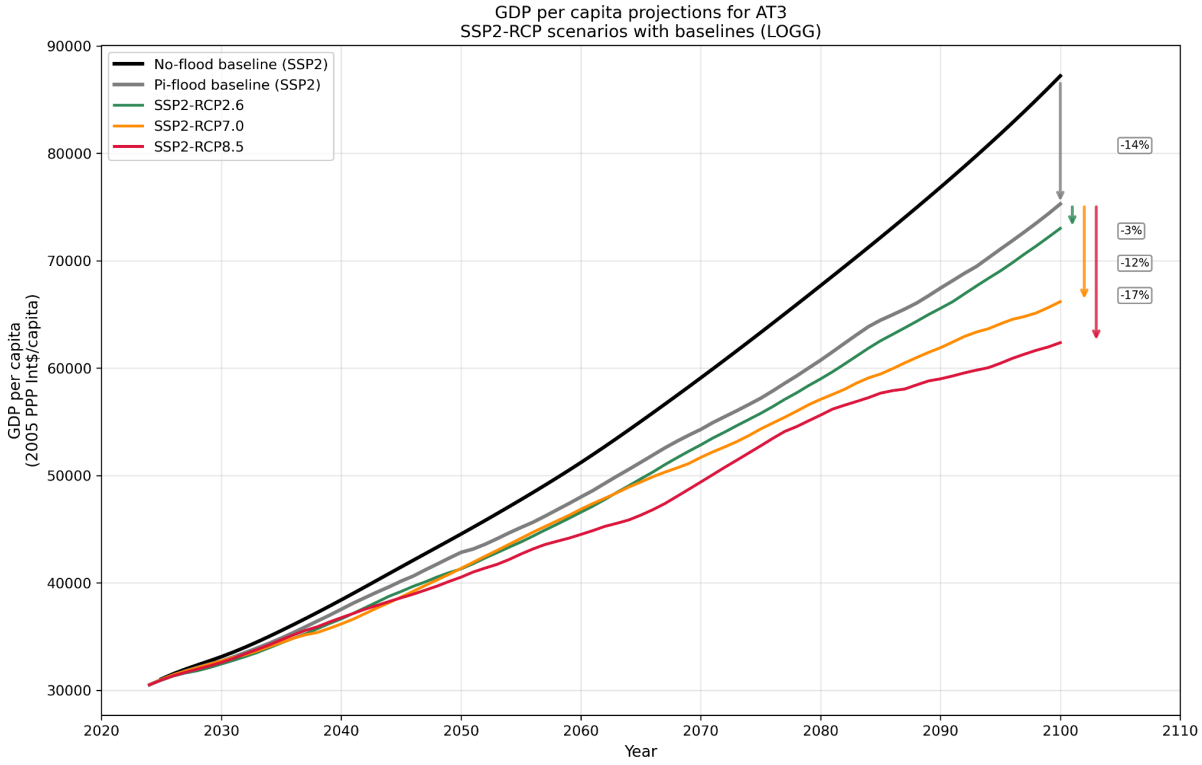

Figure 12. *Projected GDP per capita time series of example region AT3 (Western Austria) for SSP2 and RCP2.6 (green), 7.0 (yellow) and 8.5 (red), as well as two baselines. The no-flood baseline (black) does not include any perturbation of SSP2-GDP and -population projections, while the preindustrial-control baseline (grey) includes the fluvial flood-perturbation caused by preindustrial climate conditions. For perturbed GDP per capita trajectories, the multi-model ensemble mean (across five different GCM forcings) per year is plotted. For the sake of simplicity, the uncertainty range, defined as the min-max range of the multi-model ensemble (thus only present for perturbed trajectories), is not plotted here. It can be found in the overview of plots for all NUTS1 regions in Annex D Item D.1.*

The parameters for the calculation of the growth-adjusted discounted rate are taken from Ricke et al. (2018) (ρ = 2%, η = 1.5; results for other discounting choices can be found in the Annex D.2). Figure 13 shows the exemplary time series of the French NUTS1 region FRH (Britanny). Under the low-emissions scenario (SSP2-RCP2.6), DAD initially increases to approximately 0.5% of 2025 GDP per capita by 2060, followed by a decline to around 0.35% by 2100. In contrast, both higher emission scenarios (SSP2-RCP7.0 and SSP2-RCP8.5) show negative impacts in the short term, before steadily increasing to approximately 0.55% of 2025 GDP per capita by 2100. Notably, the uncertainty bands are fairly large, because we choose the min-max range across the different GCMs. (For the upcoming peer-reviewed publication of this work, several hydrological models will

be assessed, adding another uncertainty dimension). The uncertainty narrows considerably after 2060 across all scenarios.

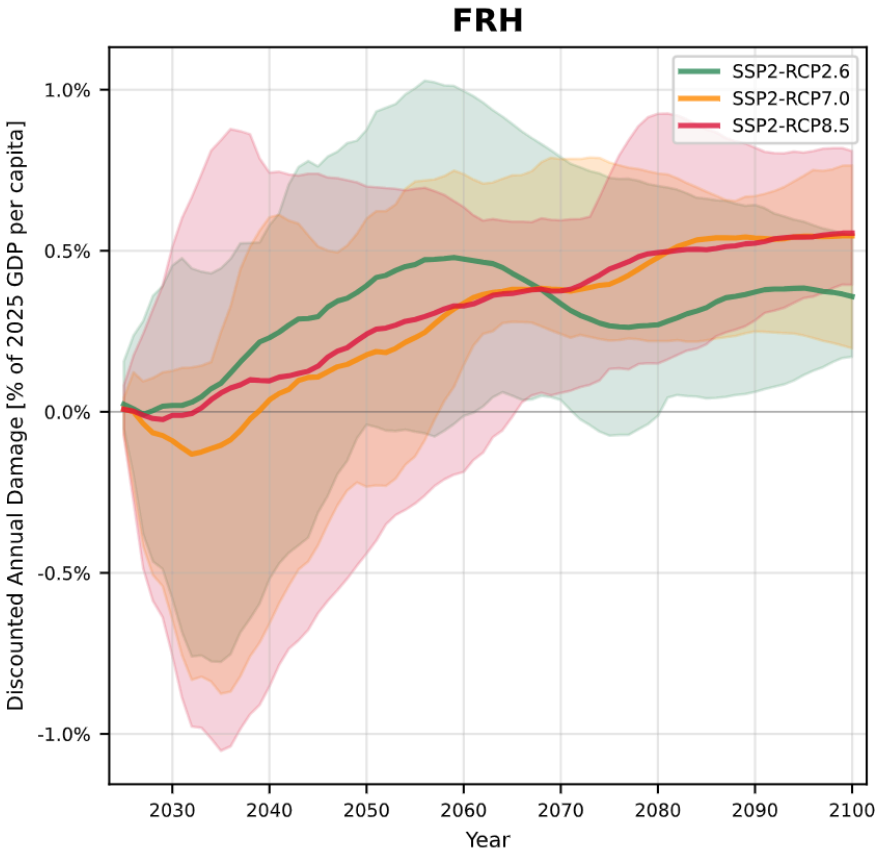

Figure 13. *Discounted Annual Damage per year (multi-model ensemble mean across 5 climate forcings) as % of 2025 GDP per capita of example region FRH (Britanny). Discounting to base year 2025 based on Ricke et al. (2018) parameters (ρ = 2%, η = 1.5). Uncertainty range defined as min-max range across ensemble. Plots for all regions and alternative discounting choices in Annex.*

The overview of DAD time series across all NUTS1 regions (Annex D.2) shows that higher DADs in the late 21st century, compared to the present day, can be observed for the majority of regions. This is in spite of the relatively conservative discounting assumptions, which downgrade future damages. For less conservative discounting assumptions, e.g. those of the Stern review (Stern, 2008; ρ = 0.1%, η = 1.01), DADs increase more strongly towards the end of the 21st century (see Annex D.2). For a majority of regions, towards the end of the 21st century the DADs are higher for RCP8.5 than for RCP 7.0 and RCP 2.6. However, this is not necessarily the case over the entire time period. For a lot of the regions, the DADs are even temporally negative, meaning that the GDP per capita of the RCP trajectory lays above the trajectory of the preindustrial-control baseline. Generally, the trajectories are rather unique for each NUTS1 region, and can even substantially

vary within the same country. This highlights the strong regional specificity of flood impacts due to the localized nature of flood hazards.

Next, we assess the average DAD per NUTS1 region over the projected time frame, visualized on a map in order to identify spatial patterns. We find strong subnational differences in DADs in all three RCP scenarios, once again indicating the necessity to assess flood impacts on a subnational level. For RCP2.6, we find substantial flood damages for parts of Europe, mostly ranging between 0.5% to 1.5% of 2025 GDP per capita (Figure 14). The hotspots for flood impacts are Central Europe and around the Alpine regions. This is likely caused by an increase of extreme precipitation events under global warming (Di Sante et al., 2021). Meanwhile, in the Southern Mediterranean projected flood impacts are decreasing, likely due to a decrease of precipitation (Di Sante et al., 2021). For North-Eastern Europe, our projections also show negative DADs, i.e., less flood impacts than in a preindustrial climate; this is likely caused by a reduction of snow accumulation during winter due to large increase of late winter temperatures (Di Sante et al., 2021).

For RCP7.0 (Figure 15), the Alpine hotspot for flood risk remains, except for Switzerland (CH0), which surprisingly exhibits negative DADs in this scenario. In addition, strong flood effects in Western Germany and the Benelux countries are no longer visible. The predictions of Di Sante et al. (2021) regarding a flood-risk decrease in North-Eastern Europe and in the Southern Mediterranean are however still apparent.

RCP8.5 then paints a clearer picture again, especially regarding the large Central European and Alpine flood hotspot. In addition, Northern France is predicted to be partially strongly affected by flood impacts under this scenario. Meanwhile, the Northern European flood risk decrease appears to be smaller compared to RCP2.6 and 7.0, while the Southern Mediterranean remains relatively unchanged.

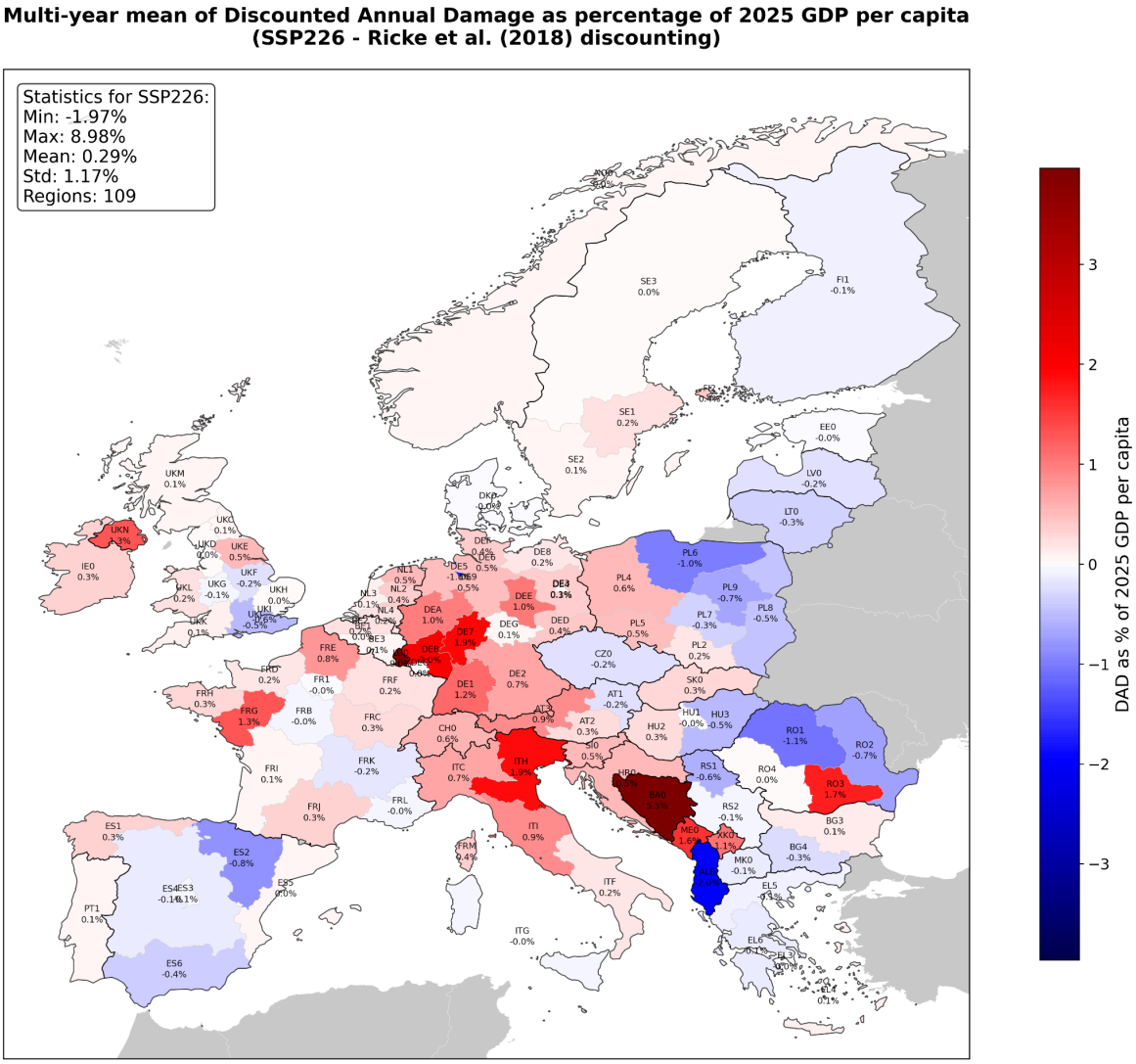

Figure 14. *Mean Discounted Annual Damage as a percentage of 2025 GDP per capita over the projected time span of 2025 – 2100 for SSP2-RCP2.6. Positive DAD values (red) represent (on average) climate change-induced economic damages, i.e. decreased GDP per capita levels compared to a preindustrial-control climate due to the long-term effects of fluvial floods. Negative DAD values (blue) represent (on average) climate change-induced economic benefits, i.e. increased GDP per capita levels compared to a preindustrial-control climate due to the lack of long-term effects of fluvial floods.*

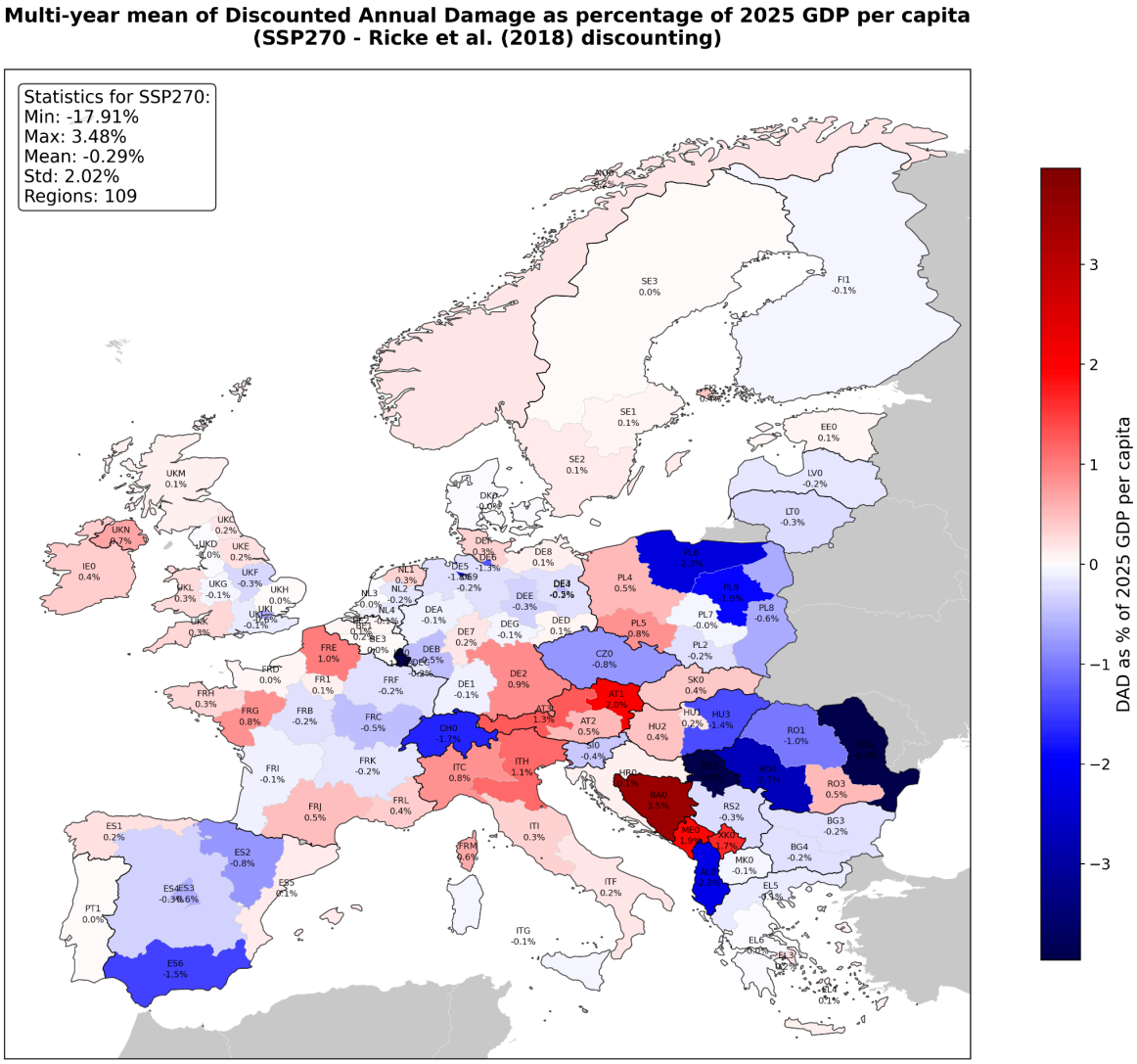

Figure 15. *Same as Figure 14 but for SSP2-RCP7.0.*

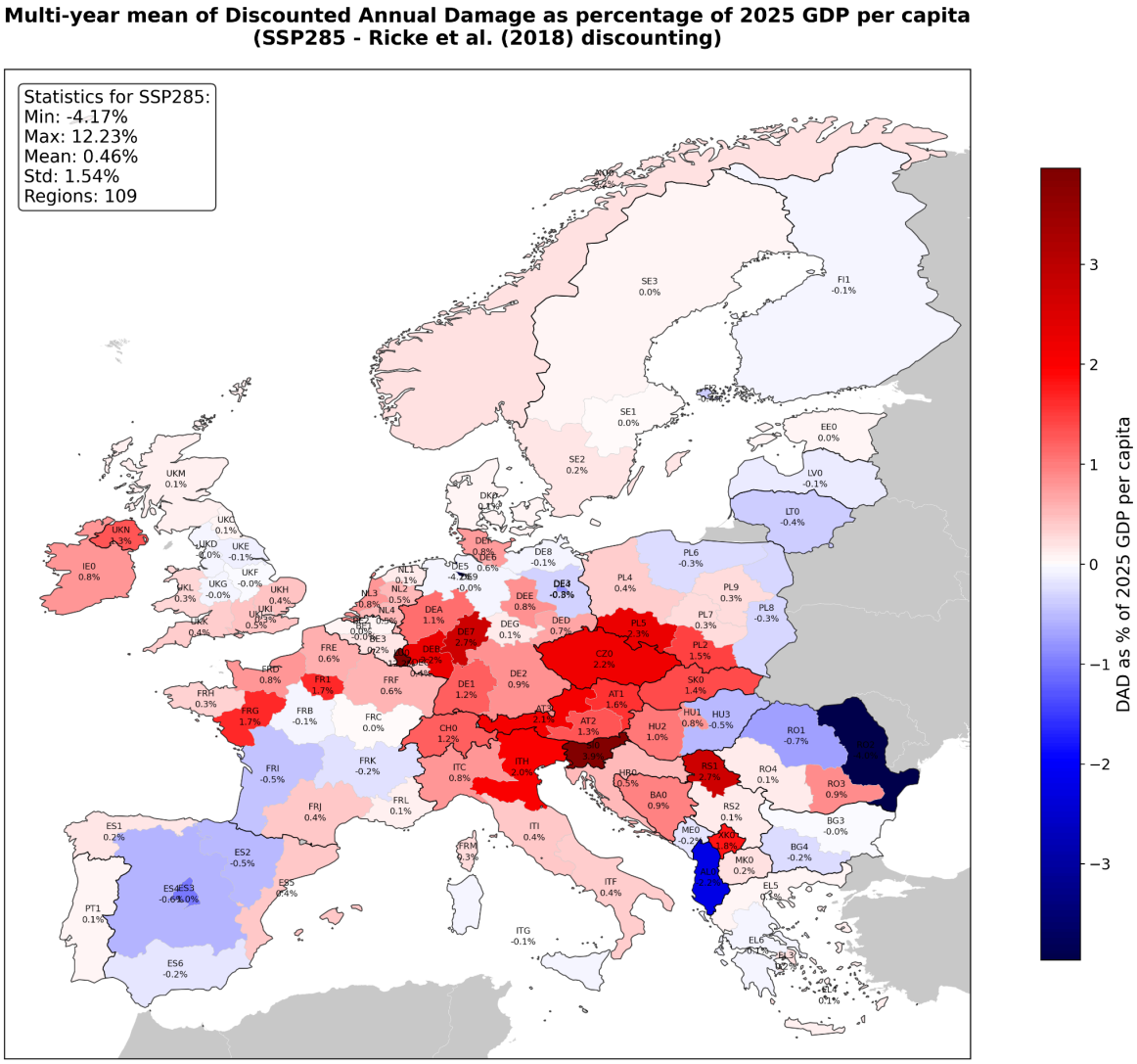

Figure 16. *Same as Figure 14 but for SSP2-RCP8.5.*

3.4 Conclusion/Key takeaways

We assess the economic damage caused by river floods in Europe on the sub-national level. Our findings underline the importance to account for the long-term impact of floods on economic growth. We find floods to reduce growth for at least one decade. Thus, the overall costs are much larger than the direct costs of these disasters.

Additionally, we measure flood impacts in terms of discounted annual damage for different emission pathways. We find that, on the regional level, these damages can be substantial and amount to the equivalent of 0.5% - 2% in yearly damages, expressed in terms of the 2025 regional economic output. As an example, for year four after the 2021 Ahrtal flood in Germany, cumulative

damages already amount to around 6 %[2] of the affected region's 2021 output (NUTS3-region DEB12, Landkreis Ahrweiler). Based on our findings, this damage may increase for another 6 years, or even longer, leading to significantly decreased economic output compared to a development GDP per capita trajectory not affected by the flood. This shows that floods have the potential to shape the development pathways of regions and countries, and stress the importance of climate change adaptation to increasing flood risks in 'hot-spot' regions.

Flood damages are highly heterogeneous across regions, and there are many regions suffering less damage than in a stable pre-industrial climate. Damage trends thereby follow observed changes in flood risk derived from observational river flood discharges (Blöschl et al. 2019), and projections of mean peak flows (Di Sante, Coppola, and Giorgi 2021). We find significant subnational differences in projected flood impacts for all three assessed emissions scenarios. This is highly significant, as to date, many flood impact assessments are conducted on a national level, hiding substantial regional differences in flood risks.

Our damage estimates are subject to substantial climate and hydrological model uncertainties. Further, the normative on how societies weigh future compared to present damage strongly impacts on damage estimates.

Our flood estimates provide climate econometrics (top-down) estimates of flood impacts. Within ACCREU, these estimates will be contrasted with damage assessments from computable general equilibrium (CGE) models (ICES-MH, ICES-REG, COIN-INT) and integrated assessment models (WITCH and MIMOSA), see Deliverables 4.1, 4.2 and 4.4. This comparison will provide a very concrete test case helping to close the current gap in understanding regarding the stark differences between top-down and bottom-up estimates of the economic impacts of climate change, which were also highlighted in Chapter 16 of the working group 2 contribution to IPCC's 6th Assessment Report (O'Neill et al. 2022).

[2] Estimated based on reported GDP per capita from ARDECO and an estimated counterfactual, no-flood trajectory, which follows the average GDP per capita growth of the years 2010 – 2019 (1.9 % p.a.).

4 Supply Chain Spillovers Intensify the Economic Impact of Local Climate Anomalies

4.1 Introduction

Recent studies demonstrate that macroeconomic performance deteriorates in response to climate anomalies (Akyapi et al. 2025, Callahan and Mankin 2023, Miller et al. 2021, Marbler 2022). However, existing research typically estimates climate-induced economic damage based solely on local weather variation, relying on the implicit assumption that the economic impacts of adverse weather conditions are confined to the affected region only. This assumption is increasingly problematic in an era of deep global economic integration, where disruptions in one region can rapidly propagate through global supply chains. Therefore, this subtask analyzes whether global supply chains amplify the macroeconomic damage of local climate shocks.

To address this question, this task constructs a novel dataset combining global multi-regional input-output (MRIO) tables with high-resolution meteorological data, enabling the identification of water availability shocks originating across the globe and their transmission via supply chains. Using this dataset, an econometric analysis is conducted to estimate the dynamic causal effect of water availability shocks on subnational gross value added (GVA) across 41 European countries, explicitly accounting for global supply chain spillover effects. The empirical analysis is grounded in a general equilibrium model of multi-regional production networks (Acemoglu et al. 2012, 2016), allowing for a structurally consistent assessment considering supply chain interlinkages.

This subtask advances the climate-economy literature in several ways. First, it provides novel empirical evidence that supply chain linkages significantly amplify the macroeconomic damage of local climate shocks. Second, it identifies the dynamic causal effects of water availability shocks on subnational GVA and explores the underlying channels through which they operate. Third, the analysis shows that regions in countries with inherently drier climates are disproportionately vulnerable, experiencing the largest damage when exposed to supply chain-transmitted water scarcity shocks. Finally, through a counterfactual analysis, this subtask quantifies the cumulative GVA losses across Europe attributable to water scarcity shocks between 2000 and 2019, accounting for global supply chain spillover effects.

4.2 Methods

4.2.1 Data

The empirical analysis is built upon three core datasets: (1) subnational gross value added (GVA) at the NUTS-3 level across Europe, (2) global multi-regional input-output (MRIO) tables capturing global supply chain linkages, and (3) gridded meteorological data on water availability anomalies.

Subnational gross value added (GVA). Annual subnational GVA (in constant euros), gross fixed capital formation (in constant euros), and employment data at the level of NUTS-3 level in Europe are sourced from the Annual Regional Database of the European Commission's Directorate General for Regional and Urban Policy (ARDECO). Data flagged as interpolated or estimated in

ARDECO are omitted. For Belarus, Bosnia and Herzegovina, Georgia, Moldavia, and Ukraine, i.e., countries not covered by ARDECO, subnational GVA data are obtained from national statistical agencies. To ensure consistency, this subnational information is used to disaggregate national-level data from Eurostat and the World Bank, using a methodology analogous to that employed in ARDECO. The final subnational economic dataset spans 1,548 subnational regions across 41 European countries (see Appendix E.1), providing granular spatial coverage essential for capturing local economic responses to climate shocks.

Multi-regional input-output data. This subtask uses the EORA26 MRIO database (Lenzen et al. 2012, 2013), which provides annual, bilateral input-output tables for 26 sectors across 188 countries and the rest of the world, including detailed transactions and final demand matrices. To trace the propagation of water availability shocks through global supply chains, direct and indirect country-by-country interlinkages are derived by performing the following steps: First, as water availability shocks cannot be disaggregated by sector, the sectoral information in the transactions and the final demand matrices are aggregated to an aggregate sector by country. Second, the total output per country is derived from these transactions and the final demand matrices. Third, the technical coefficient matrix is computed by dividing each country's input use by its total output. Finally, the Leontief inverse of this matrix is calculated, which quantifies the total direct and indirect input requirements across the global production network. The elements of the Leontief inverse matrix (Appendix E.2) enable the identification of how shock in one country propagates through the global supply chain.

Climate data. Monthly gridded meteorological data on precipitation and potential evapotranspiration are drawn from the Multi-Source Weighted-Ensemble Precipitation (MSWEP) and ERA5-Land reanalysis datasets (Beck et al. 2019; Muñoz-Sabater et al. 2021; Singer et al. 2021), with at a spatial resolution of 0.1° x 0.1° (approximately 10 km x 10 km) over the period 1981-2019.

The climatic water balance, a proxy for water availability (see, e.g., Konapala et al. 2020; Oki and Kanae 2006; Vicente-Serrano et al. 2010, 2015), is calculated as the difference between precipitation and potential evapotranspiration. Since this metric integrates both water supply (precipitation) and demand (evaporation and transpiration), it captures the joint effects of precipitation and temperature on hydrological conditions (Konapala et al. 2020; Vicente-Serrano et al. 2010), going beyond simple rainfall-based measures of water availability (Marbler, 2024). For instance, elevated temperatures can exacerbate droughts by increasing evaporation and plant transpiration (Allen et al. 2006; Konapala et al. 2020; Vicente-Serrano et al. 2015). Since the climatic water balance is derived from meteorological conditions exclusively, it is independent of socio-economic activity, allowing the identification of plausible causal effects in the econometric analysis (Carleton and Hsiang 2016; Dell et al. 2014; Hsiang 2016; Kolstad and Moore 2020).

Annual water availability shocks at the grid cell-level are defined as standardized anomalies relative to the 1991-2020 climatological mean. These location-specific anomalies represent deviations from long-term local climate conditions expressed in standard deviations, enabling cross-time and cross-location comparability across the globe. Negative values indicate water

scarcity (below average water availability), while positive values indicate water surplus (above-average availability).

To account for non-linear impacts of extreme hydrological conditions, where the effect of droughts may differ from that of wet anomalies, a piecewise linear transformation is applied at the grid cell-level (Hsiang, 2016). This transformation allows for distinct linear responses to shocks exceeding -0.5 standard deviations for water scarcity and +0.5 standard deviations for water surplus. The resulting grid-cell level annual shocks (Appendix E.3A) are then spatially aggregated to the national level using area-weighted averages (Appendix E.3B), matching the spatial resolution of the MRIO tables.

4.2.2 Econometric Implementation

To estimate the dynamic causal effects of supply chain-transmitted water availability shocks on regional GVA, local projections (LP) (Jordà 2005), a widely adopted method in empirical macroeconomics for identifying impulse response function (see, e.g., (e.g., Akyapi et al. 2025; Baron et al. 2021; Bilal and Känzig 2024), are employed. The LP approach allows for a flexible modeling of dynamic responses (Jordà and Taylor 2025). The key identification strategy is based on the following regression specification:

$$\Delta_h Y_{i,\,t+h} = \beta_1^h \Delta W_{c,t}^{-SC} + \beta_2^h \Delta W_{c,t}^{+SC} + \sum_{l=1}^{L} [\gamma_{1,l}^h \Delta W_{c,t-l}^{-SC} + \gamma_{2,l}^h \Delta W_{c,t-l}^{+SC} + \delta_l^h \Delta ln\, y_{i,t-l}] + \alpha_i^h + \phi_t^h + \epsilon_{i,c,t}^h;\ h = 0,\ldots, H,$$

where $\Delta_h Y_{i,\,t+h} = ln\, Y_{i,t+h} - ln\, Y_{i,t-1}$ denotes the change in the natural logarithm of subnational GVA (NUTS-3 level) in region *i* from year *t-1* to *t+h*. $W_{c,t}^{-SC}$ and $W_{c,t}^{+SC}$ represent supply chain-adjusted water availability shocks across countries, *c*, and time, *t*. $\Delta ln\, y_{i,t-l}$ denotes lagged growth rates of subnational GVA, where L denotes the number of lags (i.e, two in the baseline specification). ϕ_t is a full set of year fixed effects to flexibly control for global shocks and trends (e.g., pandemics, technological innovations, El Niño–Southern Oscillation events, and macroeconomic cycles), α_i are NUTS-3 fixed effects, which in the first-differenced setting correspond to region-specific time trends and help to rule out spurious correlations driven by common unobserved trends in GVA and water availability.

These supply chain-transmitted shocks $W_{c,t}^{-SC}$ and $W_{c,t}^{+SC}$ are constructed as weighted averages of globally occurring water availability shocks (Appendix E.3.C), where weights reflect the strength of bilateral direct and indirect supply chain linkages between countries (Appendix E.2). These weights are equivalent to the foreign production exposure (FPEM) metric, a recently developed input-output measure that quantifies the global supply chain reliance of a sector (Baldwin and Freeman 2022; Baldwin et al. 2023). Here, it measures the global supply chain reliance of

countries. This allows to take global supply chain spillover effects into account, capturing how a shock in one country can affect GVA in distant regions via production interlinkages.

The identifying variation arises from plausibly exogenous country-level, year-to-year fluctuations in supply-chain adjusted water availability shocks, which are independent of regional economic conditions (Hsiang, 2016). The estimated coefficients β_1^h and β_2^hrepresent the predicted change in GVA per standard deviation of a supply chain transmitted shocks, relative to a counterfactual scenario in which no such shock occurs.

As a benchmark, an alternative specification that omits supply chain spillovers is estimated. In this model, global supply chain-adjusted shocks, $W_{c,t}^{-SC}$ and $W_{c,t}^{+SC}$, are replaced with local, NUTS-3-level water availability shocks ($W_{i,t}^{-}$ and $W_{i,t}^{+}$), reflecting only direct, within region exposure. The hypothesis is that the estimated economic impacts will be systematically smaller in this local-only specification, highlighting the role of global supply chains in amplifying the macroeconomic damage of climate anomalies.

Accounting for adaptation. To assess heterogeneity in the sensitivity to water availability shocks, the econometric model is extended to allow the response of GVA to vary with long-term climate conditions and income levels, following the state-of-the-art approach in climate econometrics (Carleton et al., 2022; Rode et al. 2021). Since the long-term climate and income implicitly map out adaptive responses (Carleton et al., 2022), supply chain-adjusted averages of the two key contextual variables are introduced. Long-term water availability is computed as the 1991-2019 mean annual climatic water balance for each country, then aggregated across global supply chains using the FPEM weights to reflect a country's effective long-term water availability along its supply chain network. In the same manner, per capita income is measured as the 2000-2019 mean national GDP per capita in constant 2021 PPP US$, obtained from the World Bank's World Development Indicators, and then aggregated across supply chains.

These composite measures capture the effective climate and income environment faced by a country along its production network. This acknowledges that a drier country may source inputs from a wetter country, thereby increasing its effective water availability. In the same manner, since a higher-income country may have greater adaptive capacity, a lower-income country which sources from a higher-income country may increase its effective adaptive capacity.

The extended econometric specification is:

$$\begin{aligned}\Delta_h Y_{i,\,t+h} = {} & \beta_1^h \Delta W_{c,t}^{-SC} + \beta_2^h \Delta W_{c,t}^{+SC} + \sum_{l=1}^{L} [\gamma_{1,l}^h \Delta W_{c,t-l}^{-SC} + \gamma_{2,l}^h \Delta W_{c,t-l}^{+SC} + \delta_{1,l}^h \Delta ln\, y_{i,t-l}] \\ & + \beta_3^h \Delta W_{c,t}^{-SC} \times D_c^{SC} + \beta_4^h \Delta W_{c,t}^{+SC} \times D_c^{SC} + \sum_{l=1}^{L} [\gamma_{2,l}^h \Delta W_{c,t-l}^{-SC} + \gamma_{3,l}^h \Delta W_{c,t-l}^{+SC} + \delta_{2,l}^h \Delta ln\, y_{i,t-l}] \times D_c^{SC} \\ & + \alpha_i^h + \phi_t^h + \epsilon_{i,c,t}^h;\ h = 0,\ldots, H,\end{aligned}$$

where D_c is either the supply chain-weighted average water availability or per capita income in country c. Interaction terms allow the impact of water availability shocks to vary conditional on effective long-term climates and incomes.

Estimating historical damages. The coefficient estimates, β^h, from the local projections represent the total change in GVA over *h* years. Year-by-year incremental effects are computed as follows:

$$\Delta\beta^h = \beta^0 \; if \; h = 0 \; \wedge \; \Delta\beta^h = \beta^h - \beta^{h-1} \; if \; 1 \leq h \leq H.$$

These $\Delta\beta^h$ values reflect the impact of a year t shock on the change in GVA from year $(t + h - 1)$ to year $(t + h)$. Using these incremental log-point effects, a no-shock counterfactual series is built for each region. Starting from the observed initial baseline value, $ln\, GVA_{i,t_0}^{noShock} = ln\, GVA_{i,t_0}^{observed}$, the no-shock counterfactual series, for example for water scarcity, is recursively computed as follows:

$$ln\, GVA_{i,t}^{noShock} = ln\, GVA_{i,t-1}^{noShock} + [ln\, GVA_{i,t}^{obs.} - ln\, GVA_{i,t-1}^{obs.}] - \sum_{h=0}^{H} [\Delta\beta_1^h W_{c,t-h}^{-SC} + \Delta\beta_1^h W_{c,t-h}^{-SC} \times D_c],$$

where for each subsequent year after t_0, i.e., $t_0 + 1, \ldots, T$, the sum of all incremental shock effects is subtracted from the observed log growth. This removes the estimated log-point contribution of water scarcity shocks at each horizon from the observed log growth, $ln\, GVA_{i,t}^{obs.} - ln\, GVA_{i,t-1}^{obs.}$.

Exponentiating the counterfactual log-GVA series, $ln\, GVA_{i,t}^{noShock}$, yields the level of GVA in region i that would have prevailed in the absence of water scarcity shocks. The GVA loss in region i and year t that is attributable to water scarcity shocks is the difference between the actual and the counterfactual levels in each region–year: $Loss_{i,t} = ln\, GVA_{i,t}^{observed} - ln\, GVA_{i,t}^{noShock}$. Aggregating losses across regions and over time yields the total cumulative economic damage, in terms of GVA, attributable to water scarcity shocks from 2000 to 2019. The results section reports both annual and cumulative losses to illustrate the evolution of climate-induced economic impact over time.

4.3 Results & Discussion

This section begins by focusing first on the contemporaneous results from estimating the model outlined in the Methods section where water availability shocks are modelled with a piecewise linear function in water availability anomalies. Figure 17 reports the results for the contemporaneous effects, depicting the dose response functions of subnational GVA to supply chain-adjusted (Figure 17a) and local (Figure 17b) water availability shocks. In these figures, a year with standardized anomalies in water availability between -0.5 and 0.5 standard deviations serves as the reference depicting normal climate conditions. Each point along the dose response functions

shows the impact of a year characterized by the corresponding water availability anomaly measured in standard deviations, relative to a year with normal conditions. The histograms at the bottom of the figures depict the distribution of annual water availability anomalies across the sample.

Figure 17a reveals that both water scarcity (i.e., drier-than-usual) and water surplus (i.e., wetter-than-usual) shocks transmitted through global supply chains exert a negative effect on subnational GVA. However, while water scarcity shocks cause statistically significant and economically meaningful negative effects on value added, the effects of water surplus shocks are not statistically significant at conventional levels. A one-standard-deviation supply chain-transmitted water scarcity shock (i.e., $W^{-SC} = 0.5$) is associated with a 0.42% decline in subnational GVA in the year of occurrence ($p < 0.01$). Figure 17b presents the corresponding dose response function from the benchmark model that excludes supply chain spillover effects and accounts solely for local water availability shocks. Although the qualitative pattern of declining GVA under water availability shocks is preserved, the magnitude of the estimated effects are markedly smaller: a one-standard-deviation local water scarcity shock ($W^{-} = 0.5$) reduces GVA by only 0.17%. This represents less than half the impact observed when supply chain spillovers are accounted for, suggesting that conventional local-only estimates substantially understate the economic impact of climate shocks.

The divergence between the estimated effects implies a sizable network multiplier effect, defined as the ratio of the total effect (recovered by the supply chain model) to the direct effect (recovered by the local model). Since the local model captures approximately the direct impact of a shock, while the supply chain model derives the total effect, including spillovers, the network multiplier can be obtained by taking the ratio of the coefficients from the two models. This yields an estimated multiplier of 2.4, indicating that supply chain spillovers more than double the direct economic impact of water scarcity shocks. This shows that global supply chains play a critical role in propagating climate shocks.

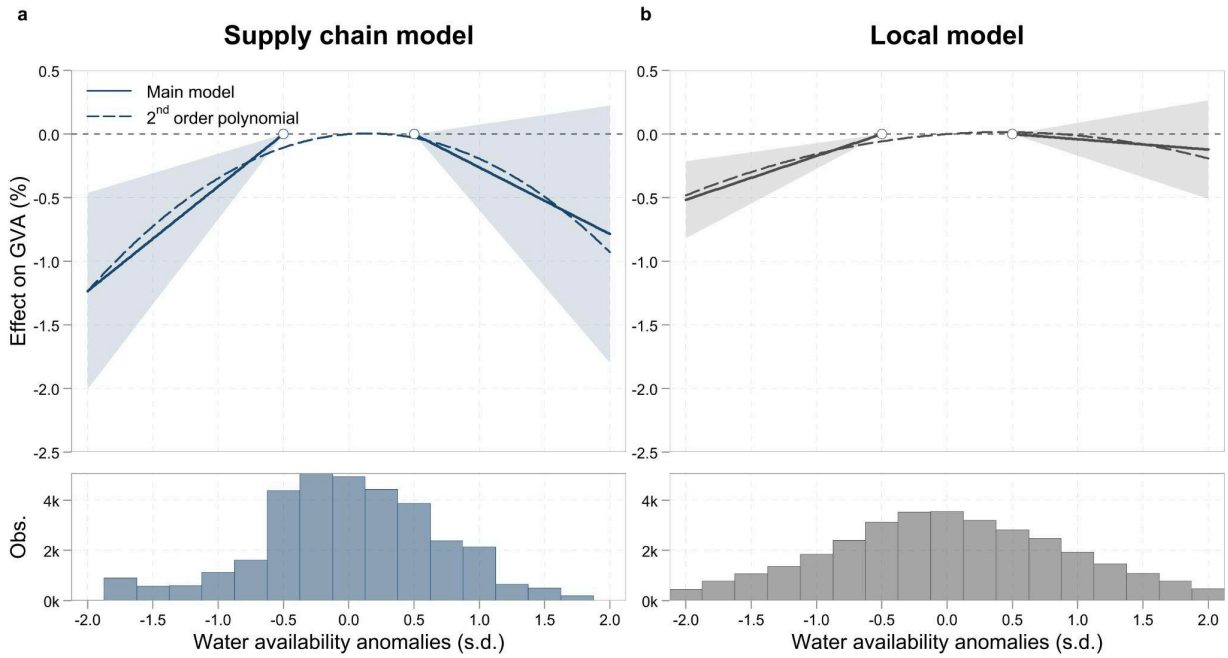

Figure 17. *The gross value added-water availability response functions. The figure plots the response of real gross value added to anomalies in water availability accounting for supply chain spillovers* ***(a)*** *and accounting for local anomalies only* ***(b)****. The x-axis depicts, from left to right, water availability anomalies ranging from extreme water scarcity shocks, i.e., −2 standard deviations, to extreme water surplus shocks, i.e., +2 standard deviations. The regression estimates are from piecewise linear functions (solid lines) and second-order polynomial functions (dashed lines). The 95% confidence bands are shown based on standard errors clustered at the country level.*

Robustness. The findings are robust to alternative model specifications. First, to test robustness against alternative functional form specifications, the piecewise linear functional form is replaced by a second-order polynomial specification. As shown in Figure 17, the response functions derived from the polynomial specification (dashed lines) closely align with those derived from the baseline piecewise linear specification in both shape and magnitude. The response of subnational GVA to water availability shocks follows an inverted U-shape: starting from extreme water scarcity, subnational value added increases with water availability up to a water surplus shock of approximately 0.5 standard deviations, beyond which further wetting leads to a decline in value added. This suggests that excessive water availability, potentially due to flooding, can also impair economic performance, in line with the findings of Chapter 3.

Second, a series of robustness tests are conducted using alternative econometric specifications (Table 14).

Table 14. *Robustness to alternative specifications.*

	Main	1 Lag	3 Lags	No trends	Country trends	Quadratic trends
Supply chain model						
$\Delta\bar{W}^{SC}$	-0.0082***	-0.0071***	-0.0095***	-0.0074**	-0.0082***	-0.0095***
	(0.0025)	(0.0022)	(0.0032)	(0.0032)	(0.0026)	(0.0031)
$\Delta\dot{W}^{SC}$	-0.0052	-0.0018	-0.0081*	-0.0048	-0.0054	-0.0048
	(0.0033)	(0.0028)	(0.0044)	(0.0035)	(0.0034)	(0.0036)
Local model						
$\Delta\bar{W}$	-0.0034***	-0.0029***	-0.0034***	-0.0032**	-0.0034***	-0.0040***
	(0.0010)	(0.0010)	(0.0012)	(0.0013)	(0.0010)	(0.0012)
$\Delta\dot{W}$	-0.0008	-1.7×10^{-5}	-0.0010	-0.0006	-0.0008	-0.0006
	(0.0013)	(0.0012)	(0.0014)	(0.0013)	(0.0013)	(0.0013)
Region FE	Yes	Yes	Yes	No	No	Yes
Country FE	No	No	No	No	Yes	No
Year FE	Yes	Yes	Yes	Yes	Yes	Yes
Region trend	No	No	No	No	No	Yes
# of lags	2	1	3	2	2	2
# of regions	1,548	1,548	1,548	1,548	1,548	1,548
# of countries	41	41	41	41	41	41
# of years (.max)	36	37	35	36	36	36
Observations	33,370	34,918	31,822	33,370	33,370	33,370

Standard errors clustered at the country level in parentheses.
*Signif. Codes: ***: 0.01, **: 0.05, *: 0.1.*

These include variations in the number of lags (one, two, or three) for both the dependent variable and the shock regressors. The results remain qualitatively and quantitatively unchanged across all specifications (columns 1-3). Furthermore, omitting NUTS-3-specific time trends (column 4), replacing NUTS-3 by country-specific time trends (column 5), or introducing NUTS-3-specific quadratic time trends (column 6) does not alter the estimated impact of water availability shocks. This consistency across alternative functional forms and controls underscores the robustness of the findings.

Notably, the negative effect of water surplus shocks remains statistically insignificant across all specifications. The explanation for this null result may be that the annual water availability measure applied captures slow-onset drought exposure better than sudden-onset flooding conditions (Marbler, 2024). Since heavy rainfall events usually occur during single days or even within hours of a single day, the annual accumulation of water availability may hide these extremes. For this reason, the remainder of this task focuses the analysis on water scarcity shocks. However, in all specifications, water surplus shocks are retained as control variables to avoid omitted variable bias and to ensure accurate estimation of the water scarcity effects.

4.3.1 Long-term Effects

Figure 18 reports the dynamic causal effects of water availability shocks on subnational GVA added, where the dynamic effect over time is derived from local projections over a six-year horizon. The figures reveal the response of GVA to a one-standard-deviation supply chain-adjusted (Figure 18a) and a local (Figure 18c) water scarcity shock up to five years after the shock. Each point along the impulse response functions reveals the cumulative effect at a specific year after the shock occurred. Additionally, for a scenario where a region is shocked three times within a ten-year period, the corresponding GVA trajectories after each shock and for a no-shock counterfactual are illustrated (Figures 18 b,d).

Figure 18a presents the dynamic response of real gross value added to a one-standard-deviation supply chain-transmitted water scarcity shock ($W^{-SC} = 0.5$) over a 6-year horizon. The impulse response function reveals a significant and persistent economic drag: GVA declines in the year of the shock and remains below its no-shock trajectory for several years. The cumulative negative effect peaks approximately three years after the shock, with value added approximately 1.4% lower than it would have been in the absence of the shock. This corresponds to a threefold amplification of the contemporaneous effect. After this peak, the effect attenuates, stabilizing at a persistent 1% reduction in GVA by years four and five.

This prolonged response highlights the lasting macroeconomic damage of supply chain-transmitted water scarcity shocks. Relative to the no-shock trajectory, regions experience persistent gross value added losses that last for multiple years (Figure 18b). Although the losses of a single shock are not permanently accumulating, the persistence of the negative effect creates a gap between the actual and the counterfactual GVA trajectories. Hence, under repeated exposure to such shocks the growing cumulative damage generates substantial long-term losses.

Figure 18b illustrates this accumulation of losses in a scenario where a region experiences three one-standard-deviation water scarcity shocks over a ten-year period (at t = 0, 4, and 8). Compared to a baseline no-shock growth path of 3% per year, the three shocks cause a 2.8% decline in the region's GVA by year ten. Crucially, the actual economic damage over the ten-year period is larger.

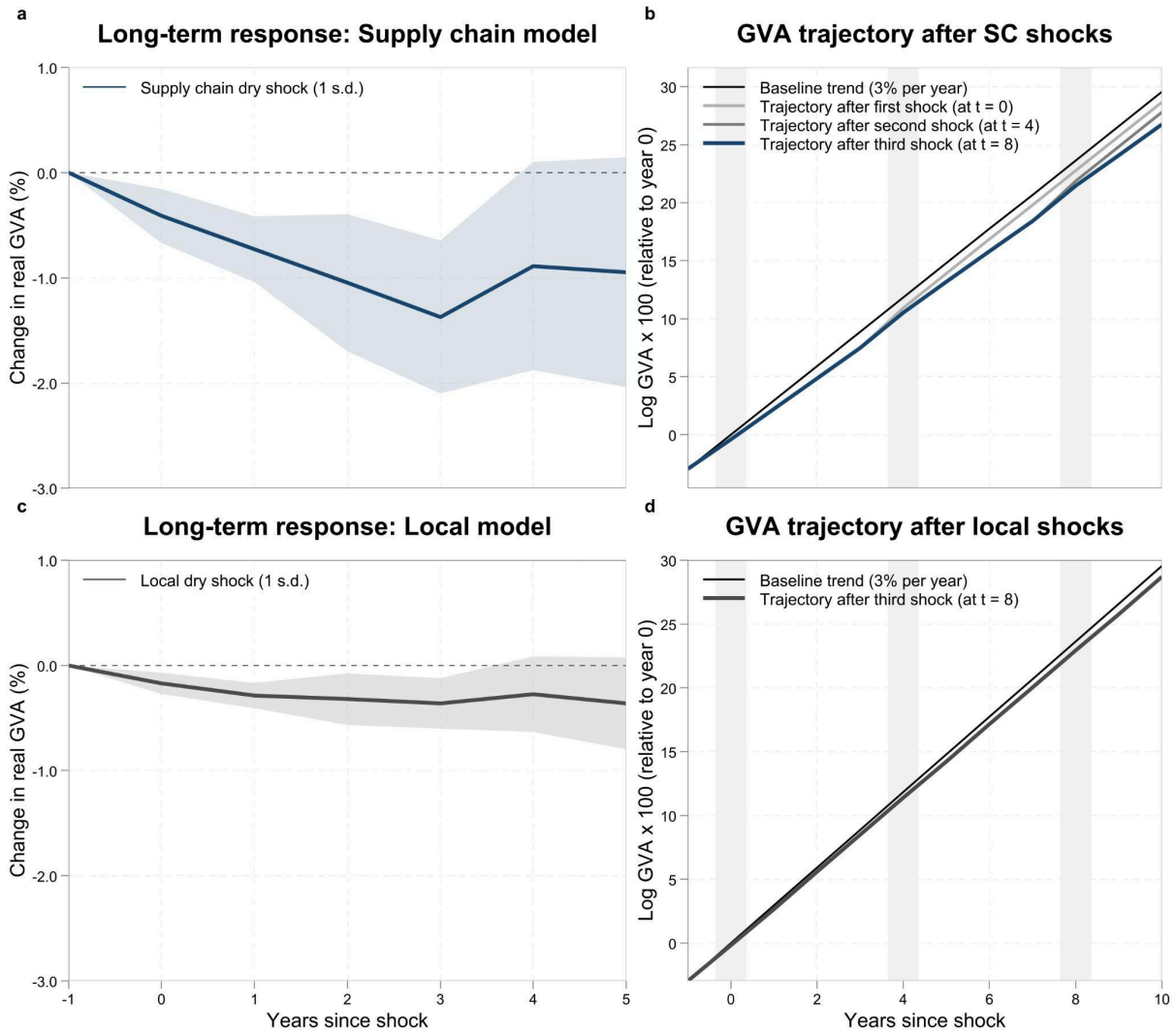

Figure 18. Impulse responses and GVA trajectories. a, c. *The panels plot the impulse responses derived from local projections, showing cumulative effects up to five years after the exposure to a one standard deviation supply chain-transmitted* ***(a)*** *and a purely local* ***(c)*** *water scarcity shock in year 0. The 95% confidence bands shown are based on standard errors clustered at the level of countries.* ***b.*** *The panel compares a baseline trajectory of gross value added which grows by a constant 3% per year (thin black line) to the alternative trajectories after the exposure to one (light gray line), two (dark gray line), and three (thick blue line) water scarcity shocks that are transmitted via global supply-chains.* ***d.*** *The panel compares a baseline trajectory of gross value added which grows by a constant 3% per year (thin black line) to the alternative trajectories after the exposure to three water scarcity shocks that are purely local (thick gray line).*

The total GVA losses are the cumulative annual deviations from the counterfactual no-shock trajectory, highlighting the compounding risk of repeated climate shocks. In Figure 18b, this corresponds to the area between the curves of the observed (thick blue line) and the counterfactual GVA trajectories (thin black line).

In contrast, when supply chain spillover effects are excluded (Figure 18c), the estimated effects are substantially weaker. A local one-standard-deviation water scarcity shock (i.e., $W^{-SC} = 0.5$) induces a peak loss in GVA of only 0.36% after three years. This is almost less than a quarter of the effect observed when supply chain spillovers are taken into account. In the three one-standard-deviation shocks scenario over a ten-year period (Figure 18d), the local model suggests a GVA reduction of just 0.9% by year ten and substantially lower cumulative impacts than the supply chain model.

Overall, these findings demonstrate that supply chain spillover effects amplify both the contemporaneous and the long-term impact of water scarcity on subnational GVA. Ignoring supply chain spillovers leads to a systematic underestimation of the total long-term losses, particularly when losses accumulate over time due to repeated exposure to these shocks.

Robustness. To assess the robustness of the identified impulse responses, a jackknife analysis is conducted, sequentially omitting one country at a time and re-estimating the model. The resulting impulse responses remain stable across all iterations (Figure 19a and 19c), demonstrating that no single country drives the results. This suggests that the results are not sensitive to outliers or idiosyncratic country-specific dynamics.

Given the panel structure with relatively short time dimension compared to the number of regions, an additional robustness test is conducted to test for Nickel bias, which arises when regressors are only weakly exogenous in short panels (Chudik et al. 2018). Applying the half-panel jackknife fixed effects estimator proposed by Chudik et al. (2018) shows that estimated impulse responses are nearly identical to those derived from the main specification (Figure 19b and 19d). This confirms that the results are not distorted by Nickel bias and supports the validity of the identifying assumption: the year-to-year variation in water availability shocks is plausibly exogenous.

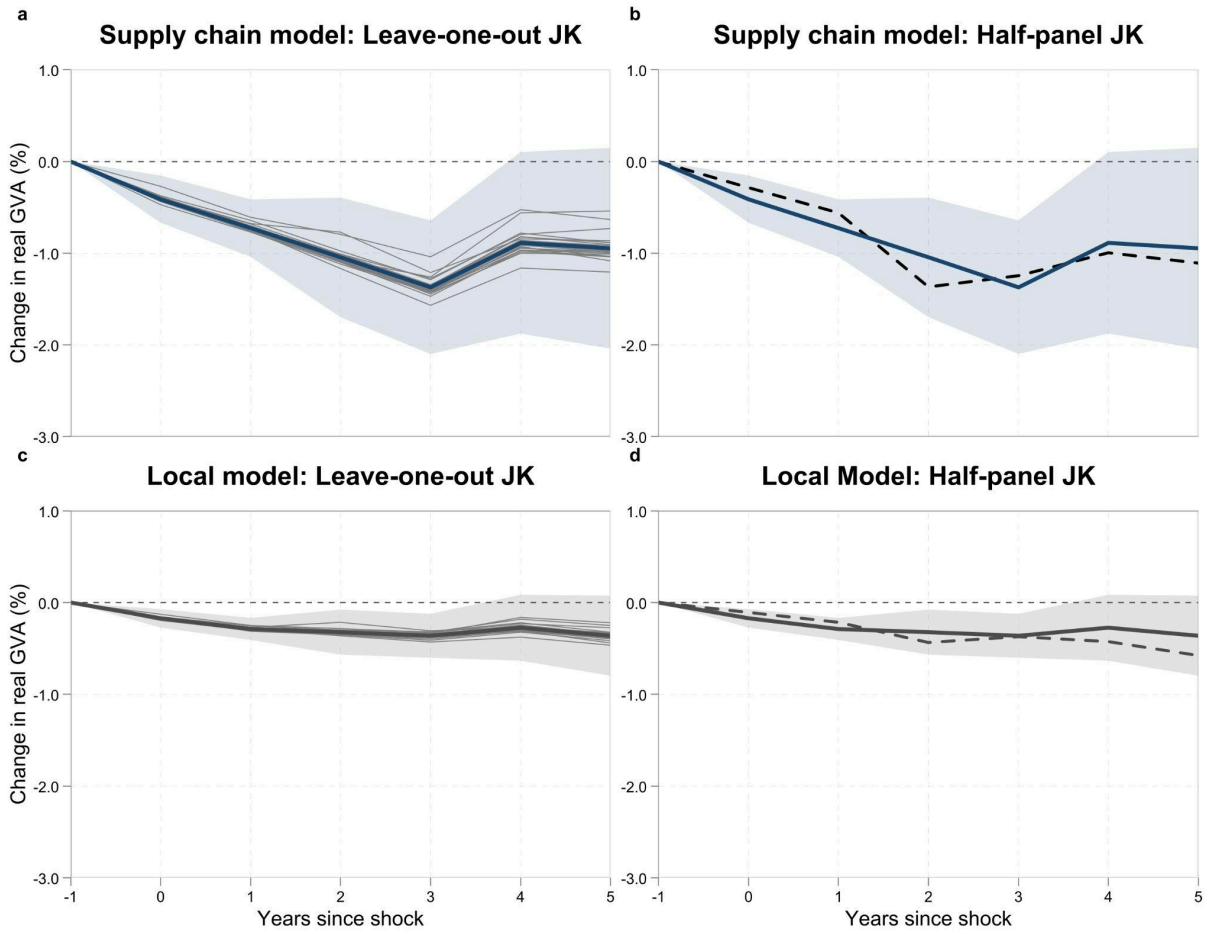

Figure 19. Robustness of impulse responses of GVA to water scarcity. *The panels plot the impulse responses derived from local projections, showing cumulative effects up to five years after the exposure to a one standard deviation supply chain-transmitted* ***(a, b)*** *and a purely local* ***(c, d)*** *water scarcity shock in year 0. Confidence bands shown are based on standard errors clustered at the level of countries.* ***a, c.*** *The panel compares the impulse-response function derived from the baseline model (thick line) to those derived from a jackknife exercise, censoring one country at a time (thin lines).* ***b, d.*** *The panel compares the impulse-response function derived from the baseline model (solid line) to the one derived from the half-panel jackknife fixed effects estimator (dashed line).*

4.3.2 Channels of Impact and Accounting for Adaptation

Having established the significant and persistent macroeconomic effects of supply chain-transmitted water scarcity shocks, this section first explores the channels through which these shocks operate and then accounts for potential adaptation in terms of heterogeneous sensitivities to these shocks.

Channels. To identify potential channels of impact, the dynamic response of key economic indicators is analyzed: employment, labor productivity, and investment (Figures 20 a-c). The analysis shows that the decline in GVA following a one-standard-deviation water scarcity shock is accompanied by declines in employment, labor productivity, and investment levels. Compared to the effects on GVA, employment shows a more moderate decline, peaking at 0.8% lower employment four years after the shock (Figure 20a). Similarly, the negative effects on labor productivity peak at minus 0.7% three years later and recover thereafter (Figure 20b). Investment, however, shows the most pronounced and lasting decline: the negative effects are accumulating over the entire 6-year horizon, leading to a 4% reduction in capital formation five years after the shock (Figure 20c). This sustained drop in capital formation indicates that firms delay or scale back investment decisions in response to supply chain-transmitted water scarcity shocks. This could reflect the associated uncertainty in times of shocks or, for example, reduced cashflow due to constrained access to more expensive intermediate inputs.

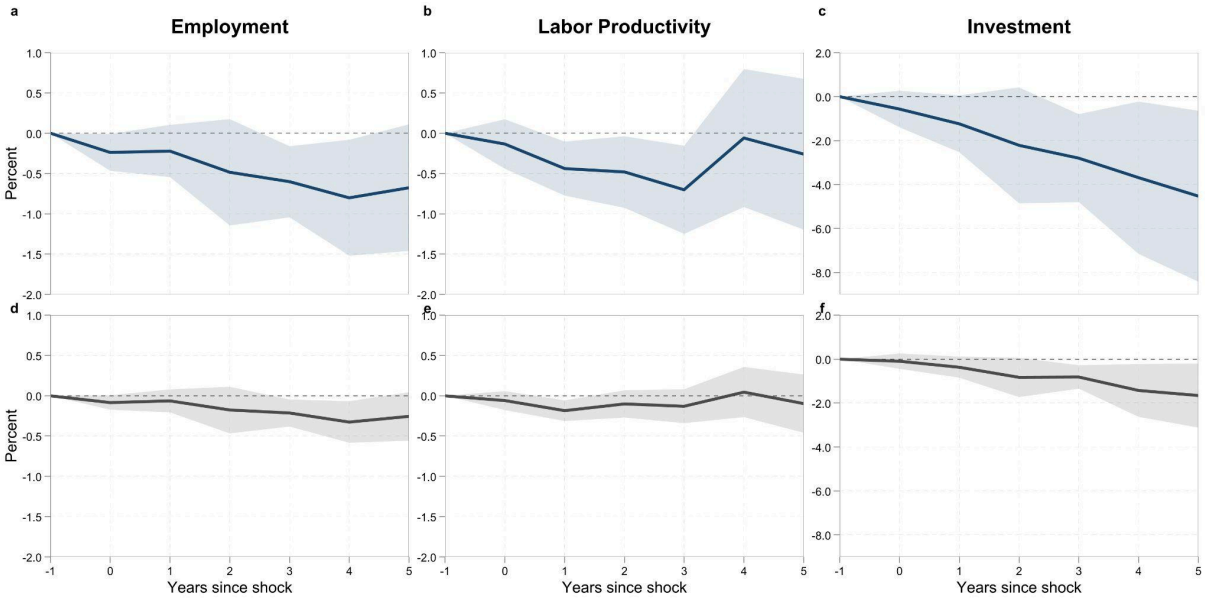

Figure 20. Transmission channels. *Impulse responses of employment, labor productivity, and investment to a one-standard-deviation supply chain-transmitted* ***(a, b, c)*** *and purely local* ***(d, e, f)*** *water scarcity shock. Employment: number of workers. Labor productivity: GVA over employment. Investment: Gross fixed capital formation. 95% confidence bands are based on standard errors clustered at the country level.*

Critically, the magnitude of these effects is amplified when supply chain spillovers are accounted for. For example, the investment decline when supply chain spillovers are considered (Figure 20a) is more than twice as large as the decline estimated in the local-only specification (Figure 20f).

Adaptation. Next, an analysis is conducted to test whether the sensitivity to supply chain-transmitted water scarcity shocks varies with per capita income and long-term climate conditions. Since per capita income and long-term climate conditions map out underlying adaptation mechanisms, i.e., adaptation due to increased adaptive capacity and repeated exposure to local climatic conditions (Carleton et al. 2022, Rode et al. 2021), supply chain-weighted averages of per capita income and long-term water availability are utilized to account for potential adaptation along the supply chain.

Figure 21a shows that higher income per capita does not significantly reduce the sensitivity to water scarcity shocks. The responses of GVA in the average regions within countries of the lowest and highest income terciles are statistically indistinguishable from the response in the average region. This suggests that, despite higher adaptive capacity due to greater financial resources, wealthier regions do not show stronger resilience to supply chain-transmitted water scarcity shocks.

In contrast, Figure 21b reveals strong heterogeneity by long-term water availability. The responses of GVA in the average regions within countries in the driest and wettest tercile of countries are statistically significantly different from the response in the average region. In particular, regions in countries with lower supply chain-weighted water availability experience the largest and most persistent losses. While the average region in the wettest tercile of countries recovers fully within five years after the one-standard-deviation shock, GVA in the average region in the driest tercile of countries remains 2.9% below its no-shock trajectory after five years. This gap indicates that regions in drier countries are not better adapted to water scarcity. In fact, they appear more vulnerable than regions in wetter countries, possibly because they are more dependent on water-intensive intermediate inputs and less buffered against water scarcity by domestic water availability.

Similar, but less pronounced effects are identified in the local-only specification (see Appendix E.6).

These results provide no evidence of adaptation to water scarcity shocks. On the contrary, the findings suggest that exposure to long-term water stress, whether domestic or through supply chains, increases the sensitivity to water scarcity, and that economic development alone is not sufficient to build resilience. Adaptation is currently not occurring at the scale or in the form required to mitigate the economic damage from supply chain-transmitted water scarcity shocks.

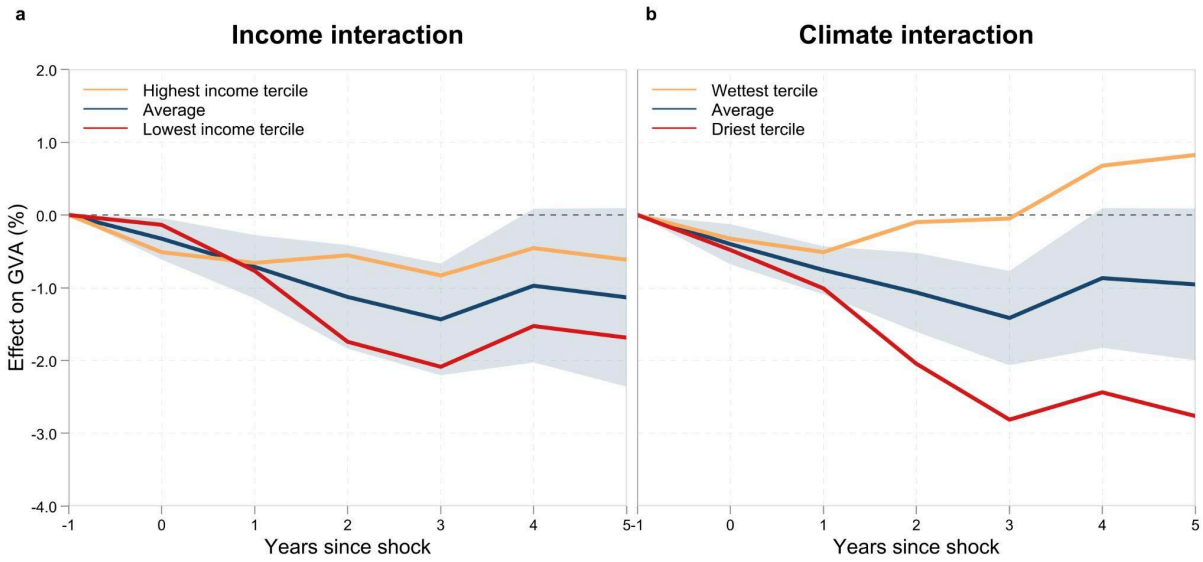

Figure 21. Heterogeneous impulse responses. *The panels plot the impulse response functions of GVA to a one-standard-deviation supply chain-adjusted water scarcity shocks, allowing for differential responses conditional on the supply chain-adjusted income per capita level* ***(a)*** *and the supply chain-adjusted long-term water availability* ***(b)****. Shown are cumulative effects, derived from local projections, up to five years after the exposure to the shock. Red and orange lines depict impulse responses for the average region within the lowest and highest income* ***(a)*** *or the driest and wettest* ***(b)*** *tercile of countries, respectively. Blue lines depict impulse responses for the average region in terms of income* ***(a)*** *and water availability* ***(b)*** *across countries. 95% confidence bands based on standard errors clustered at the country-level are shown for the average region.*

Building on these results, in the next step the climate-specific impulse responses are utilized to estimate the historical GVA losses across Europe attributable to water scarcity shock between 2000 and 2019, accounting for supply chain spillovers and heterogeneity in sensitivity. This counterfactual analysis illustrates where and how climate risks have materialized over time.

4.3.3 Historical Water Scarcity Damages in Europe

To quantify the economic damage in terms of GVA losses in Europe due to water scarcity shocks, a counterfactual GVA trajectory without these shocks is constructed for each NUTS-3 region which has valid GVA data from 2000 to 2019. The counterfactual is derived using the climate-specific impulse response functions from the local projections model (Appendix E.4-5), the observed year-by-year supply chain-transmitted and local water scarcity shocks, the supply chain-weighted and regional long-term water availabilities, and the observed subnational NUTS-3-level GVA time series.

This results in time series of NUTS-3-specific GVA changes which are attributable to supply chain-transmitted and local water scarcity shocks between 2000 and 2019. Based on these GVA changes, NUTS-3-specific GVA trajectories are recovered that represent what GVA would have been in the absence of water scarcity shocks. The divergence between the observed and the

counterfactual GVA levels captures the economic damage caused by water scarcity shocks. Aggregating across NUTS-3 regions and years gives the total cumulative economic damage in terms of foregone GVA in Europe that is attributable to supply chain-transmitted and local-only water scarcity shocks.

Figure 22a shows that between 2000 and 2019, supply chain-transmitted water scarcity shocks have incurred a cumulative loss of €12.4 trillion (2015-equivalent Euros) in foregone real GVA across Europe. In relative terms, this loss is equivalent to nearly three-quarters of Europe's total GVA in 2019. Figure 22b shows the observed and the counterfactual trajectories of GVA in Europe over 2000-2019. Without supply chain-transmitted water scarcity shocks during 2000–2019, total GVA across Europe would have been approximately 9% higher by 2019. These findings underscore the significant and substantial economic damage incurred by water scarcity on economic activity, particularly when supply chain spillovers are taken into account.

Figure 22d reveals strong regional heterogeneity in the distribution of losses within Europe. The driest countries in Southern and Eastern Europe suffer the largest economic damage caused by supply chain-transmitted water scarcity shocks. By 2019, the absence of these shocks during 2000-2019 would have led to 15–25% higher GVA in Cyprus (25.7%), Malta (24.3%), Greece (23.3%), Türkiye (21.9%), Spain (21.7%), Portugal (18.4%), Bulgaria (16.8%), Hungary (15.5%), Romania (15.1%), and Serbia (15.1%). In contrast, wetter countries in Northern and Western Europe are far less sensitive to supply chain-transmitted water scarcity shocks. By 2019, without the shocks during 2000-2019, GVA would have increased by less than 0.5% in Island, Norway, Switzerland, Montenegro, Slovenia, UK, Ireland, and Albania. These findings highlight the pronounced disparities in economic risk caused by water scarcity across European regions.

The comparison of economic damages predicted by the supply chain model and the local-only model underscores the importance of incorporating global supply chain spillover effects in climate impact assessments. When supply chain spillover effects are omitted, and only local water scarcity shocks are considered, the estimated cumulative loss in European GVA amounts to €3.9 trillion over 2000-2019. This means that the local-only model captures less than a third of the total damage predicted by the model that incorporates supply chain spillover effects (Figure 22a). This discrepancy highlights the role of global supply chains in amplifying the economic damage of adverse climatic shocks. Neglecting global supply chain spillovers can lead to a significant underestimation of the true economic cost of climate shocks.

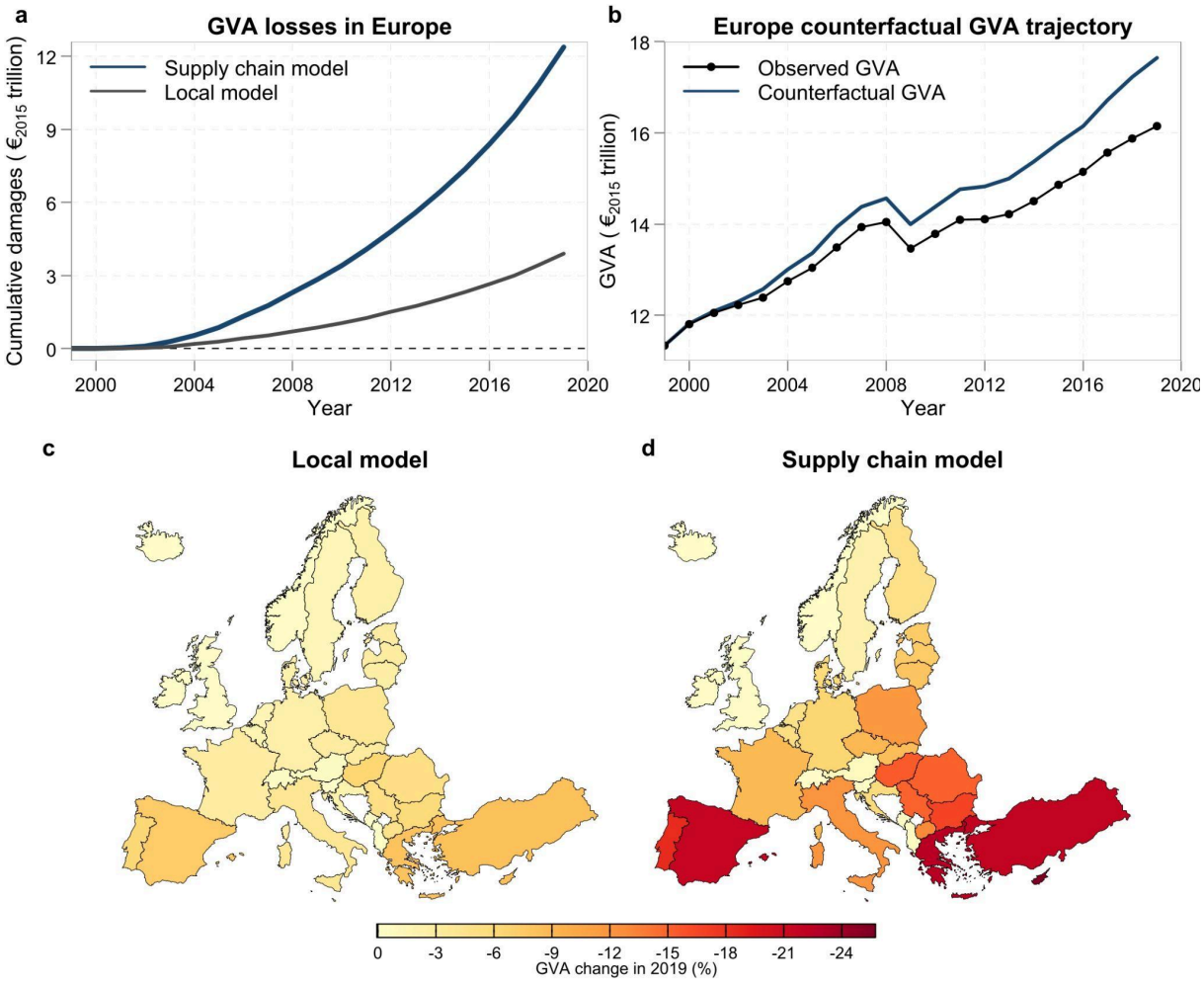

Figure 22. Macroeconomic effects of water scarcity. a. *Cumulative losses in real gross value added in Europe caused by water scarcity shocks during 2000-2019, accounting for supply chain spillovers (black line) and purely local exposure (gray line).* ***b.*** *Observed trajectory of Europe's total real gross value added (dotted black line) versus counterfactual trajectory without water scarcity shocks accounting for supply chain spillovers (blue line).* ***c, d****. Gross value added change per country in 2019 caused by local* ***(c)*** *and supply chain-transmitted* ***(d)*** *water availability shocks during 2000-2019. All monetary values shown are in constant 2015 Euros.*

4.4 Conclusion/Key takeaways

This subtask demonstrates that spillovers through global supply chains can amplify the macroeconomic damage of local climate anomalies. Combining high-resolution meteorological data with global multi-regional input-output tables, a novel measure of supply chain-transmitted water availability anomalies originating around the globe is constructed. Combining this with information on subnational real GVA data at the NUTS3-level across 41 countries in Europe, the dynamic causal effect of water availability shocks on regional value added is estimated, explicitly accounting for supply chain spillover effects.

The findings of this subtask reveal that supply chain-transmitted water scarcity shocks generate persistent, negative effects on regional GVA, particularly in the driest countries. Crucially, the results highlight that neglecting global supply chain spillover effects results in a severe underestimation of the economic damage. In the case of water scarcity shocks, neglecting supply chain spillover effects results in damage estimates that capture only about one-third of the total GVA losses. When supply chain spillovers are not accounted for, the cumulative water scarcity damages in Europe amount to €3.9 trillion over the period 2000–2019, which is a vast underestimation of the €12.4 trillion in cumulative GVA losses when global supply chain spillovers are accounted for.

The key contribution of this task lies in highlighting that global supply chains are a critical transmission mechanism through which local climate anomalies can generate large-scale macroeconomic losses. To capture the total macroeconomic losses from climate change, it is essential to account for these supply chain linkages. Local exposure is only part of the picture; the global network of production and trade can turn localized climate shocks into macroeconomic headwinds that cross borders.

A limitation of this study is its reliance on country-level multi-regional IO tables. Currently, no subnational multi-regional IO tables with global coverage exist. Yet, such data would be essential for accurately identifying local hotspots that are both highly exposed to climate-related hazards and serve as key production hubs for the global economy. Future research should therefore aim to construct global subnational multi-regional IO tables to enable more granular risk assessments.

5 Impacts of compound wildfires

5.1 Introduction

A wildfire is an uncontrolled fire event that can spread rapidly through fire-prone areas, including forests, grasslands, shrublands, agricultural and urban areas. Wildfires are generally powered by dry conditions, flammable vegetation and other positive fuel loads, and they are often exacerbated by wind. The European Climate Risk Assessment (EUCRA) report, published by the European Environment Agency (EEA) in 2024, has identified wildfires as one of the major climate risks threatening Europe's ecosystems, human health, infrastructure, and economic stability, in particular sectors like tourism and forestry (EEA, 2024). As a natural phenomenon, wildfires have a complex and multifaceted impact on biodiversity, acting dually as a threat to many species and as a natural ecological process. However, it is human activity that plays the dominant role in wildfire ignition (Farid et al. 2024). Globally, and particularly in developed and densely populated areas, most wildfires are linked to human activities. In Southern Europe and globally, an estimated 90% of wildfires are caused by humans, often due to negligence, agricultural burning, or intentional ignition. Natural causes like lightning account for the remaining 10%, mostly in remote or forested areas. Northern Europe historically has experienced lower wildfire activity, but human-caused fires are increasing due to warming and land-use changes (EEA, 2024). Human-caused wildfires can occur outside the natural fire seasons, and in areas close to human settlements, which increases the risk to people and infrastructure. According to the recent review by Farid et al. (2024), wildfires started from human activities tend to be larger than lightning-caused ones, especially in regions of high fuel loads and dry conditions.

Wildfires are increasingly recognized as compound events (e.g. Abatzoglou et al. 2020; Fan et al., 2023; Kumar and Collins, 2025; Richardson et al., 2022). Zscheischler et al. (2018) defines compound weather/climate events as the combination of multiple drivers and/or hazards that contribute to societal or environmental risk. Table 15 lists some of the common drivers of compound wildfires reported in literature. For example, a wildfire may be triggered during a heatwave that coincides with drought conditions, creating an environment where vegetation is extremely dry and flammable. These conditions are often worsened by strong winds, which can make the fire spread rapidly and unpredictably. Wildfires can also lead to compound (cascading) hazard chains such as enhanced susceptibility to landslides or floods in burned areas (Xu et al., 2023), or compound health risks when smoke coincides with extreme heat, affecting vulnerable populations (Jones-Ngo et al., 2025; Rosu et al. 2025). For example, Dulin et al. (2025) show how sequences of wildfires followed by heavy rainfall can enhance flooding and infrastructure damage in California catchments, whereas Waggenbrenner et al. (2021) reviewed post-wildfire hydrologic recovery in Mediterranean-type global climates; while this study finds a large spatial variability, it confirms severe compound impacts from post-fire flash floods and erosion risks.

Climate change is affecting many of the risk drivers listed in Table 15. According to the Sixth Assessment Report (AR6) of the IPCC (Seneviratne et al. 2021), human-induced climate change has increased the frequency and intensity of fire weather conditions, especially hot and dry extremes. This has resulted in longer fire seasons in many places due to increasing temperatures

and shifting precipitation patterns, with ideal fire environments. Meanwhile, compound events — such as concurrent heatwaves and droughts — are becoming more common and are strongly linked to increased wildfire risk. A recent paper by Cunningham et al. (2024) suggests that the frequency of the most extreme wildfire events has more than doubled over the past 21 years based on satellite observations, despite a potential reduction in the total area burned on earth. They further highlight that fire behavior is worsening in several regions — particularly the boreal and temperate conifer biomes — with substantial implications for carbon storage and human exposure to wildfire disasters (Cunningham at al. 2024). Conversely, Schütze and Resco de Dios (2025) attribute the observed increases in the world's most extreme wildfire events to fire size and simultaneity. Regardless, both support the need for a compound event perspective when analyzing wildfires.

Table 15. *Common drivers of compound wildfire events reported in literature.*

Heatwaves, high temperatures	Prolonged heat waves can dry out vegetation, making them more flammable
Drought	Extended drought reduces moisture in vegetation and soil, increasing fire susceptibility
Low humidity	Dry air accelerates the drying of fuels and promotes ignition
Strong winds	Strong winds can lead to rapid spreading of flames and carry embers to new areas
Lightning strikes	Lightning constitutes a major natural ignition source, especially in remote areas
Vegetation type	Some plants burn easily, exacerbating the spread of the fire
Topography	In some places, topography can play an important role for the spread of a wildfire (e.g. combined with wind and vegetation)
Fuel accumulation	Dead trees, dry leaves, and underbrush act as fuel
Forest degradation	Forest degradation, including drought-induced dieback and pest outbreaks, contributes to fuel accumulation and fire spread
Forest management practices	Lack of controlled burns or forest thinning can lead to excessive fuel buildup
Agricultural practices	Slash-and-burn techniques or crop residue burning can lead to unintended wildfires, often out-of-season

Human activities	Campfires and outdoor burning can escape control and ignite wildfires. Also, sparks from power lines, electrical faults, engines and vehicles can ignite wildfires. Intentional ignition is a significant cause of wildfire ignition in some places.
Urban-rural (wildland) interface	Expansion of homes into fire-prone areas increases ignition sources and risk.

So far, very few studies have analyzed European wildfires from a compound event perspective. Hence, existing studies have mainly focused on California and the Western part of the United States. In the following, we analyze the potential compound drivers for Southern Europe (e.g., Spain, Portugal, Italy, Greece, Türkiye, Balkans). Based on statistics from the European Forest Fire Information System (EFFIS) and Copernicus' European State of the Climate, in 2025 over 1 million hectares were burned across the EU, with Southern Europe accounting for the vast majority. Conservative multi-year estimates by EFFIC suggest that Southern Europe accounts for 70–80% of total wildfire burned area and incidents in Europe, whereas Central and Northern Europe only contributes 20–30% with smaller burned areas, although this number is gradually increasing due to climate change.

5.2 Methods

5.2.1 Methodology

This study extends previous work presented in Milestone 2.1 ("Wildfire estimates", Month 17) and Deliverable 2.4 ("Impacts on ecosystems & biodiversity", Month 25) of the ACCREU project.

To assess the role of different drivers of compound wildfires, we (i) develop a data-driven wildfire risk model for Southern Europe that combines potentially compounding factors (see Table 15) including climate variables, land use, human activity, and topography, to estimate the probability of wildfire occurrence for given daily weather conditions; (ii) use explainable AI artificial intelligence (AI) to evaluate the contribution of different predictors to the wildfire risk; and (iii) simulate wildfire risk under current and future climatic conditions using regional climate model simulations from the ClimEx-II ensemble (Asselin et al., 2024). The modeling framework is outlined in Figure 23.

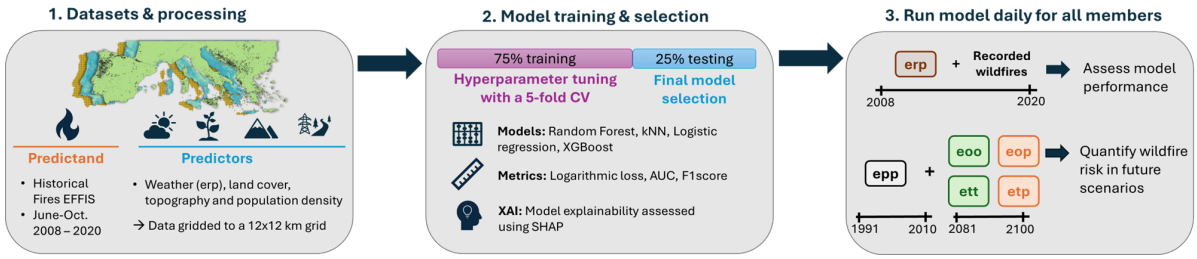

Figure 23. Workflow of the data-driven wildfire risk model for Southern Europe. *The framework integrates data processing, model training and explainability, and daily simulations across ClimEx-II ensemble members to assess historical performance and future wildfire risk.*

Records of European wildfires occurring between 2008 and 2020 that resulted in burned areas exceeding 50 were obtained from EFFIS. These wildfires cover the European fire season from June to October. The predictors were selected based on a literature review and include human infrastructure and land use (Bountzouklis et al., 2023; Oliveira et al., 2012; Zhai et al., 2023), as well as topographical and climate data (Polash, 2022; Dorph et al., 2022; Milanovic et al. , 2021). In total, 25 variables were aggregated into a common 12 × 12 km grid, providing a balance between computational efficiency and the ability to capture regional variation in the data.

Four different machine learning (ML) models were trained based on the data collected using the Scikit-learn Python library: Support Vector Machine (SVM), Random Forest (RF), k-Nearest Neighbors (kNN), and Logistic Regression (LR). These models were chosen based on their interpretability, robustness, and performance. In addition, they are commonly used for classification tasks in climate modelling studies (Polash, 2022; Milanovic et al. , 2021; Oliveira et al., 2012). The tuning of model hyperparameters was performed on the training data with a 5-fold cross-validation using the F1 score. The final model selection was performed using the testing data and evaluated using three metrics: the F1 score, logarithmic loss, and Area Under the Curve (AUC).

75% of the data from the period 2008 to 2020 were used for training the models, and the remaining 25% for testing. Unique combinations of location and date, distinct from the historical wildfire records, were selected to generate a balanced dataset consisting of 50% data with wildfire occurrence and 50% data without wildfires. A value of 1 (0) was assigned to the fire (no fire) data, and the corresponding 25 predictors were appended. Similar to Oliveira et al. (2012), pairs of predictors with a Pearson's correlation coefficient greater than 0.75 were identified, and one of the correlated predictors was removed. This process dropped five features to reduce the multicollinearity. Finally, the remaining twenty predictors were standardized by subtracting the mean and dividing by the standard deviation.

5.2.2 Climate and topographic data

Regional climate model simulations produced within the ClimEx-II project that aligns with the ACCREU scenario matrixare used to quantify both current and future risks of wildfires from a compound event perspective. For the historical period, we use ClimEx-II simulations forced by

ERA5 (Muñoz-Sabater et al. 2021). A detailed description of ClimEx-II can be found in Asselin et al. (2024). The ClimEx-II regional climate model ensemble is a single-model initial condition large ensemble (SMILE) and thereby differs from multi-model climate model ensembles, e.g. CORDEX (Jacob et al., 2020). All ClimEx-II simulations are carried out using the Canadian regional climate model, CRCM5, which in turn is forced by either ERA5 reanalysis data or the Max Planck Institute for Meteorology's Earth System Model version 1.2 Grand Ensemble (MPI-ESM-1.2; Mauritsen et al. 2019, Olonscheck et al. 2023). Only the first four members (rXi1p1f1, with X=1-4) of the global ensemble were used in ClimEx-II (MPI-ESM-LR-1.2, Olonscheck et al. 2023). The four ensemble members (labelled "e", "f", "g" and "h") vary due to the different initial conditions of the simulations. For each of these members, three different configurations are explored: (a) present land cover and climate forcing ("p", or control); (b) future climate forcing ("o" for RCP2.6 and "t" for RCP7.0) with unchanged land cover ("p"); and finally future climate forcing with land use and land cover change corresponding to the SSP1 ("o") and SSP3 ("t") global narratives. Projections of land use and land cover changes (maps) are based on the Land Use Harmonized Dataset Version 2 (LUH2; Hurtt et al., 2020). By means of the land-use translator by Hoffmann et al. (2023), land cover maps based on land use transitions for the year 2100 in SSP1-2.6 and SSP3-7.0 (Hoffmann et al., 2022) were derived from LUH2. The land use change maps provide fractions of 16 plant-functional types (PFTs) over Europe in 2015 which were simplified to 6 land cover categories for the ClimEx-II experiments.

Figure 24 illustrates how the different land surface configurations reflect the ACCREU scenario framework. In terms of land use and land cover change, the SSP2 land cover scenario essentially represents unchanged conditions (P). Meanwhile, SSP1 and SSP3 land covers can be assumed to represent different adaptation scenarios with respect to the SSP2 baseline. We note that not all nine scenario combinations are covered by the available climate data (i.e. RCP2.6, 4.5 and 7.0; with low, moderate and high adaptation, respectively).

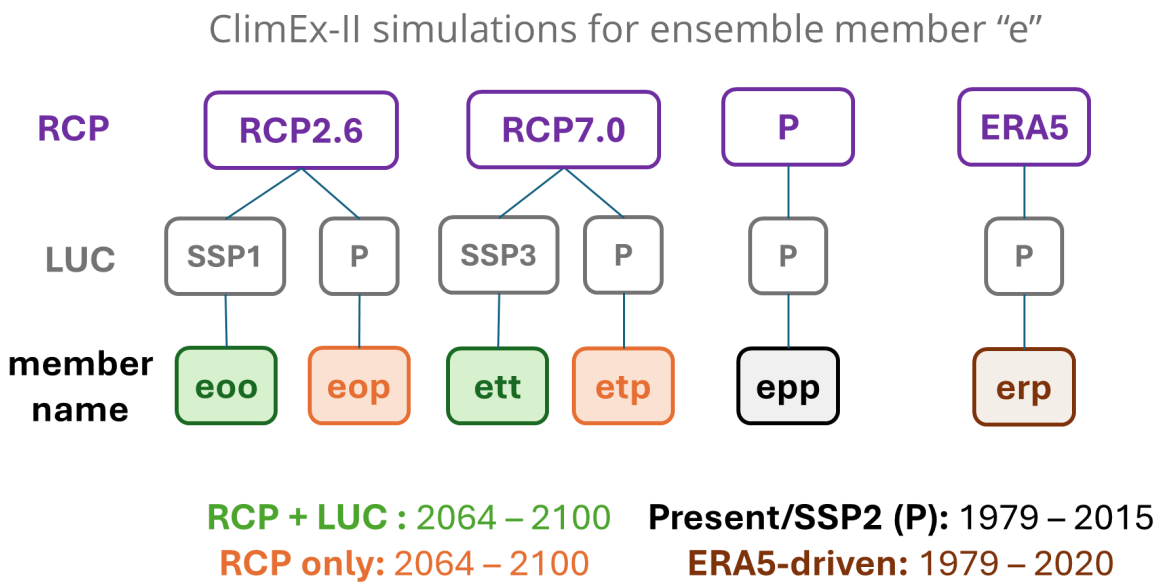

Figure 24. ClimEx-II simulations. *The different ensemble members are named in the following way: the first letter (e, f, g, or h) distinguishes individual members (here only e); the second letter refers to the climate forcing (o = RCP2.6, t = RCP7.0), while the third letter refers to the land use and land cover scenario (o = SSP2.6, t = SSP7.0, and p = present conditions/SSP2)*

5.2.3 ML model performance

Figure 25 (left) depicts the performance of the four different ML models that were trained (see Sec. 5.2.1). As illustrated below, all four models performed very well, with XGBoost having the highest AUC and F1 scores (0.91, 0.83). The second-best model is the Random Forest model, which has almost identical scores. In the following, we use results from the best-performing XGBoost model, while noting that our results are robust across models.

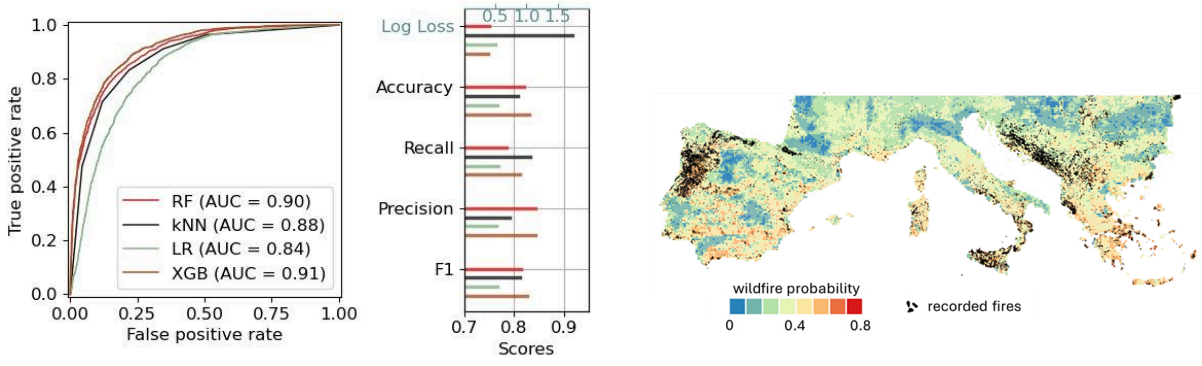

Figure 25. *(left) "ROC" curves and other performance metrics for the RF, kNN, LR, and XGB models. (right) Comparison of mean XGBoost wildfire probability with the historical record of fires (fire season 2008-2020).*

The map on the left side of Figure 25 indicates the predicted wildfire risk (color scale) using the XGBoost model together with the location of historical wildfires. By visual inspection it is clear that there is a correlation between the predicted wildfire risk and the observations, e.g. areas which suffered a large number of wildfires from 2008-2020 are accordingly assigned a high risk by our model as we would expect.

5.3 Results & Discussion

5.3.1 Explainability & compound factors

We use the SHapley Additive exPlanations (SHAP) method to assess the contribution of the wildfire drivers to each individual prediction (Lundberg and Lee, 2017). The SHAP method can be used with any machine learning model and is founded on solid mathematical principles. It is often used for building trust in AI models by explaining decisions. The SHAP analysis was performed on the testing data to evaluate how the fine-tuned XGBoost model quantified the fire risk in Southern Europe. The mean absolute SHAP values show the influence of the top-twelve-ranked features on model prediction (Figure 26, left). Meanwhile, the force (layered violin) plot indicates the corresponding relationship between the feature values, including both magnitude and positive and negative directions, and how this affects model prediction (Figure 26, right).

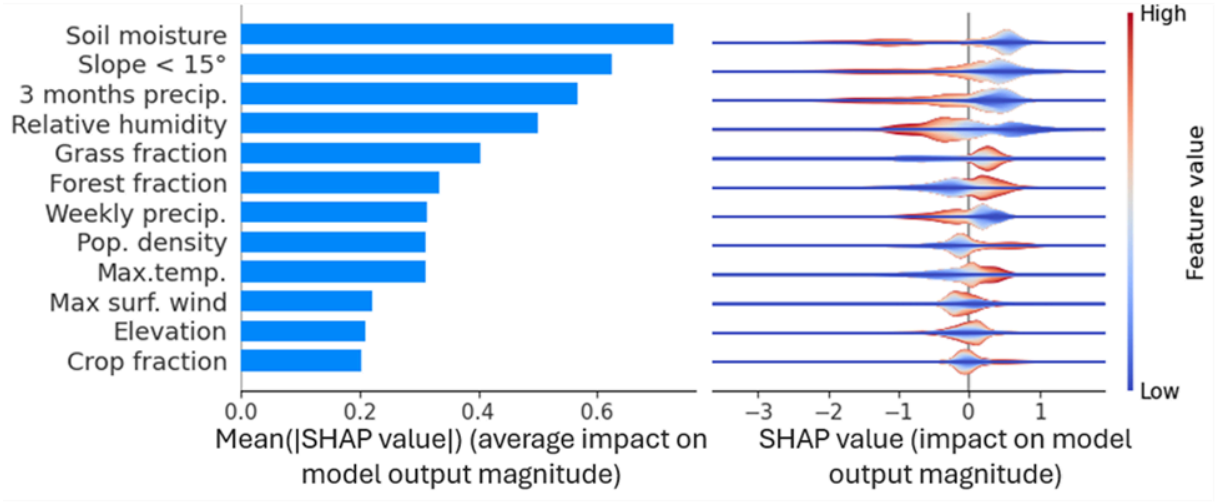

Figure 26. Top-twelve predictors of wildfires ranked by mean absolute SHAP values and their distribution. *(left) Mean absolute SHAP values, indicating their relative impact on model output magnitude (i.e. wildfire risk). (right) Distribution of SHAP values. Each dot is a SHAP value for a single prediction, showing how much that feature contributed to the model's output for that instance (i.e., red = high, blue = low), that is, how each feature pushes the prediction up or down.*

Table 16 lists the twelve primary drivers of wildfire activity in Southern Europe, identified by our machine learning model.

Table 16. *Top twelve important predictors of wildfire activity in Southern Europe identified by the ML model.*

Soil moisture	Fraction of soil volume occupied by water (m^3/m^3)
Slope < 15°	Proportion (0–1) of the grid cell area where the slope is below 15°
3-months precipitation sum	m
Relative humidity	%
Grass fraction	Proportion (0–1) of the grid cells covered by each different land cover type. The classes have been obtained following the categories from Zhai et al. (2023) and CORINE land cover (EEA, 2020)
Forest fraction	
Weekly precipitation sum	m
Population density	Ratio of inhabitants per grid cell (persons/km^2). From the WorldPop Global Population dataset. https://doi.org/10.1038/sdata.2017.4
Max. temperature	°C
Max. surface wind	m/s
Elevation	Average elevation above the sea level for the grid cell
Crop fraction	See forest and grass fractions above.

Our model clearly confirms previous findings (Table 15), estimating the relative feature importance of the different potential compound drivers. Soil moisture, 3-months precipitation sum, weekly precipitation sum and relative humidity are all found to play similar roles for wildfire risks related to drought and temperature-related extreme conditions (right side of Figure 26). Similarly, land surface characteristics, in particular, grass and forest fractions, stand out. Interestingly, when land surface variables play a dominant role for the magnitude of the model output (red colors) the sign is generally positive, whereas when the hydrometeorological parameters dominate, the sign is negative. Two of the twelve parameters shown above are not included in Table 15: slope and

elevation. While the elevation overall is found to be of lesser importance (but still in the top 50% of the 25 features we consider in this study), the slope and — more generally — terrain features are clearly very important drivers of wildfires. This suggests that high resolution models are needed to properly represent wildfires in current and future climates.

5.3.2 Future projections of wildfires: the compound role of land use change

To elicit the compounding role of land use and land cover change, we apply the trained wildfire risk model to future climate projections from the ClimEx-II ensemble of regional climate model simulations. Figure 27 depicts the future changes in mean wildfire probability for four of the ensemble members, all representing the same driving global climate model ("eoo", "eop", "ett", and "etp") as well as the baseline simulation ("epp") (Figure 24). Similar analyses were carried out for all ensemble members. The future changes are calculated as the difference (anomaly) between the mean fire probability averaged over the fire season (June – October) for a future period(2081 – 2100) and a present-day period(1991 – 2010, e.g. member "epp"). The two top panels show results for RCP2.6 assuming SSP1 and SSP2 (present-day) land use, respectively. The next two panels show analogous results for RCP7.0 assuming SSP3 and SSP2 (present-day) land use, respectively, while the lowest panel shows the results of the baseline simulation.

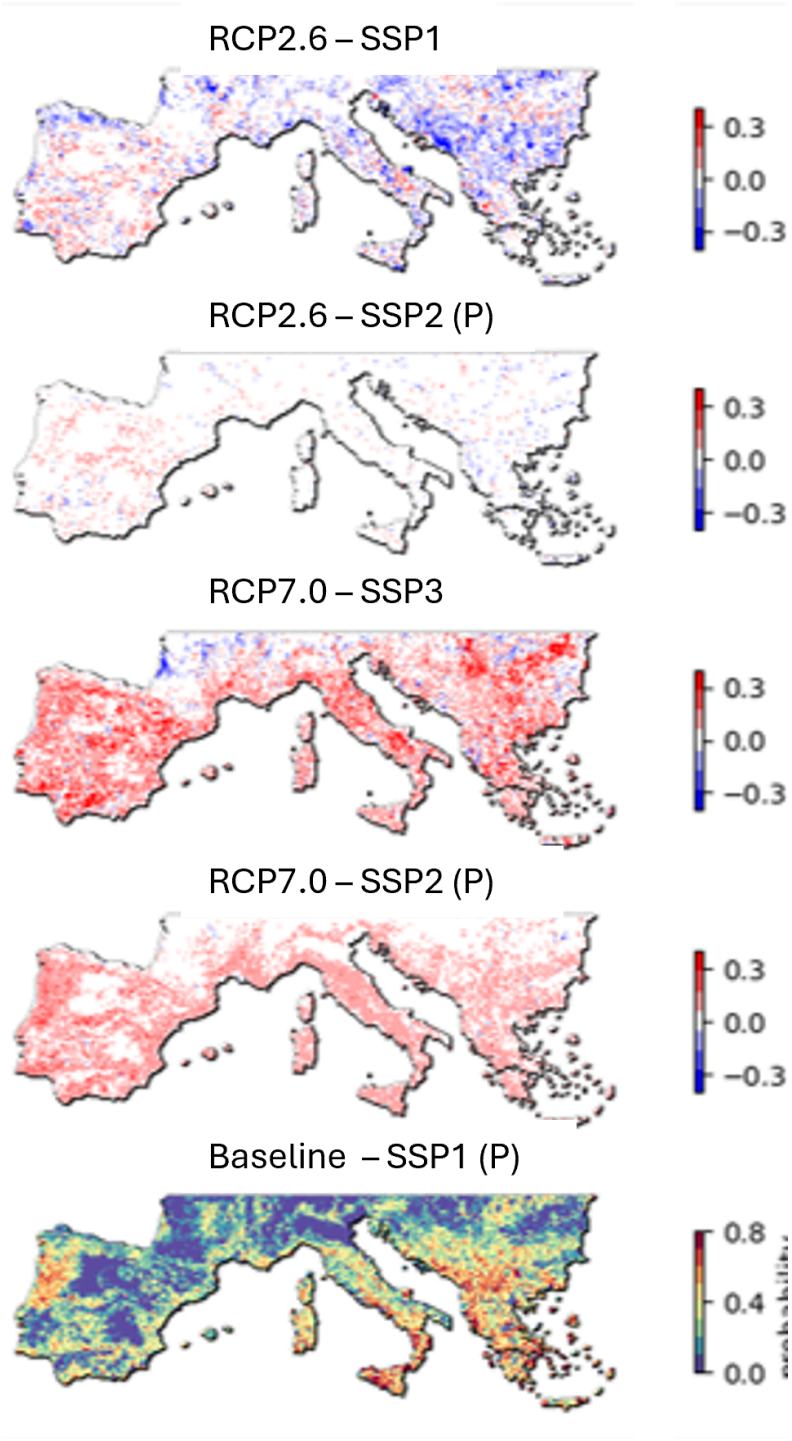

Figure 27. Future changes in mean wildfire probability for the eoo, eop, ett and epp ensemble members. *The future anomaly is calculated as the difference between the mean fire probability averaged over the fire season (June – October) between future (2081 – 2100) and present simulations (epp 1991 – 2010).*

For the RCP2.6 (2081 – 2100) scenario with largely unchanged land cover (SSP2), we observe few and very local changes in wildfire risk compared to the baseline simulations. Conversely, if we impose the SSP1 land use and land cover change scenario (Figure 28), which may be considered a "high" adaptation scenario, we observe a significant decrease in wildfire risk associated with increasing fractions of forest and croplands and a decrease in grasslands. For the RCP7.0 scenario with unchanged/SSP2 land cover, we observe a compounded increase in wildfire risk almost everywhere driven by anthropogenic warming, resulting in more favorable wildfire conditions generally. This trend is even stronger in most places when we adopt the SSP3 land use and land cover scenario, featuring a significant decrease in croplands and an increase in forest (another "high" adaptation scenario).

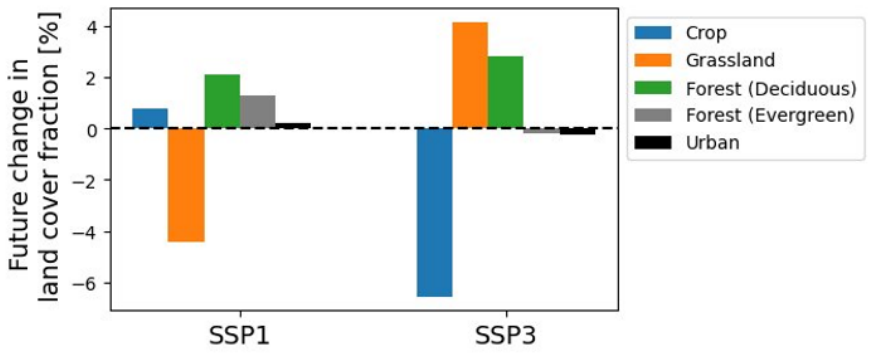

Figure 28. *Future changes in land cover fraction over Southern Europe in the SSP1 and SSP3 scenarios.*

It is evident from this analysis that increasing the European forest cover, as indicated in the EU Forest Strategy for 2030, which is part of the European Green Deal and the EU Biodiversity Strategy for 2030, carry the risk of increasing wildfires in the Mediterranean — at least in the short and medium term — unless substantial mitigation is achieved. Hence, improved forest management and substantial adaptation at the local and landscape level will be urgently needed to cope with increasing wildfire risks under sustained high levels of anthropogenic warming in order to achieve these long-term sustainability and biodiversity goals.

5.3.3 Compound wildfire risk — a case study

One of the main conclusions by Zscheischler et al. (2018) is that compound events are in general highly localized. To test the abovementioned findings, we therefore also investigate the compound risk for a case study in the Campania region. The same region is investigated in WP3 of the ACCREU project (case study CS2.1).

As the foundation for this analysis, we define a number of climate indicators (Table 17), which specifies when a day can be classified as extreme. The percentiles for these indicators were calculated from the ClimEx-II climate simulations, i.e., aggregating the results of the four historic ensemble members.

Table 17. *Extreme indicators.*

Indicator	Description	Season	
		DJF	JJA
Hot days	Max temperature > 95th percentile	X	X
Cold days	Min temperature < 5th percentile	X	
Warm nights	Min temperature> 95th percentile		X
Windy days	Daily wind speed> 99th percentile	X	X
Rx1day	Max daily precipitation	X	X
CDD	Consecutive dry days	X	X
CWD	Consecutive wet days	X	X
R20	Daily precipitation > 20 mm	X	X

For each season (winter - DJF, summer - JJA) and each ensemble member (covering a total of 120 model years), we count the number of days exceeding the climate indicator threshold. This provides for each year a seasonal count of extreme days. From these seasonal counts, we build a historical distribution, from which we infer the 95^{th}-percentile as the threshold for extreme seasons. A current or future year is now marked as extreme if the number of extreme days in that season exceeds the historical 95^{th}-percentile threshold (Figures 29 and 30; upper right). For example, if the 95^{th} percentile of "hot days" corresponds to 10 days per season, and through June - August in 1990 ,we observe 11 hot days then that year is classified as a hot-day extreme. Finally, we compute how often such extremes co-occur in the historical and future periods.

The results of the abovementioned analysis for the current baseline (1991-2010) and future RCP7.0-SSP2 (2081-2100) scenario is shown in Figures 29 and 30.

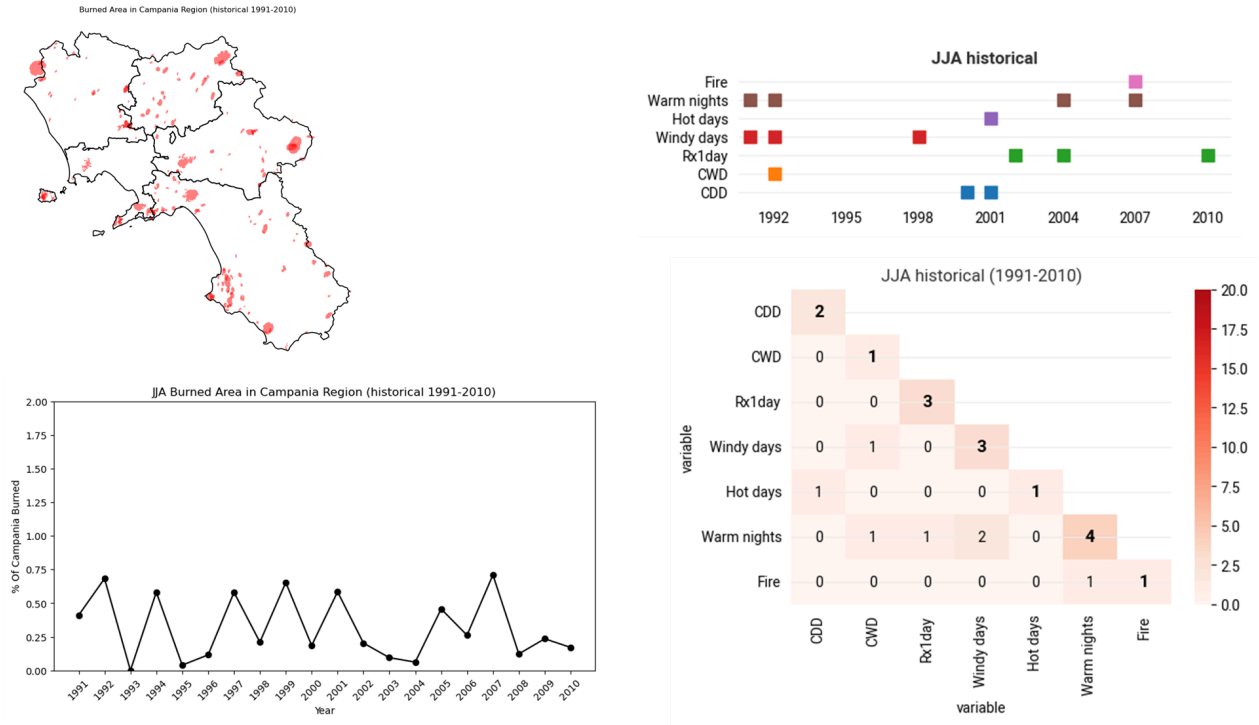

Figure 29. Current compound risks related to overlapping climatic indicators, including wildfire (Campania region, Italy). *The top left map indicates burned areas in the baseline period 1991-2010 for JJA (June-August) in the Campania region, Italy (WP3, case study 2.1). The lower left plot shows the annual percent of burned area in Campania due to wildfires. The top right graph depicts the annual occurrence of daily extreme events (Table 17) over the baseline period, measured by different climatic indicators; Rx1day indicates the maximum daily precipitation, CWD and CDD is a measure of consecutive wet and dry days, respectively. The lower right graphic counts the number of overlapping extreme years in the period, where the legend indicates the corresponding number of extreme days per year.*

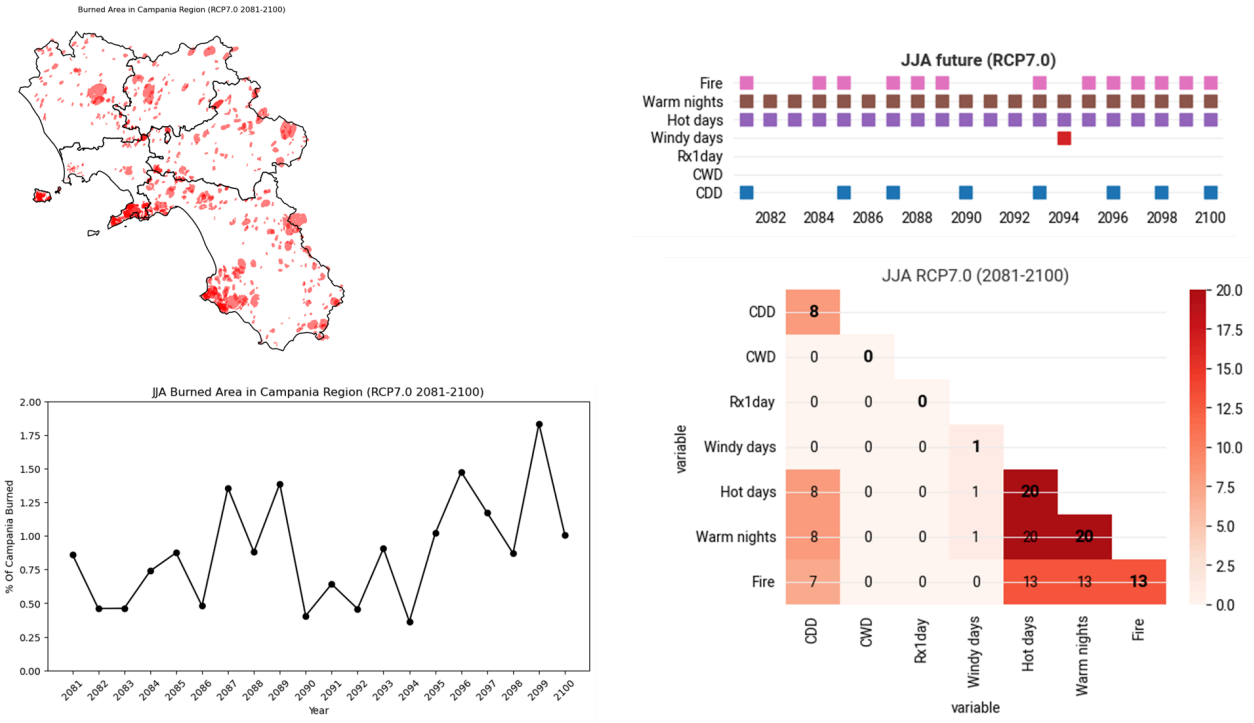

Figure 30. Future compound risks related to overlapping climatic indicators, including wildfire, under the RCP7.0 scenario (Campania region, Italy). *This figure is similar to Figure 29, except it shows results for the period 2081-2100 under the RCP7.0 scenario with unchanged (SSP2) land use. A significant increase in the potential risk of compound wild fires is clearly observed.*

Comparing Figures 29 and 30, we see that the number of extreme wildfire years grows from one in the current climate to 13 (in a 20-year period) under the RCP7.0 scenario with a SSP2-type land cover. Correspondingly, if we assumed an SSP3-type land cover with increased afforestation and decreased croplands (c.f Figure 28), one might expect an even more dramatic increase in the risk of wildfires. We also note that extreme wildfire years overlap years having a large number of consecutive dry days (7), hot days (13) and warm nights (13), confirming that an increased risk of wildfire may be associated with compound factors (drought, heat waves).

5.4 Conclusion/Key takeaways

Wildfires are inherently driven by different factors, including local hydrometeorology, topography, land use and land cover, as well as human factors. In this task, we investigate some of these key drivers using two different methods. First, a machine learning model is trained for the Mediterranean region and used to identify and rank the most important features from a selection of 25 different potentially compounding factors. Second, we collect statistics on seasonally overlapping climate indicators for present and future climate simulations drawn from the ClimEx-II regional climate model ensemble. Based on this analysis, it is evident that hot and dry conditions as

expected play a key role. This conclusion is supported by a case study in Campania, Italy (case study 2.1, D3.2). But also topography and land cover is found to be very important, which suggests that high-resolution data and modelling are required to aptly capture the dynamics of present and future wildfires. Here, we find that the usual static land surface scheme employed in most regional climate models is likely to skew results. Hence, this study shows an increasing risk of wildfires under the RCP7.0-SSP3 scenario, which assumes a significant transformation from croplands to forest (e.g., a “high adaptation” scenario) as opposed to a RCP7.0-SSP2 scenario, where the land cover mimics current conditions. Similarly, for the sustainable and highly mitigated RCP2.6-SSP1 scenario, we find an overall decreasing risk of wildfires (increases in wildfire risk are still found in some locations) following a transformation of grasslands to other land surface types, compared to the RCP2.6-SSP2 scenario resembling present-day conditions. Needless to say, this stresses the importance of considering the compound effect of climate warming and land use and land cover change when assessing the future impacts of wildfires on, e.g., ecosystems, infrastructure, and the economy.

This study has at least one main limitation. Although we have not explicitly estimated changes in occurrence probability, as for instance done in a publication by the Society of Actuaries Research Institute. (2024), we have principally demonstrated the increased probability of wildfire due to temporally and spatially compounding factors. However, we do not investigate the potential relation between wildfire extremeness and compounding drivers, e.g., as proposed by Cunningham et al. (2024) and Schütze &Resco de Dios (2025). This is in part due to the fact that wildfires are subject to human suppression and firefighting activities. Thus, the records of European burnt areas provided by EFFIS carry a size bias, which depends on fire spread and human influence. While this factor was excluded from the current study, it will be the subject of future work.

References

Abatzoglou, J. T., Juang, C. S., Williams, A. P., Kolden, C. A., & Westerling, A. L. (2021). Increasing synchronous fire danger in forests of the western United States. *Geophysical Research Letters*, *48*, e2020GL091377. https://doi.org/10.1029/2020GL091377

Acemoglu, D., Akcigit, U., & Kerr, W. (2016). Networks and the Macroeconomy: An Empirical Exploration. *NBER Macroeconomics Annual*, *30*(1), 273–335.

Acemoglu, D., Carvalho, V. M., Ozdaglar, A., & Tahbaz-Salehi, A. (2012). The Network Origins of Aggregate Fluctuations. *Econometrica*, *80*(5), 1977–2016.

Acevedo, S., Mrkaic, M., Novta, N., Pugacheva, E., & Topalova, P. (2020). The Effects of Weather Shocks on Economic Activity: What are the Channels of Impact? *Journal of Macroeconomics*, *65*, 103207.

Akyapı, B., Bellon, M., & Massetti, E. (2025). Estimating Macro-Fiscal Effects of Climate Shocks from Billions of Geospatial Weather Observations. *American Economic Journal: Macroeconomics*, *Forthcoming*.

Allen, R., Pruitt, W., Wright, J., Howell, T., Ventura, F., Snyder, R., Itenfisu, D., Steduto, P., Berengena, J., Baselga-Yrisarry, J., Smith, M., Pereira, L., Raes, D., Perrier, A., Alves, I., Walter, I., & Elliott, R. (2006). A Recommendation on Standardized Surface Resistance for Hourly Calculation of Reference ETo by the FAO56 Penman-Monteith Method. *Agricultural Water Management*, *81*(1), 1–22.

Asselin, O., Leduc, M., Paquin, D., de Noblet-Ducoudré, N., Rechid, D., & Ludwig, R. (2024). Blue in green: Forestation turns blue water green, mitigating heat at the expense of water availability. *Environmental Research Letters*, *19*(11), 114003. https://doi.org/10.1088/1748-9326/ad796c

Baldwin, R., & Freeman, R. (2022). Risks and Global Supply Chains: What We Know and What We Need to Know. *Annual Review of Economics*, *14*(1), 153–180.

Baldwin, R., Freeman, R., & Theodorakopoulos, A. (2023). Hidden Exposure: Measuring US Supply Chain Reliance (NBER Working Paper No. 31820). National Bureau of Economic Research. https://doi.org/10.3386/w31820

Baron, M., Verner, E., & Xiong, W. (2021). Banking Crises Without Panics. *The Quarterly Journal of Economics*, *136*(1), 51–113.

Barrot, J.-N., & Sauvagnat, J. (2016). Input Specificity and the Propagation of Idiosyncratic shocks in Production Networks. *The Quarterly Journal of Economics*, *131*(3), 1543–1592.

Beck, H. E., Wood, E. F., Pan, M., Fisher, C. K., Miralles, D. G., Van Dijk, A. I., McVicar, T. R., & Adler, R. F. (2019). MSWEP V2 Global 3-Hourly 0.1 Precipitation: Methodology and Quantitative Assessment. *Bulletin of the American Meteorological Society*, *100*(3), 473–500.

Bierkens, M. F. P., & Van Beek, L. P. H. (2009). Seasonal predictability of european discharge: NAO and hydrological response time. *Journal of Hydrometeorology*, *10*(4), 953–968. https://doi.org/10.1175/2009JHM1034.1

Blöschl, G., Hall, J., Viglione, A., Perdigão, R. A. P., Parajka, J., Merz, B., Lun, D., Arheimer, B., Aronica, G. T., Bilibashi, A., Boháč, M., Bonacci, O., Borga, M., Čanjevac, I., Castellarin, A., Chirico, G. B., Claps, P., Frolova, N., Ganora, D., … Živković, N. (2019). Changing climate both increases and decreases European river floods. *Nature*, *573*(7772), 108–111. https://doi.org/10.1038/s41586-019-1495-6

Bountzouklis, C., Fox, D. M., & Di Bernardino, E. (2023). Predicting wildfire ignition causes in southern France using explainable artificial intelligence (XAI) methods. *Environmental Research Letters*, *18*(4), Article acc8ee. https://doi.org/10.1088/1748-9326/acc8ee

Burke, M., Hsiang, S. M., & Miguel, E. (2015). Global non-linear effect of temperature on economic production. *Nature*, *527*(7577), 235–239. https://doi.org/10.1038/nature15725

Caloia, F. G., van Ginkel, K. C. H., & Jansen, D. (2023). Floods and financial stability: Scenario-based evidence from below sea level (DNB Working Paper No. 796).

Callahan, C. W., & Mankin, J. S. (2023). Persistent Effect of El Niño on Global Economic Growth. *Science*, *380*(6649), 1064–1069.

Carleton, T., & Hsiang, S. (2016). Social and Economic Impacts of Climate. *Science*, *353*(6304), aad9837.

Carleton, T., Jina, A., Delgado, M., Greenstone, M., Houser, T., Hsiang, S., Hultgren, A., Kopp, R. E., McCusker, K. E., Nath, I., Rode, A., Sharman, N., Rising, J., & Yuan, J. (2022). Valuing the Global Mortality Consequences of Climate Change Accounting for Adaptation Costs and Benefits. *The Quarterly Journal of Economics*, *137*(4), 2037–2105.

Chudik, A., Pesaran, M. H., & Yang, J.-C. (2018). Half-Panel Jackknife Fixed-Effects Estimation of Linear Panels with Weakly Exogenous Regressors. *Journal of Applied Econometrics*, *33*(6), 816–836.

Cunningham, C. X., Williamson, G. J., & Bowman, D. M. J. S. (2024). Increasing frequency and intensity of the most extreme wildfires on Earth. *Nature Ecology & Evolution*, *8*, 1420–1425. https://doi.org/10.1038/s41559-024-02452-2

de Bruijn, K., Wagenaar, D., Slager, K., de Bel, M., Burzel, A., Beckers, J., Bouwer, L., & Diermanse, F. (2015). Updated and improved method for flood damage assessment: SSM2015 (version 2) (pp. 115).

de Moel, H., Endendijk, T., van Ederen, D., Juch, S., & van Ginkel, K. (2025). Gebruik van de schadefunctie overstromingsschade residentieel vastgoed door de financiële sector (Deltares rapport 11211522-004). Deltares, Vrije Universiteit & Achmea.

Dell, M., Jones, B., & Olken, B. (2014). What Do We Learn From the Weather? The New Climate-Economy Literature. *Journal of Economic Literature*, *52*(3), 740–98.

Di Sante, F., Coppola, E., & Giorgi, F. (2021). Projections of river floods in Europe using EURO-CORDEX, CMIP5 and CMIP6 simulations. *International Journal of Climatology*, *41*(5), 3203–3221. https://doi.org/10.1002/joc.7014

Dorph, A., Marshall, E., Parkins, K. A., & Penman, T. D. (2022). Modelling ignition probability for human and lightning-caused wildfires in Victoria, Australia. *Natural Hazards and Earth System Sciences*, *22*, 3487–3499. https://doi.org/10.5194/nhess-22-3487-2022

Dulin, S., Smith, M., Ellinport, B., Carr, J., Chu, J., Afshan, S., Lohadefsky, S., Lin, H., Kumar, M., & Sahin, N. (2025). Quantifying the compounding effects of natural hazard events: a case study on wildfires and floods in California. *npj Natural Hazards*, *2*, 40. https://doi.org/10.1038/s44304-025-00090-7

Endendijk, T., Botzen, W. W., de Moel, H., Aerts, J. C., Slager, K., & Kok, M. (2023). Flood vulnerability models and household flood damage mitigation measures: An econometric analysis of survey data. *Water Resources Research*, *59*(8), e2022WR034192.

Endendijk, T., Botzen, W. W., De Moel, H., Aerts, J. C., Duijndam, S. J., Slager, K., & Kok, M. (2023). Experience from the 2021 floods in the Netherlands: household survey results on impacts and responses. *Journal of Coastal and Riverine Flood Risk*, *2*. https://doi.org/10.59490/jcrfr.2023.0009

Endendijk, T., Botzen, W. W., de Moel, H., Slager, K., Kok, M., & Aerts, J. C. (2024). Enhancing resilience: Understanding the impact of flood hazard and vulnerability on business interruption and losses. *Water Resources and Economics*, *46*, 100244.

European Banking Authority. (2023). 2023 EU-wide stress test: results. July 28, 2023.

European Environment Agency. (2016). EU-DEM: Digital Elevation Model [Data set]. Copernicus Programme. https://ec.europa.eu/eurostat/web/gisco/geodata/digital-elevation-model/eu-dem

European Environment Agency. (2020). CORINE Land Cover 2018 (raster 100 m), Europe, 6-yearly [Data set]. Copernicus Programme. https://doi.org/10.2909/960998c1-1870-4e82-8051-6485205ebbac

European Environment Agency. (2024). European Climate Risk Assessment (EEA Report No. 01/2024). Publications Office of the European Union. https://www.eea.europa.eu/en/analysis/publications/european-climate-risk-assessment. https://doi.org/10.2800/204249

Fan, X., Chen, Y., Zhang, Q., Zhang, D., Fu, K., Burrows, A. S., & Li, D. (2023). Escalating hot–dry extremes amplify compound fire weather. *Earth's Future*, *11*(9), e2023EF003825. https://doi.org/10.1029/2023EF003825

Fan, X., Zscheischler, J., Seneviratne, S. I., & Li, D. (2023). Escalating hot-dry extremes amplify compound fire weather risk. *Earth's Future*, *11*(8), e2023EF003976. https://doi.org/10.1029/2023EF003976

Farid, A., Alam, M. K., Goli, V. S. N. S., Akin, I. D., Akinleye, T., Chen, X., Cheng, Q., Cleall, P., Cuomo, S., Foresta, V., Guo, W., Goharipour, H. R., Ke, Y., Lai, S., Liu, X., Mayorga, L., Miao, Y., Mohammadi, S., Olarinoye, T., ... Singh, K. (2024). A review of the occurrence and causes for

wildfires and their impacts on the geoenvironment. *Fire*, *7*, 295. https://doi.org/10.3390/fire7080295

Hallema, D. W., Robinne, F.-N., & Bladon, K. D. (2018). Reframing the challenge of global wildfire threats to water supplies. *Earth's Future*, *6*(6), 772–776. https://doi.org/10.1029/2018EF000867

Hoffmann, P., Reinhart, V., & Rechid, D. (2022). LUCAS LUC future land use and land cover change dataset for Europe (Version 1.1) [Data set]. https://doi.org/10.26050/WDCC/LUC_future_EU_v1.1

Hoffmann, P., Reinhart, V., Rechid, D., de Noblet-Ducoudré, N., Davin, E. L., Asmus, C., Bechtel, B., Böhner, J., Katragkou, E., & Luyssaert, S. (2023). High-resolution land use and land cover dataset for regional climate modelling: Historical and future changes in Europe. *Earth System Science Data*, *15*, 3819–3852. https://doi.org/10.5194/essd-15-3819-2023

Hsiang, S. (2016). Climate Econometrics. *Annual Review of Resource Economics*, *8*, 43–75.

Hudson, P., Botzen, W. W., & Aerts, J. C. (2019). Flood insurance arrangements in the European Union for future flood risk under climate and socioeconomic change. *Global Environmental Change*, *58*, 101966.

Hurtt, G. C., Chini, L., Sahajpal, R., Frolking, S., Bodirsky, B. L., Calvin, K., Doelman, J. C., Fisk, J., Fujimori, S., Klein Goldewijk, K., Hasegawa, T., Havlik, P., Heinimann, A., Humpenöder, F., Jungclaus, J., Kaplan, J. O., Kennedy, J., Krisztin, T., Lawrence, D., ... Zhang, X. (2020). Harmonization of global land use change and management for the period 850–2100 (LUH2) for CMIP6. *Geoscientific Model Development*, *13*, 5425–5464. https://doi.org/10.5194/gmd-13-5425-2020

Jacob, D., Teichmann, C., Sobolowski, S., Bissolli, P., Christensen, O. B., Feldmann, H., Nikulin, G., Bülow, K., Modali, K., & Vautard, R. (2020). Regional climate downscaling over Europe: Perspectives from the EURO-CORDEX community. *Regional Environmental Change*, *20*(51). https://doi.org/10.1007/s10113-020-01606-9

Joint Research Centre. (n.d.). Annual Regional Database of the European Commission (ARDECO) (No. 2025.04; Version 2025.04) [Dataset]. Retrieved September 26, 2025, from https://territorial.ec.europa.eu/ardeco/explorer

Jones-Ngo, C. G., Liu, J. C., & Mickley, L. J. (2025). Increasing exposures to compound wildfire smoke and extreme heat hazards in California (2011–2020). *Earth's Future*, *13*(5), e2024EF005189. https://doi.org/10.1029/2024EF005189

Jordà, Ò. (2005). Estimation and Inference of Impulse Responses by Local Projections. *American Economic Review*, *95*(1), 161–182.

Jordà, Ò., & Taylor, A. M. (2025). Local projections. *Journal of Economic Literature*, *63*(1), 59-110.

Klein Goldewijk, K., Beusen, A., Van Drecht, G., & De Vos, M. (2011). The HYDE 3.1 spatially explicit database of human-induced global land-use change over the past 12,000 years. *Global Ecology and Biogeography*, *20*(1), 73–86. https://doi.org/10.1111/j.1466-8238.2010.00587.x

Kolen, B., & Nicolai, R. (2025). New framework to generate event set for risk based spatial planning and financial decisions for Dutch Flood. *Journal of Coastal and Riverine Flood Risk*, *4*.

Kolstad, C., & Moore, F. (2020). Estimating the Economic Impacts of Climate Change Using Weather Observations. *Review of Environmental Economics and Policy*, *14*(1), 1–24.

Konapala, G., Mishra, A., Wada, Y., & Mann, M. (2020). Climate Change Will Affect Global Water Availability Through Compounding Changes in Seasonal Precipitation and Evaporation. *Nature Communications*, *11*(1), 1–10.

Krichene, H., Vogt, T., Piontek, F., Geiger, T., Schötz, C., & Otto, C. (2023). The social costs of tropical cyclones. *Nature Communications*, *14*(1), Article 1. https://doi.org/10.1038/s41467-023-43114-4

Kumar, M., & Collins, M. (2025). Compounding effects of climate change and WUI expansion quadruple the likelihood of extreme-impact wildfires in California. *npj Natural Hazards*, *1*, Article 67. https://doi.org/10.1038/s44304-025-00067-6

Lange, S., & Büchner, M. (2021). ISIMIP3b bias-adjusted atmospheric climate input data (Version 1.1) [Dataset]. ISIMIP Repository. https://doi.org/10.48364/ISIMIP.842396.1

Lenzen, M., Kanemoto, K., Moran, D., & Geschke, A. (2012). Mapping the Structure of the World Economy. *Environmental Science & Technology*, *46*(15), 8374–8381.

Lenzen, M., Moran, D., Kanemoto, K., & Geschke, A. (2013). Building Eora: A Global Multi-Region Input–Output Database at High Country and Sector Resolution. *Economic Systems Research*, *25*(1), 20–49.

Lepore, C., & Mok, J. (2024). Beyond the dikes: flood scenarios for financial stability risk analysis (International Monetary Fund Working Paper No. 2024/197). https://doi.org/10.5089/9798400289545.001

LIWO [Landelijk Informatiepunt Water en Overstromingen]. (2024). Kaarten. URL https://basisinformatie-overstromingen.nl

Lundberg, S. M., & Lee, S.-I. (2017). A unified approach to interpreting model predictions. *Advances in Neural Information Processing Systems*, *30*, 4765–4774.

MacKinnon, J. G., Nielsen, M. Ø., & Webb, M. D. (2023). Fast and Reliable Jackknife and Bootstrap Methods for Cluster-Robust Inference. *Journal of Applied Econometrics*, *38*(5), 671–694.

Marbler, A. (2022). Agriculture Drives the Effect of Rainfall on Economic Production. Available at SSRN. https://dx.doi.org/10.2139/ssrn.4459158

Marbler, A. (2024). Water Scarcity and Local Economic Activity: Spatial Spillovers and the Role of Irrigation. *Journal of Environmental Economics and Management*, *124*, 102931.

Mauritsen, T., Bader, J., Becker, T., Behrens, J., Bittner, M., Brokopf, R., Brovkin, V., Claussen, M., Crueger, T., Esch, M., Fast, I., Fiedler, S., Fläschner, D., Gayler, V., Giorgetta, M., Goll, D. S., Haak, H., Hagemann, S., Hedemann, C., ... Marotzke, J. (2019). Developments in the MPI-M Earth System Model version 1.2 (MPI-ESM1.2) and its response to increasing CO_2. *Journal*

of Advances in Modeling Earth Systems, *11*(4), 998–1038. https://doi.org/10.1029/2018MS001400

Milanovic, S., Milanovic, S. D., Markovic, N., Pamucar, D., Gigovic, L., & Kostic, P. (2021). Forest fire probability mapping in Eastern Serbia: Logistic regression versus random forest method. *Forests*, *12*, 1–17. https://doi.org/10.3390/f12010005

Miller, S., Chua, K., Coggins, J., & Mohtadi, H. (2021). Heat Waves, Climate Change, and Economic Output. *Journal of the European Economic Association*, *19*(5), 2658–2694.

Müller Schmied, H., Trautmann, T., Ackermann, S., Cáceres, D., Flörke, M., Gerdener, H., Kynast, E., Peiris, T. A., Schiebener, L., Schumacher, M., & Döll, P. (2024). The global water resources and use model WaterGAP v2.2e: Description and evaluation of modifications and new features. *Geoscientific Model Development*, *17*(23), 8817–8852. https://doi.org/10.5194/gmd-17-8817-2024

Muñoz-Sabater, J., Dutra, E., Agustí-Panareda, A., Albergel, C., Arduini, G., Balsamo, G., Boussetta, S., Choulga, M., Harrigan, S., Hersbach, H., Martens, B., Miralles, D. G., Piles, M., Rodríguez-Fernández, N. J., Zsoter, E., Buontempo, C., & Thépaut, J. N. (2021). ERA5-Land: A state-of-the-art global reanalysis dataset for land applications. *Earth System Science Data*, *13*(9), 4349–4383. https://doi.org/10.5194/essd-13-4349-2021

O'Neill, B., van Aalst, M., Ibrahim, Z. Z., Berrang Ford, L., Bhadwal, S., Buhaug, H., Diaz, D., Frieler, K., Garschagen, M., Magnan, A., Midgley, G., Mirzabaev, A., Thomas, A., & Warren, R. (2022). Key risks across sectors and regions. In H.-O. Pörtner, D. C. Roberts, M. M. B. Tignor, E. S. Poloczanska, K. Mintenbeck, A. Alegría, M. Craig, S. Langsdorf, S. Löschke, V. Möller, A. Okem, & B. Rama (Eds.), *Climate Change 2022: Impacts, Adaptation and Vulnerability. Contribution of Working Group II to the Sixth Assessment Report of the Intergovernmental Panel on Climate Change*. Cambridge University Press.

Oki, T., & Kanae, S. (2006). Global Hydrological Cycles and World Water Resources. *Science*, *313*(5790), 1068–1072.

Oliveira, S., Oehler, F., San-Miguel-Ayanz, J., Camia, A., & Pereira, J. M. (2012). Modeling spatial patterns of fire occurrence in Mediterranean Europe using multiple regression and random forest. *Forest Ecology and Management*, *275*, 117–129. https://doi.org/10.1016/j.foreco.2012.03

Olonscheck, D., Suarez-Gutierrez, L., Milinski, S., Beobide-Arsuaga, G., Baehr, J., Fröb, F., Kadow, C., Kirchner, I., Li, H., Marotzke, J., Müller, W. A., Notz, D., Pfahl, S., Pongratz, J., Putrasahan, D. A., Roberts, C. D., von Storch, J., Tian, F., Wiedermann, M., ... Dobrynin, M. (2023). The new Max Planck Institute grand ensemble with CMIP6 forcing and high-frequency model output. *Journal of Advances in Modeling Earth Systems*, *15*(10), e2023MS003790. https://doi.org/10.1029/2023MS003790

Paprotny, D. (2023). Pan-European exposure maps and uncertainty estimates from HANZE v2.0 model, 1870-2020 (Version v2.0.3) [Dataset]. Zenodo. https://doi.org/10.5281/ZENODO.6783201

Paprotny, D. (2024). Flood protection and vulnerability estimates for Europe, 1950-2020 [Dataset]. Zenodo. https://doi.org/10.5281/zenodo.10911302

Paprotny, D., 't Hart, C. M. P., & Morales-Nápoles, O. (2025). Evolution of flood protection levels and flood vulnerability in Europe since 1950 estimated with vine-copula models. *Natural Hazards*, *121*(5), 6155–6184. https://doi.org/10.1007/s11069-024-07039-5

Paprotny, D., Tilloy, A., Treu, S., Buch, A., Vousdoukas, M. I., Feyen, L., Kreibich, H., Merz, B., Frieler, K., & Mengel, M. (2025). Attribution of flood impacts shows strong benefits of adaptation in Europe since 1950. *Science Advances*, *11*(33), eadt7068. https://doi.org/10.1126/sciadv.adt7068

Paudel, Y., Botzen, W. J. W., Aerts, J. C. J. H., & Dijkstra, T. K. (2015). Risk allocation in a public–private catastrophe insurance system: an actuarial analysis of deductibles, stop-loss, and premiums. *Journal of Flood Risk Management*, *8*(2), 116-134.

Polash, B. (2022). MODIS-FIRMS and ground-truthing-based wildfire likelihood mapping of Sikkim Himalaya using machine learning algorithms. *Natural Hazards*, *110*, 899–935. https://doi.org/10.1007/s11069-021-04973-6

Richardson, D., Abatzoglou, J. T., & Williams, A. P. (2022). Global increase in wildfire potential from compound fire weather and drought. *npj Climate and Atmospheric Science*, *5*, Article 48. https://doi.org/10.1038/s41612-022-00248-4

Ricke, K., Drouet, L., Caldeira, K., & Tavoni, M. (2018). Country-level social cost of carbon. *Nature Climate Change*, *8*(10), 895–900. https://doi.org/10.1038/s41558-018-0282-y

Robinne, F.-N., Hallema, D. W., Bladon, K. D., Flannigan, M. D., Boisramé, G., Bréthaut, C. M., Doerr, S. H., Di Baldassarre, G., Gallagher, L., Hohner, A. K., Khan, S. J., Kinoshita, A. M., Mordecai, R., Nunes, J. P., Nyman, P., Santín, C., Sheridan, G., Stoof, C. R., Thompson, M. P., ... Wei, Y. (2020). Scientists' warning on extreme wildfire risks to water supply. *Hydrological Processes*, *34*(19), 4048–4053. https://doi.org/10.1002/hyp.13886

Rode, A., Carleton, T., Delgado, M., Greenstone, M., Houser, T., Hsiang, S., Hultgren, A., Jina, A., Kopp, R. E., McCusker, K. E., Nath, I., Rising, J., & Yuan, J. (2021). Estimating a social cost of carbon for global energy consumption. *Nature*, *598*(7880), 308-314.

Roșu, I. A., Mourgela, R. N., Kasoar, M., Hollaway, M., Ban, N. C., Keeble, J. M., Ficus, C. A., Persad, G. G., Schwartz, H., Kumar, S. T., Nelson, B. S., Kipling, Z., Eastham, S. D., Kerr, G. H., Henderson, J., Clifton, O. E., Horton, D. E., & Archibald, A. T. (2025). Large-scale impacts of the 2023 Canadian wildfires on the Northern Hemisphere atmosphere. *npj Clean Air*, *1*, 22. https://doi.org/10.1038/s44407-025-00022-9

Scussolini, P., Aerts, J. C. J. H., Jongman, B., Bouwer, L. M., Winsemius, H. C., de Moel, H., & Ward, P. J. (2016). FLOPROS: An Evolving Global Database of Flood Protection Standards. *Natural Hazards and Earth System Sciences*, *16*(5), 1049–61. doi:10.5194/nhess-16-1049-2016

Schütze, S. J., & Resco de Dios, V. (2025). Increases in the world's most extreme wildfire events probably driven by fire size and simultaneity. *Nature Ecology & Evolution*, *9*, 1345–1348. https://doi.org/10.1038/s41559-025-02742-3

Seneviratne, S. I., Zhang, X., Adnan, M., Badi, W., Dereczynski, C., Di Luca, A., Ghosh, S., Iskandar, I., Kossin, J., Lewis, S., Otto, F., Pinto, I., Satoh, M., Vicente-Serrano, S. M., Wehner, M., & Zhou, B. (2021). Weather and Climate Extreme Events in a Changing Climate. In V. Masson-Delmotte, P. Zhai, A. Pirani, S. L. Connors, C. Péan, S. Berger, N. Caud, Y. Chen, L. Goldfarb, M. I. Gomis, M. Huang, K. Leitzell, E. Lonnoy, J. B. R. Matthews, T. K. Maycock, T. Waterfield, O. Yelekçi, R. Yu, & B. Zhou (Eds.), *Climate Change 2021: The Physical Science Basis. Contribution of Working Group I to the Sixth Assessment Report of the Intergovernmental Panel on Climate Change* (pp. 1513–1766). Cambridge University Press. https://doi.org/10.1017/9781009157896.013

Singer, M. B., Asfaw, D. T., Rosolem, R., Cuthbert, M. O., Miralles, D. G., MacLeod, D., Quichimbo, E. A., & Michaelides, K. (2021). Hourly Potential Evapotranspiration at 0.1° Resolution for the Global Land Surface from 1981-Present. *Scientific Data*, *8*(1), 1–13.

Slager, K., & Wagenaar, D. (2017). Standaardmethode 2017: Schade en slachtoffers als gevolg van overstromingen. Deltares Report 11200580-004.

Society of Actuaries Research Institute. (2024). Compound weather extreme events and their impacts. https://www.soa.org/4ab2fe/globalassets/assets/files/resources/research-report/2024/compound-weather-extreme-events.pdf

Stern, N. (2008). The Economics of Climate Change. *American Economic Review*, *98*(2), 1–37. https://doi.org/10.1257/aer.98.2.1

Sutanto, S. J., van der Weert, M., Vitolo, C., & van Lanen, H. A. J. (2020). Exploring compound and cascading dry hazards at the pan-European scale. *Science of the Total Environment*, *728*, 138548. https://doi.org/10.1016/j.scitotenv.2020.138548

ten Brinke, W. B. M., Kolen, B., Dollee, A., van Waveren, H., & Wouters, K. (2010). Contingency planning for large-scale floods in the Netherlands. *Journal of Contingencies and Crisis Management*, *18*, 55-69.

Tesselaar, M., Botzen, W. W., Haer, T., Hudson, P., Tiggeloven, T., & Aerts, J. C. (2020). Regional inequalities in flood insurance affordability and uptake under climate change. *Sustainability*, *12*(20), 8734.

Van Beek, L. P. H., Wada, Y., & Bierkens, M. F. P. (2011). Global monthly water stress: 1. Water balance and water availability. *Water Resources Research*, *47*(7). https://doi.org/10.1029/2010WR009791

van Der Knijff, J. M., Younis, J., & De Roo, A. P. J. (2010). LISFLOOD: A GIS-based distributed model for river basin scale water balance and flood simulation. *International Journal of Geographical Information Science*, *24*(2), 189–212. https://doi.org/10.1080/13658810802549154

van Dorland, R., Lenderink, G., van den Hurk, B., Ridder, N., van Heerwaarden, C., Schrier, G., Siegmund, P., & Wolters, D. (2023). *KNMI National Climate Scenarios 2023 for The Netherlands*. KNMI, De Bilt.

van Ginkel, K., Caloia, F., & Jansen, D. J. (2023). Overstromingen en financiële stabiliteit in Nederland: een toelichting voor de watersector. https://www.h2owaternetwerk.nl/h2o-podium/uitgelicht/overstromingen-en-financiele-stabiliteit-in-nederland-een-toelichting-voor-de-watersector

van Huijstee, J., van Bemmel, B., Bouwman, A., & van Rijn, F. (2018). *TOWARDS AN URBAN PREVIEW Modelling future urban growth with 2UP Background Report Towards and Urban Preview: Modelling future urban growth with 2UP*. www.pbl.nl/en

Vicente-Serrano, S., Beguería, S., & López-Moreno, J. (2010). A Multiscalar Drought Index Sensitive to Global Warming: The Standardized Precipitation Evapotranspiration Index. *Journal of Climate*, *23*(7), 1696–1718.

Vicente-Serrano, S., Van der Schrier, G., Beguería, S., Azorin-Molina, C., & Lopez-Moreno, J. (2015). Contribution of Precipitation and Reference Evapotranspiration to Drought Indices Under Different Climates. *Journal of Hydrology*, *526*, 42–54.

Volkholz, J., Zimmermann, S., & Hassel, J. (2025). Global projections of fluvial floods based on the ISIMIP3b ensemble of global hydrological models: Flooded area fraction (Version 1.0) [Dataset]. ISIMIP Repository. https://doi.org/10.48364/ISIMIP.294944

Von Peter, G., von Dahlen, S., & Saxena, S. (2024). Unmitigated disasters? Risk sharing and macroeconomic recovery in a large international panel. *Journal of International Economics*, *149*, 103920.

Wagenbrenner, J. W., Ebel, B. A., Bladon, K. D., & Kinoshita, A. M. (2021). Post-wildfire hydrologic recovery in Mediterranean climates: A systematic review and case study to identify current knowledge and opportunities. *Journal of Hydrology*, *602*, 126772. https://doi.org/10.1016/j.jhydrol.2021.126772

Ward, P. J., Jongman, B., Aerts, J. C. J. H., Bates, P. D., Botzen, W. J. W., DIaz Loaiza, A., Hallegatte, S., Kind, J. M., Kwadijk, J., Scussolini, P., & Winsemius, H. C. (2017). A global framework for future costs and benefits of river-flood protection in urban areas. *Nature Climate Change*, *7*(9), 642–646. https://doi.org/10.1038/nclimate3350

Weedon, G. P., Best, M., & Clark, D. B. (n.d.). Changes in land surface model outputs due to uncertainty in the WATCH Forcing Data.

Wenz, L., Carr, R. D., Kögel, N., Kotz, M., & Kalkuhl, M. (2023). DOSE – Global data set of reported sub-national economic output. *Scientific Data*, *10*(1), Article 1. https://doi.org/10.1038/s41597-023-02323-8

Winsemius, H. C., Aerts, J. C. J. H., Van Beek, L. P. H., Bierkens, M. F. P., Bouwman, A., Jongman, B., Kwadijk, J. C. J., Ligtvoet, W., Lucas, P. L., Van Vuuren, D. P., & Ward, P. J. (2016). Global

drivers of future river flood risk. *Nature Climate Change*, *6*(4), 381–385. https://doi.org/10.1038/nclimate2893

Xu, Z., Zhang, Y., Blöschl, G., & Piao, S. (2023). Mega forest fires intensify flood magnitudes in southeast Australia. *Geophysical Research Letters*, *50*, e2023GL103812. https://doi.org/10.1029/2023GL103812

Yamazaki, D., Kanae, S., Kim, H., & Oki, T. (2011). A physically based description of floodplain inundation dynamics in a global river routing model. *Water Resources Research*, *47*(4), 2010WR009726. https://doi.org/10.1029/2010WR009726

Zhai, J., Ning, Z., Dahal, R., & Yang, S. (2023). Wildfire susceptibility of land use and topographic features in the Western United States: Implications for the landscape management. *Forests*, *14*(4), Article 807. https://doi.org/10.3390/f14040807

Zscheischler, J., Westra, S., van den Hurk, B., Seneviratne, S. I., Ward, P. J., Pitman, A., AghaKouchak, A., Bresch, D. N., Leonard, M., Wahl, T., & Zhang, X. (2018). Future climate risk from compound events. *Nature Climate Change*, *8*, 469–477. https://doi.org/10.1038/s41558-018-0156-3

ACCREU Deliverable 2.5 Table of Annexes

Annex A: ACCREU Task 2.5 Description

Task 2.5, Extremes, catastrophic events & supply chains [M6-30] (Lead: PIK, Participants: Deltares, DTU, VU, UNIGRAZ, see D2.5 and Milestone 2.2) will develop pan-European (global) and local, event-based assessments of the impacts of extremes and catastrophic events using two approaches: in a top-down approach, the task will develop event-based damage functions for fluvial floods, and droughts accounting for the direct impacts of these events as well as possible long-term impacts on economic growth needed for the IAM analyses in WP4. A novelty compared to the state-of-the-art is the use of impact indicators (e.g., affected areas or people) derived from ISIMIP impact model runs instead of meteorological indicators (e.g., precipitation and evaporation indices) as predictors, and their statistical link with sub-national GDP panel data (e.g., DOSE dataset). Growth impacts will be firstly estimated separately for each event category and then in combination to highlight potential amplifications in growth losses from consecutive and compound events. In a bottom-up, local event-based assessment of impacts of extreme catastrophic flood scenarios will be conducted (Deltares, VU) by using spatially refined flood risk models (D-HYDRO/SOBEK) and insurance sector modelling (DIFI), offering new insights into distributional aspects of flood risk for the private sector. The analysis will directly inform WP3 adaptation case study CS 5.2. Local, event-based assessment of compound wildfire events will be carried out by using a novel probabilistic version of the ForeFire-Climate model (DTU) to inform case study CS 2.1. T2.5 will assess the indirect impact of extreme events, which are propagated over supply chains, by combining information on input-output linkages of countries' sectors and impact indicators derived from ISIMIP impact model runs. We estimate an econometric model which regresses extreme weather-induced supply chain shocks on national business structure statistics.

Annex B: Impacts of large-scale floods on financial stability

B.1 Damage to all land use categories, and casualties, for land cover exposure in 2014 and in 2022

ID	Total damage 2014	Total damage 2022	Casualties 2022
	million EUR (2011 pricelevel)	*million EUR (2022 pricelevel)*	
578	14274	19646	1564
621	10449	14180	1015
3555	23809	31304	1739
4955	8660	12564	679
5108	16906	21779	1227
11122	17987	25414	1591
13374	13804	17836	1432
13453	4201	6758	449
13550	12923	17230	2146
13753	11040	14589	1261
14185	9092	13546	472
14263	5882	8699	363
15125	4215	5542	1766
15484	3691	4788	10596
15506	6244	7685	784
17975	7535	10423	223
18310	12386	18688	562
19032	13938	18813	1288
19054	28136	39848	1944
19425	18026	24149	1550
19446	8689	11755	456
19562	16894	24811	2294

19623	9966	13522	854
19637	10803	14523	1414
19697	6323	8101	4539
19751	6241	8607	736
20667	25279	34869	1929
20674	30109	38371	1609
20970	22444	31447	1763
20989	5435	7315	581
21059	17666	*	*
21063	4390	5815	347

*This scenario is no longer available in the new database.

B.2 Damage to residential real estate for the exposure in 2014 and 2022

	Residential real estate 2014	**Residential real estate 2022**
	million EUR (2011-pricelevel)	*million EUR (2022-pricelevel)*
578	1197	1653
621	1473	1950
3555	3330	4962
4955	1713	2685
5108	2435	2999
11122	2106	3096
13374	2440	3218
13453	688	1093
13550	2740	3883
13753	1235	1697
14185	620	882
14263	533	772
15125	610	843
15484	1094	1619
15506	1114	1645
17975	520	722
18310	605	846
19032	1509	2187
19054	2904	4420
19425	1998	3005
19446	955	1397
19562	2700	3924
19623	1038	1358
19637	1303	1656
19697	1400	1877
19751	947	1299

20667	2859	4061
20674	2509	3287
20970	3041	4302
20989	1007	1448
21059	3287	0
21063	702	956

B.3 Initial selection of 24 flood scenarios

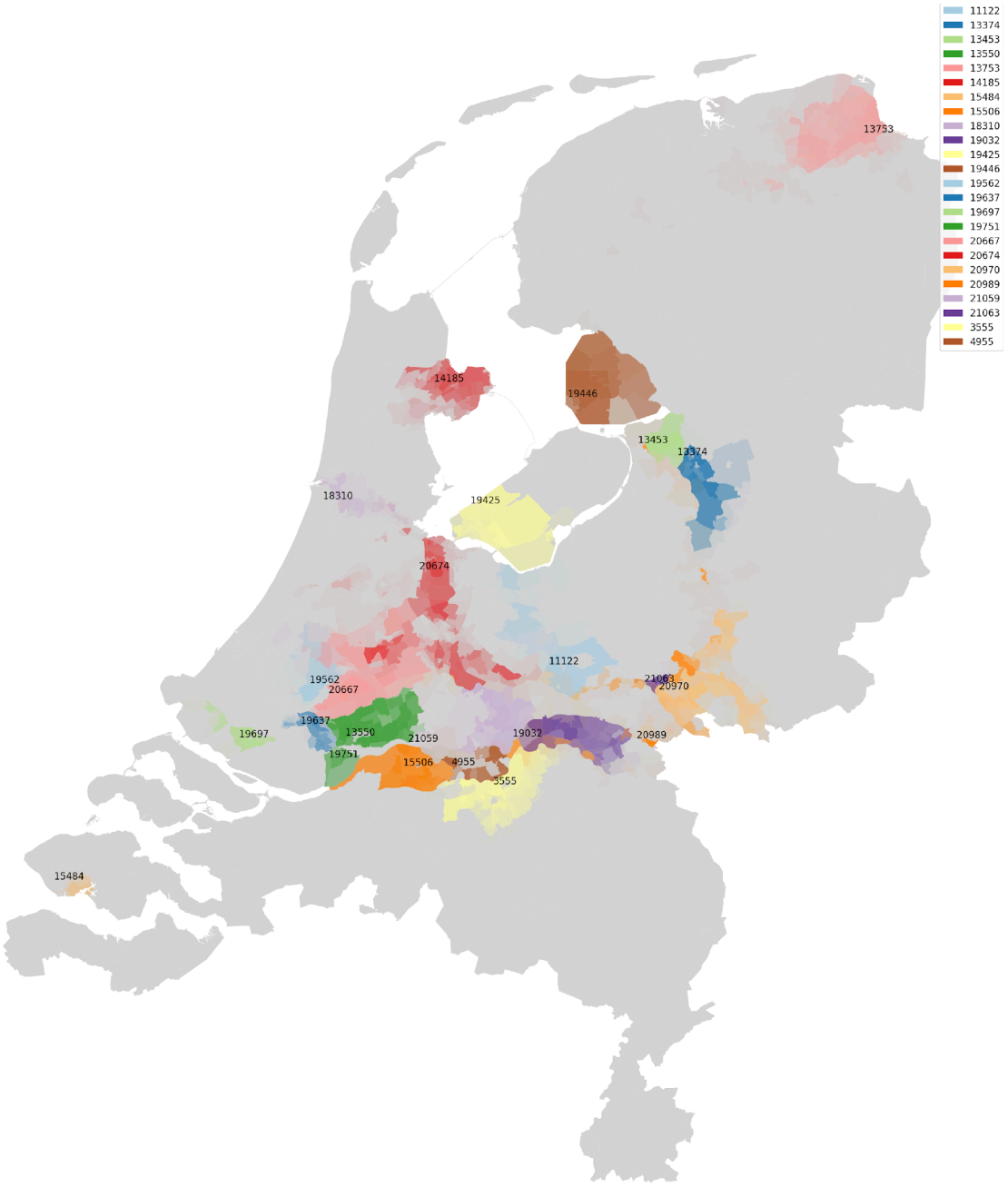

The map shows the initial selection of 24 flood scenarios, each in a different dike ring area.

B.4 Manual addition of 8 flood scenarios

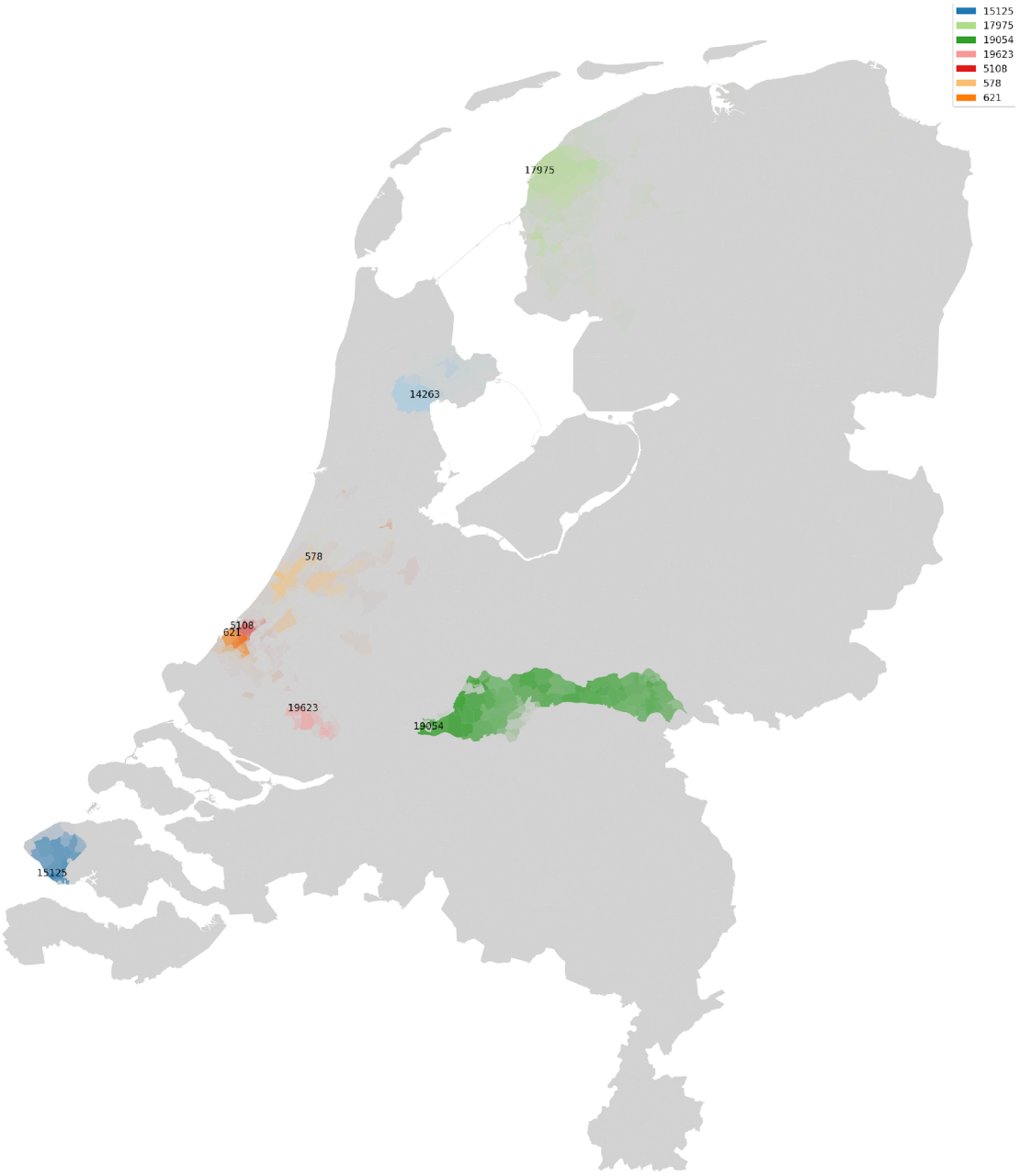

The map shows the manual additions to the initial selection of flood scenarios. These additions hit the real estate in another part of an already selected dike ring. All scenarios cause more than €500 million damage to real estate, for the 2014 land cover in the Netherlands, at 2011-price level.

Annex C: Impacts of flood risk on commercial sector

[to-do VU]

C.1 Item

Annex D: Impacts of floods on long-term economic growth

D.1 Projected GDP per capita time series per NUTS1 region

Projected GDP per capita time series per NUTS1 region for SSP2 and RCP2.6 (green), 7.0 (yellow) and 8.5 (red), as well as two baselines. The no-flood baseline (black) does not include any perturbation of SSP2-GDP and -population projections, while the preindustrial-control baseline (grey) includes the fluvial flood-perturbation caused by preindustrial climate conditions. For perturbed GDP per capita trajectories, the multi-model ensemble mean (across five GCM forcings) per year is plotted. The uncertainty range is defined as the min-max range of the multi-model ensemble and is therefore only present for perturbed trajectories.

GDP per capita projections - SSP2 - NUTS1 (Page 1/6)

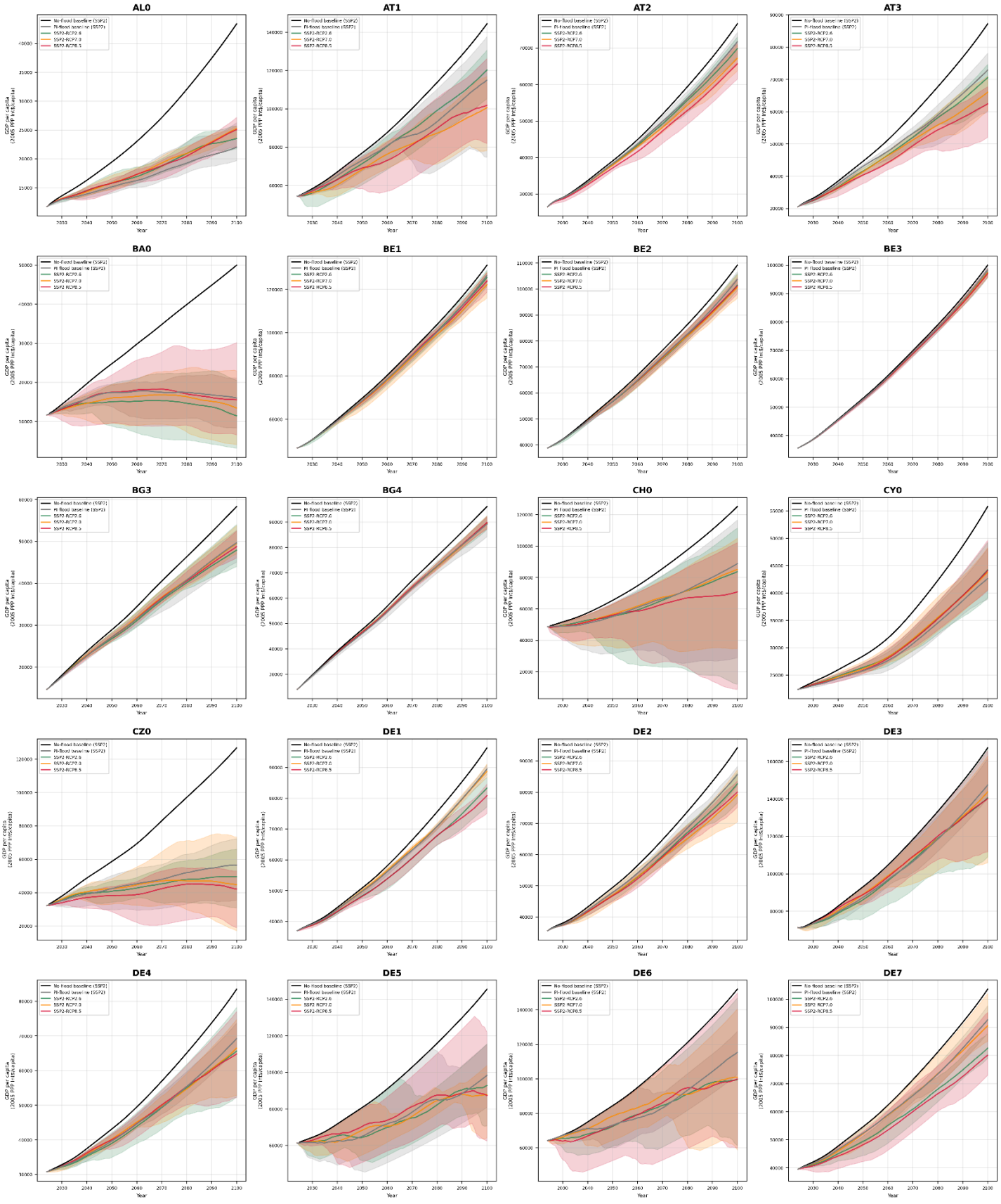

GDP per capita projections - SSP2 - NUTS1 (Page 2/6)

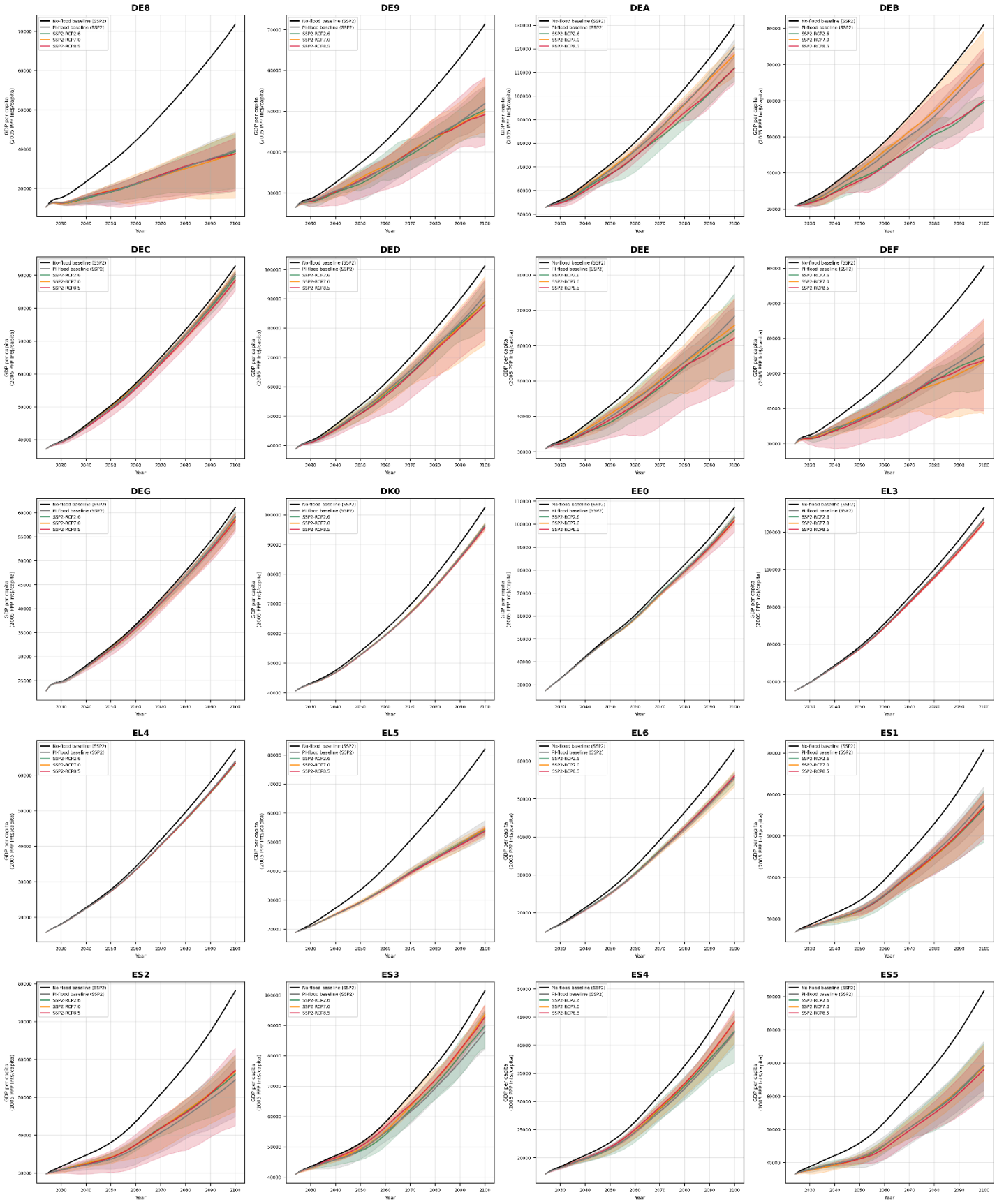

GDP per capita projections - SSP2 - NUTS1 (Page 3/6)

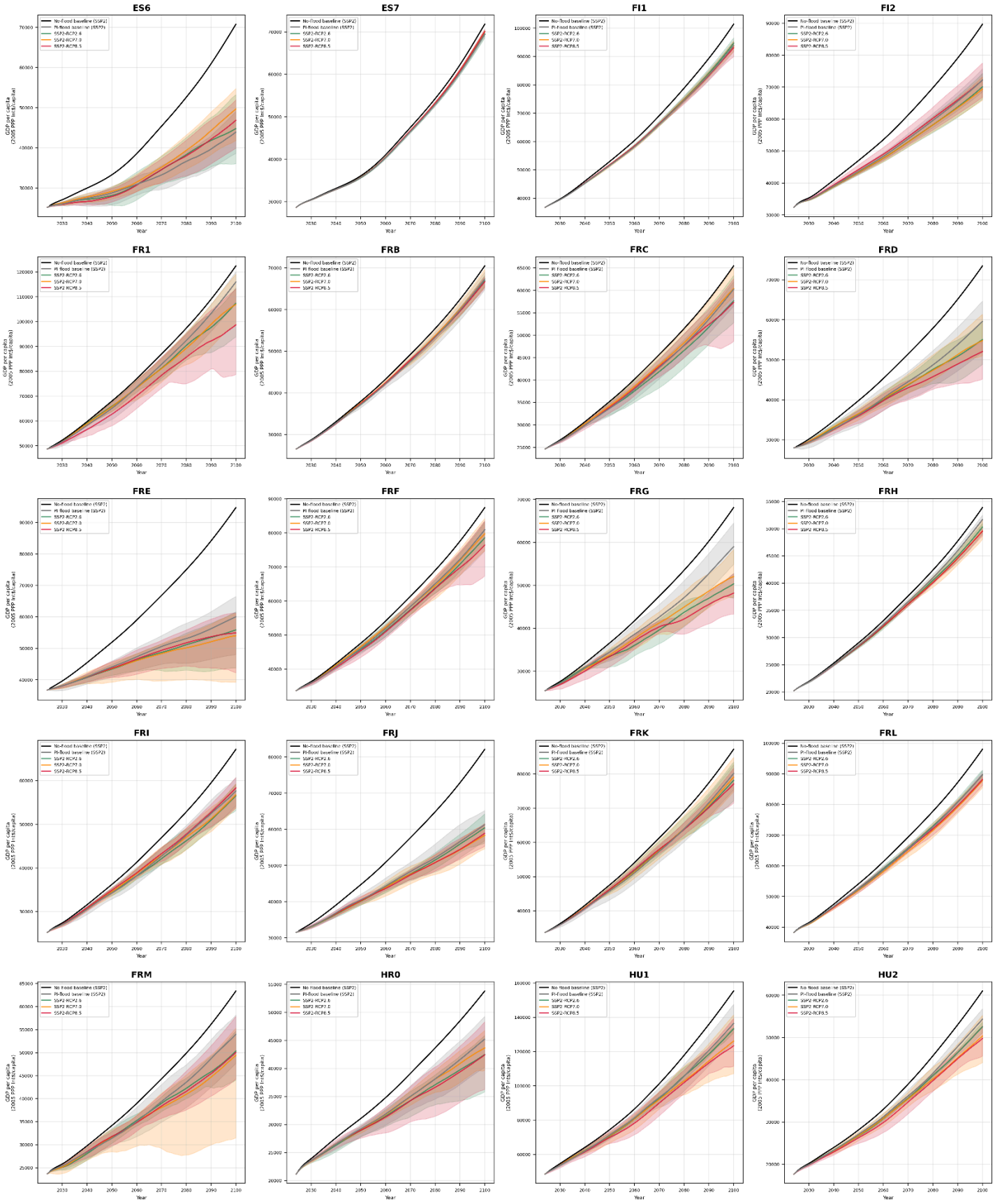

GDP per capita projections - SSP2 - NUTS1 (Page 4/6)

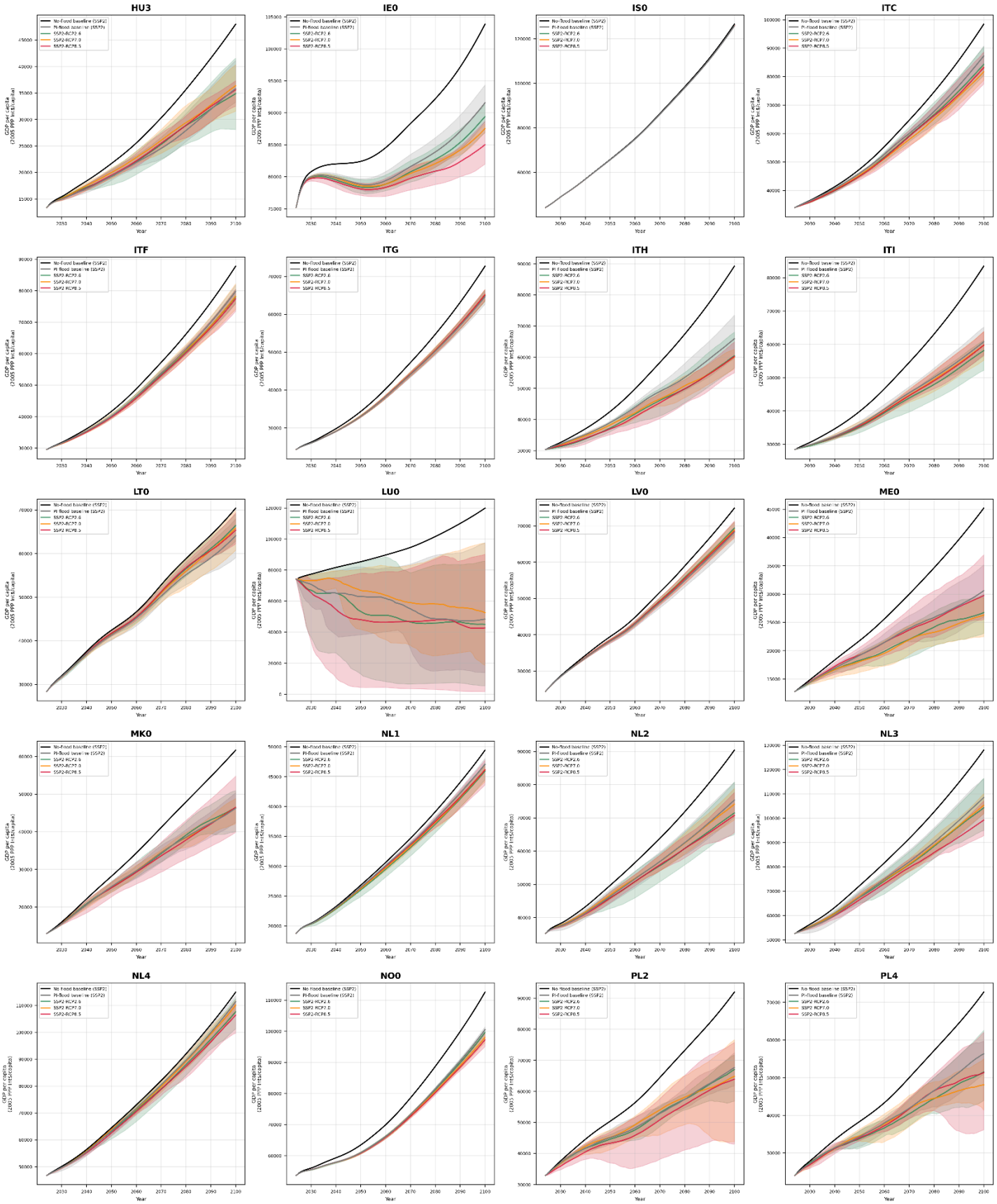

GDP per capita projections - SSP2 - NUTS1 (Page 5/6)

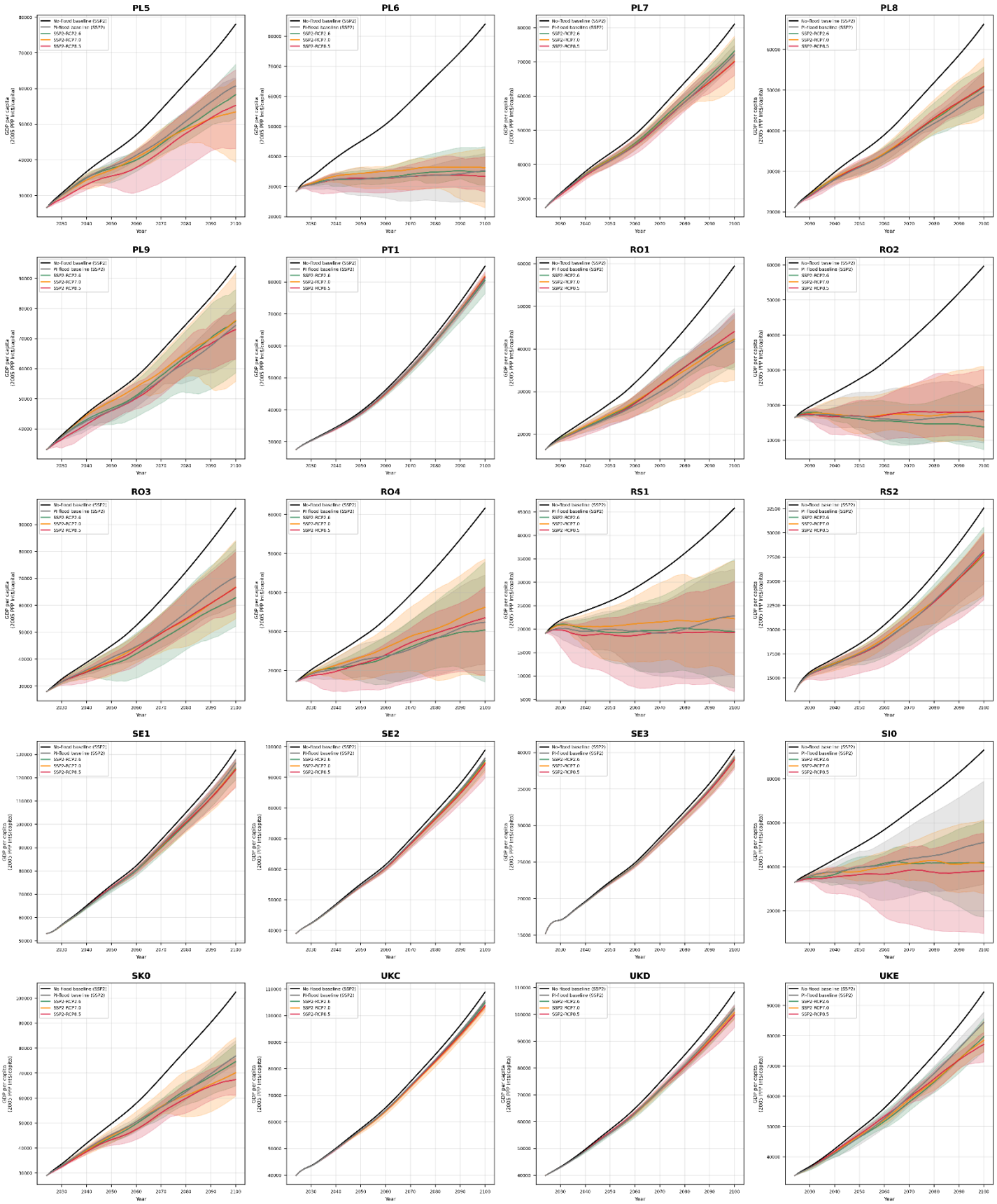

GDP per capita projections - SSP2 - NUTS1 (Page 6/6)

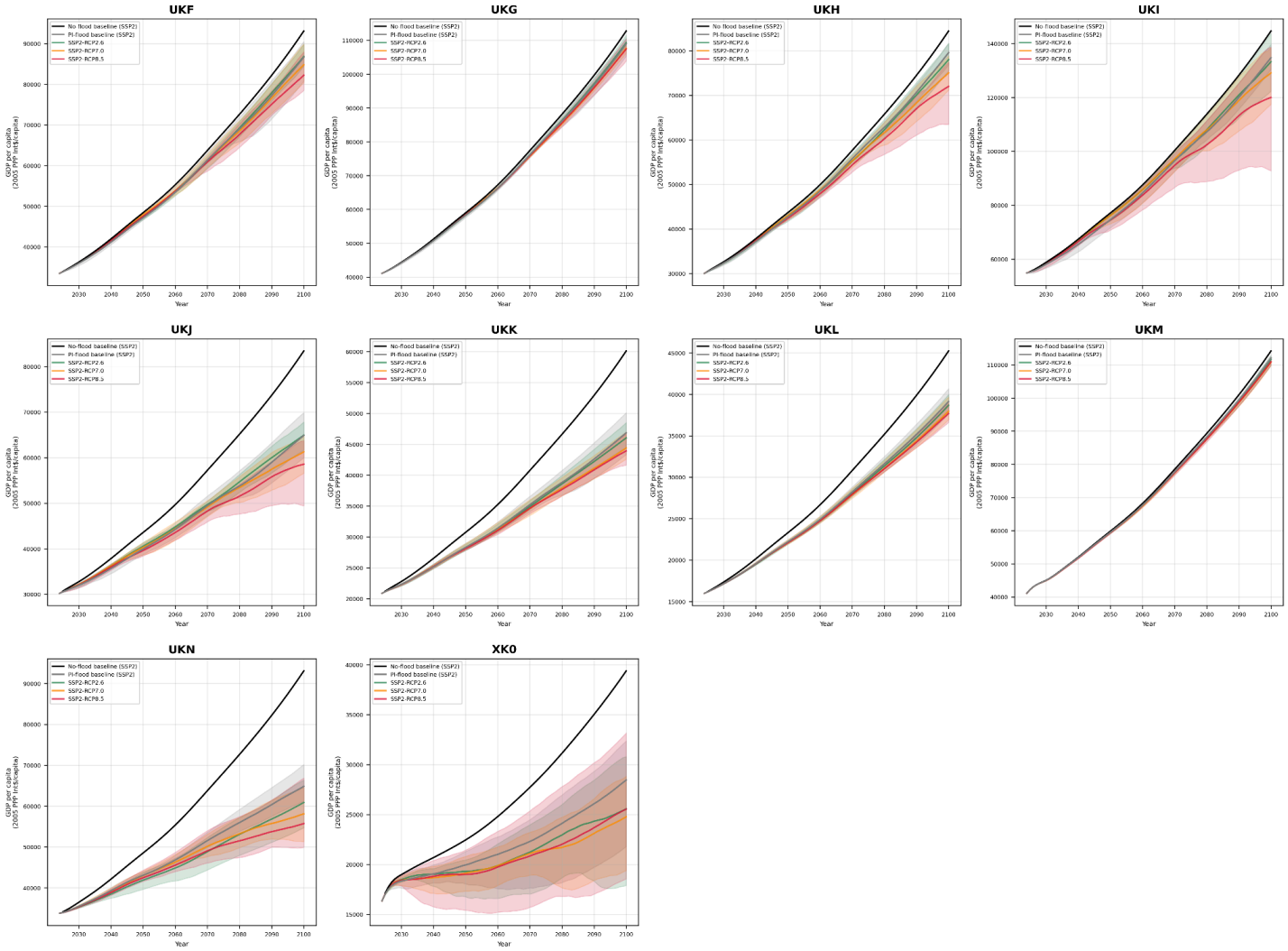

D.2 Projected Discounted Annual Damage time series per NUTS1 region for different discounting choices

Projected Discounted Annual Damage time series per NUTS1 region for SSP2 and RCP2.6 (green), 7.0 (yellow) and 8.5 (red). The values are expressed as a percentage of 2025 GDP per capita and are dependent on the discounting choice: Ricke et al. (2018; ρ=2%, η=1.5; main specification), Nordhaus's DICE model (Nordhaus, 2011; ρ=1.5%, η=1.45) or Stern Review (Stern, 2008; ρ=0.1%, η=1.01). The main curve represents the multi-model ensemble mean (across five GCM forcings) per year. The uncertainty range is defined as the min-max range of the multi-model ensemble.

Discounted Annual Damage as percentage of 2025 GDP per capita - Ricke et al. (2018) discounting - NUTS1 (Page 1/6)

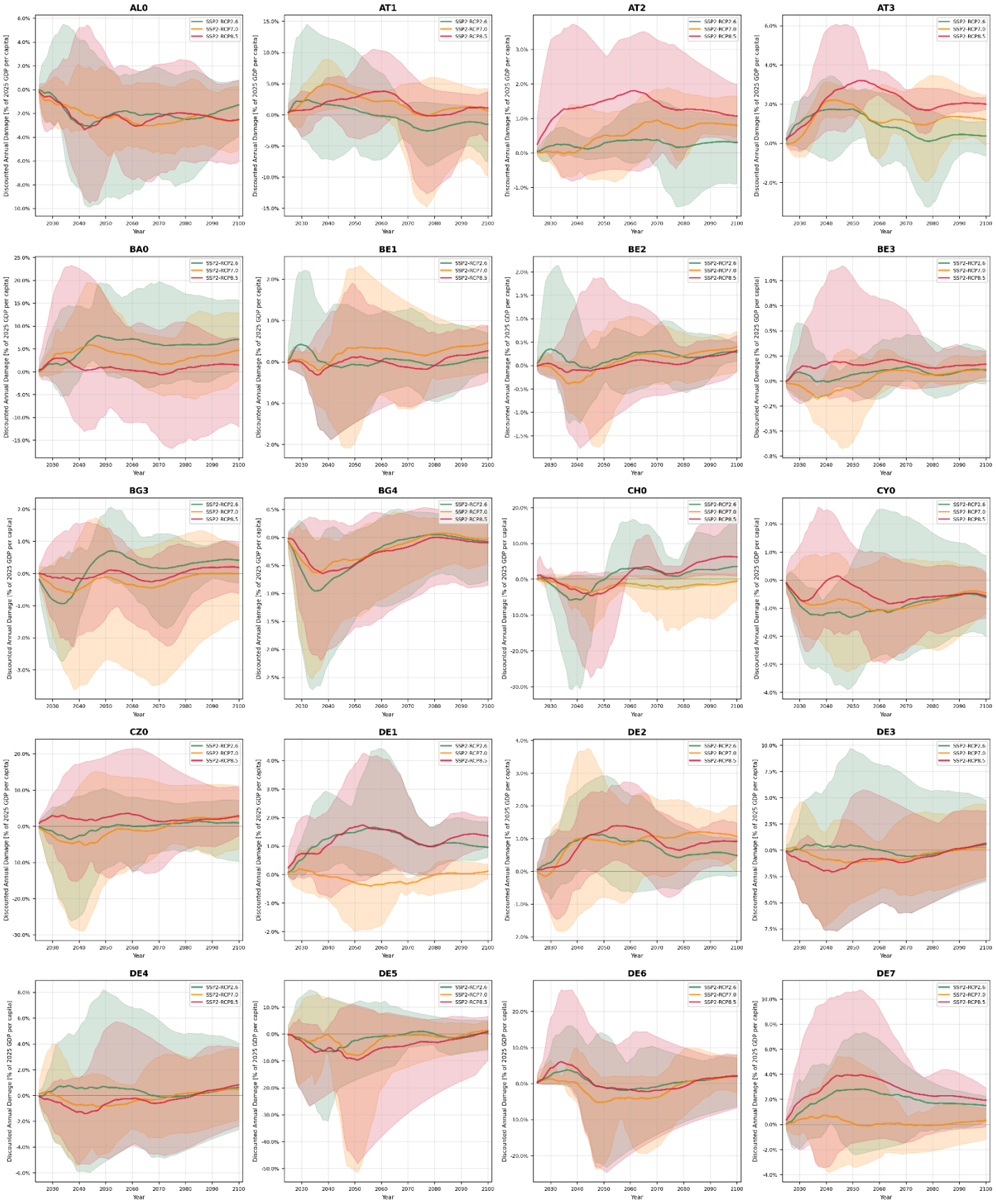

Discounted Annual Damage as percentage of 2025 GDP per capita - Ricke et al. (2018) discounting - NUTS1 (Page 2/6)

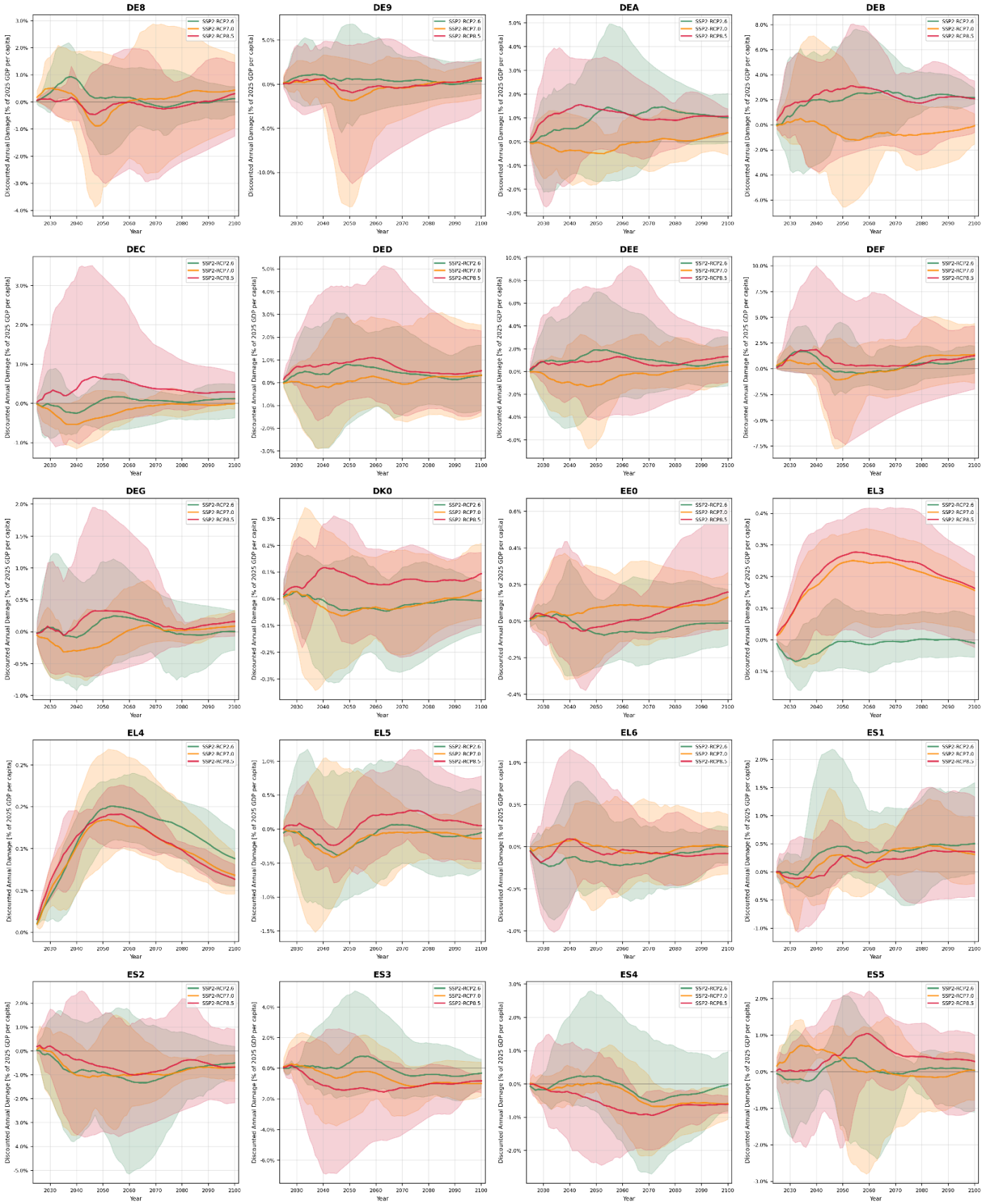

Discounted Annual Damage as percentage of 2025 GDP per capita - Ricke et al. (2018) discounting - NUTS1 (Page 3/6)

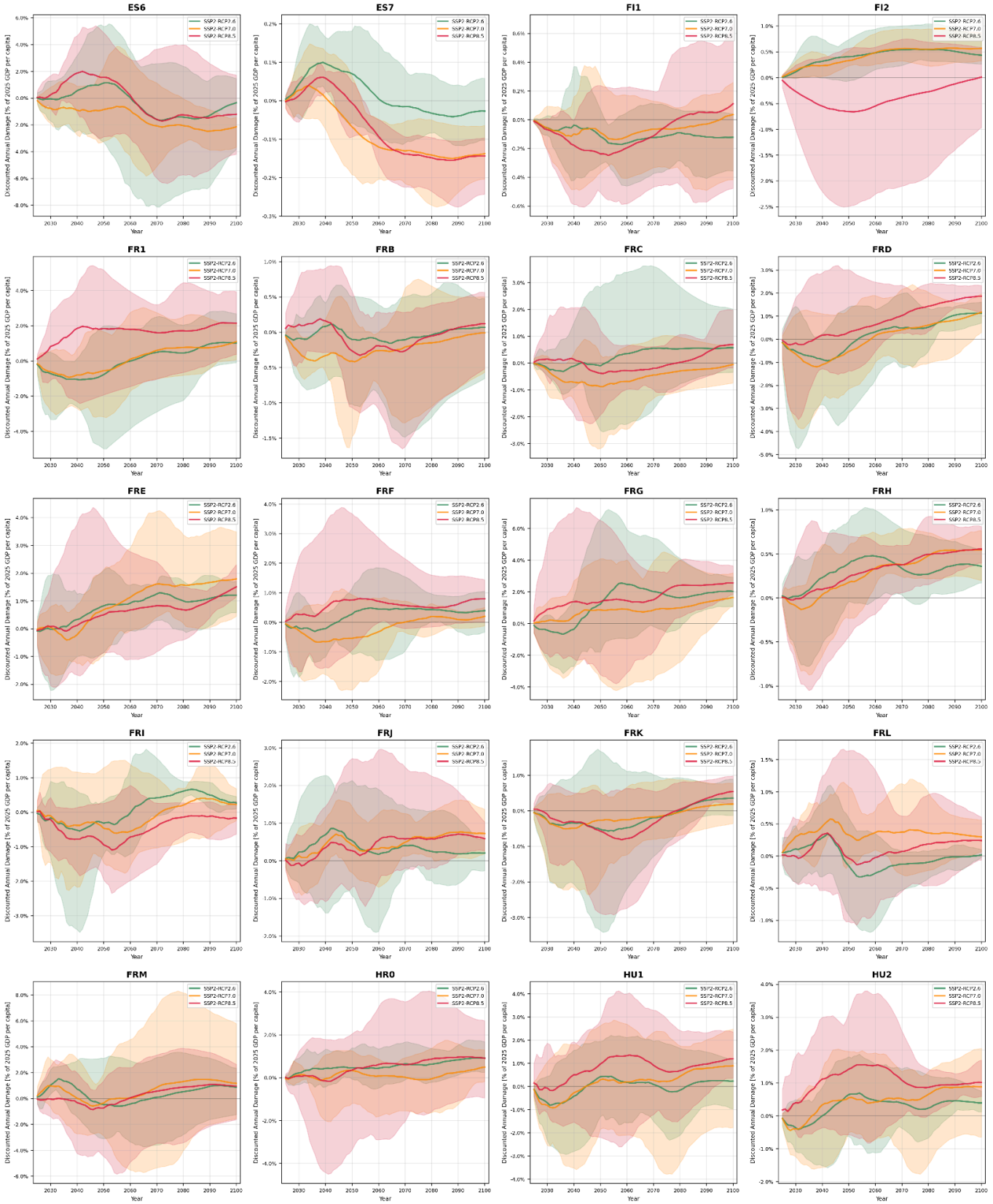

Discounted Annual Damage as percentage of 2025 GDP per capita - Ricke et al. (2018) discounting - NUTS1 (Page 4/6)

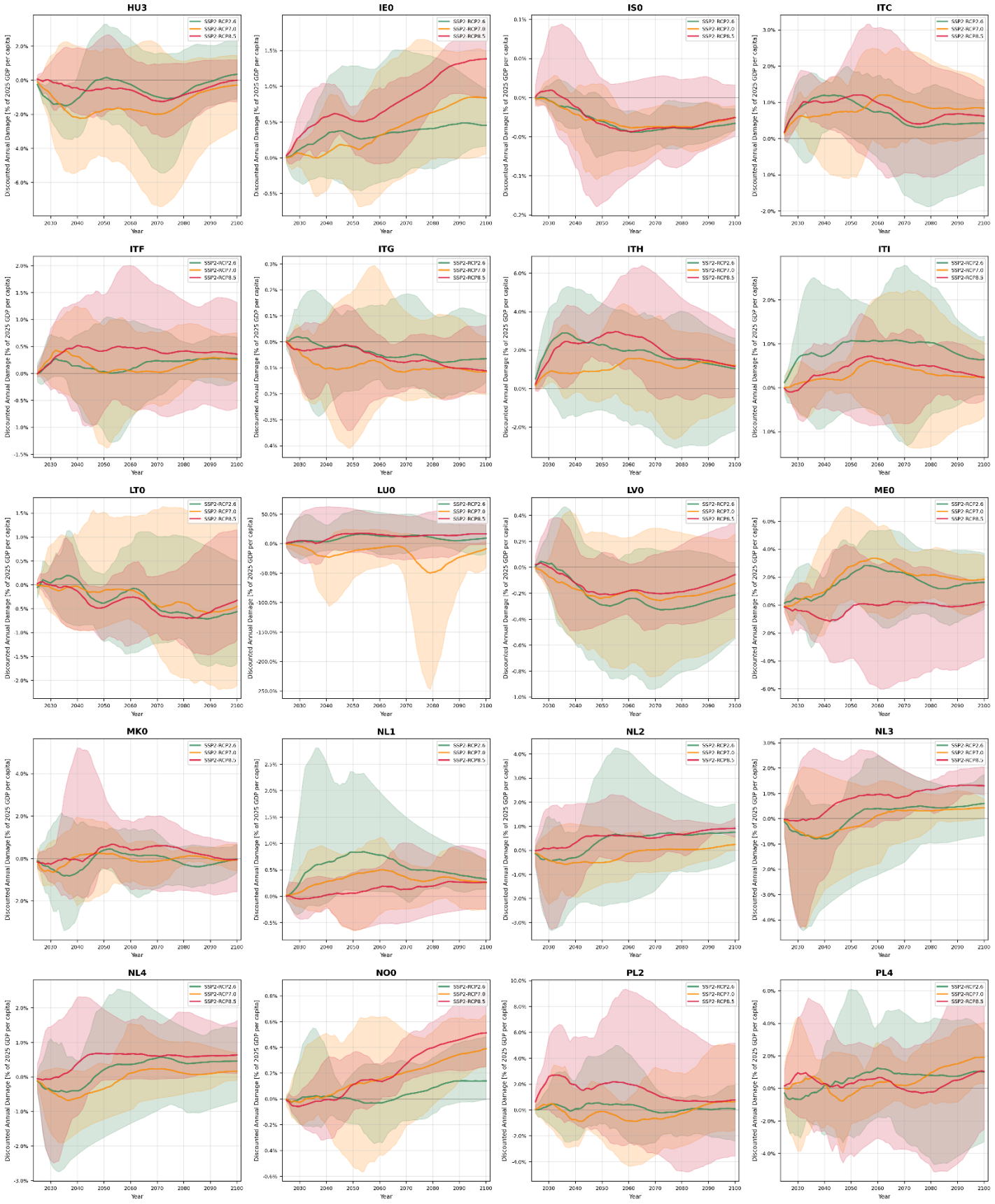

Discounted Annual Damage as percentage of 2025 GDP per capita - Ricke et al. (2018) discounting - NUTS1 (Page 5/6)

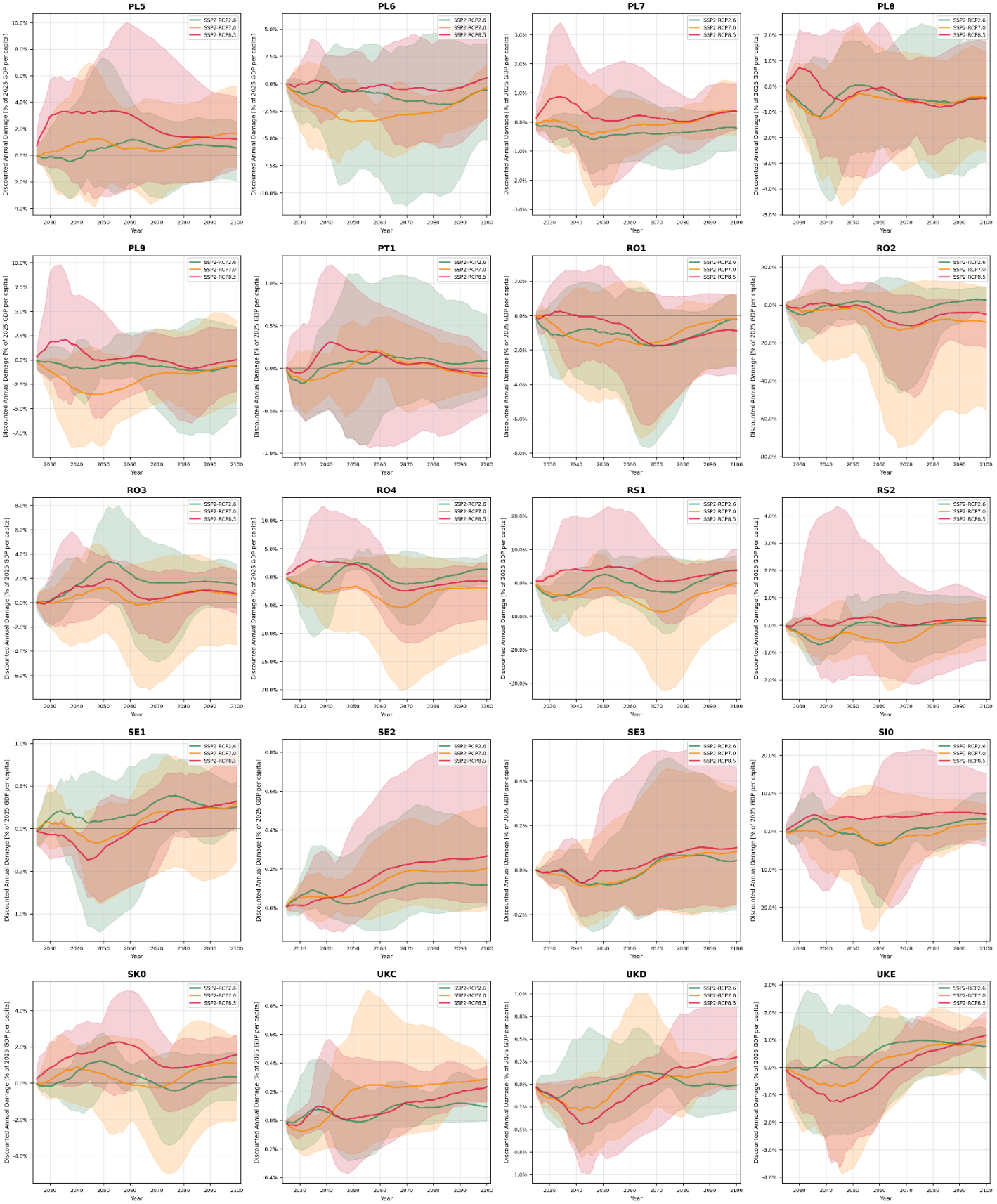

Discounted Annual Damage as percentage of 2025 GDP per capita - Ricke et al. (2018) discounting - NUTS1 (Page 6/6)

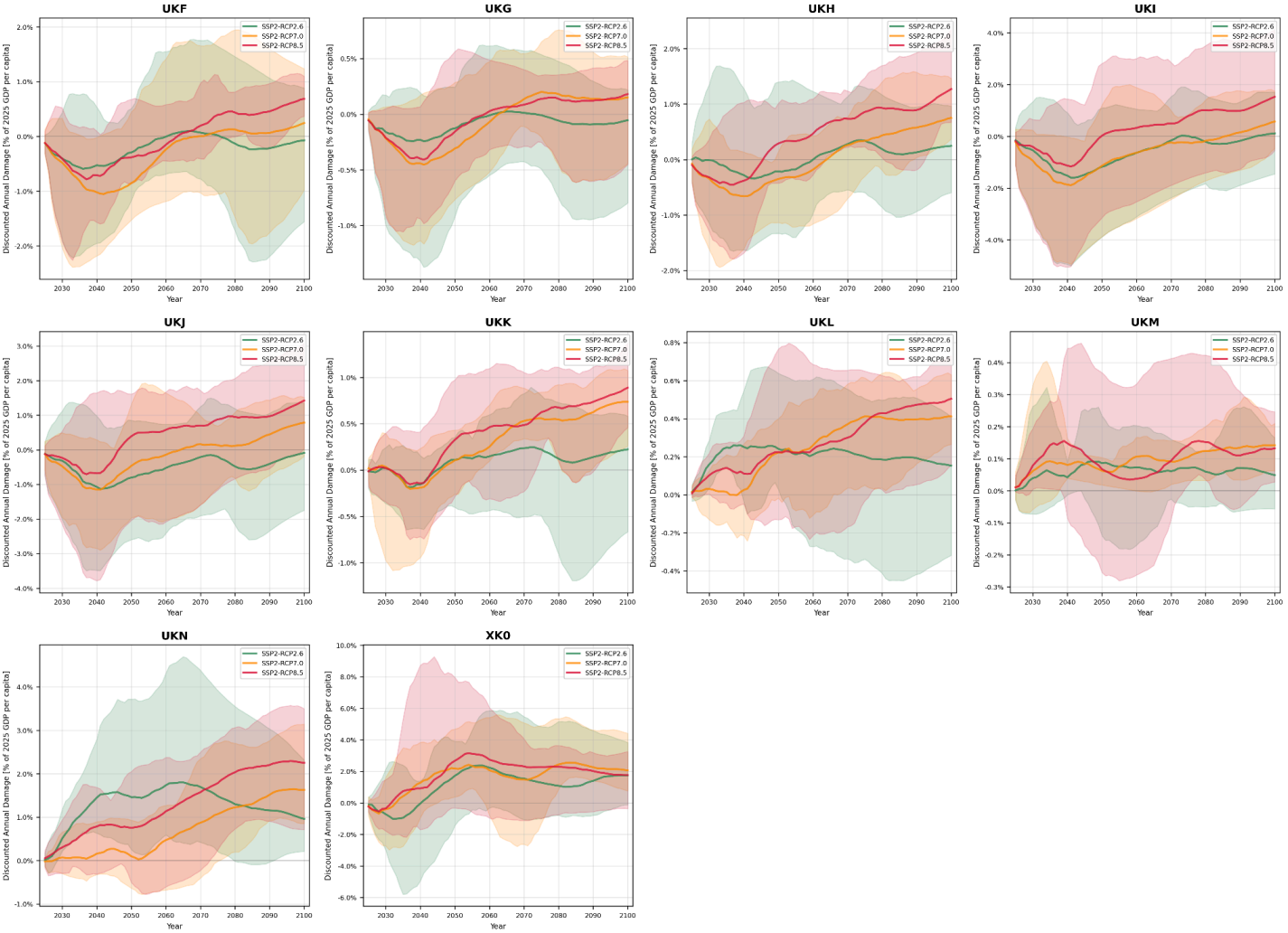

Discounted Annual Damage as percentage of 2025 GDP per capita - Nordhaus DICE model discounting - NUTS1 (Page 1/6)

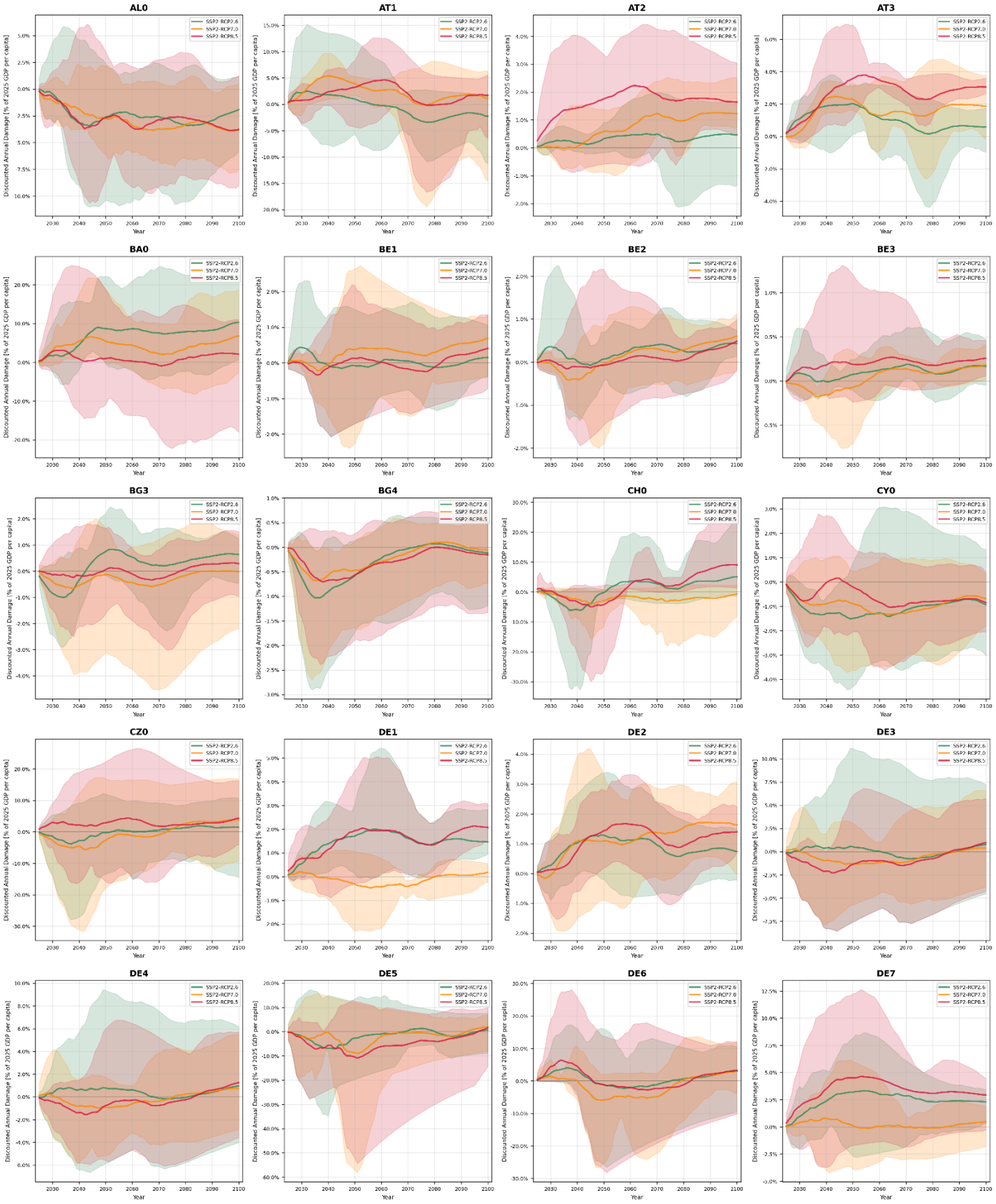

Discounted Annual Damage as percentage of 2025 GDP per capita - Nordhaus DICE model discounting - NUTS1 (Page 2/6)

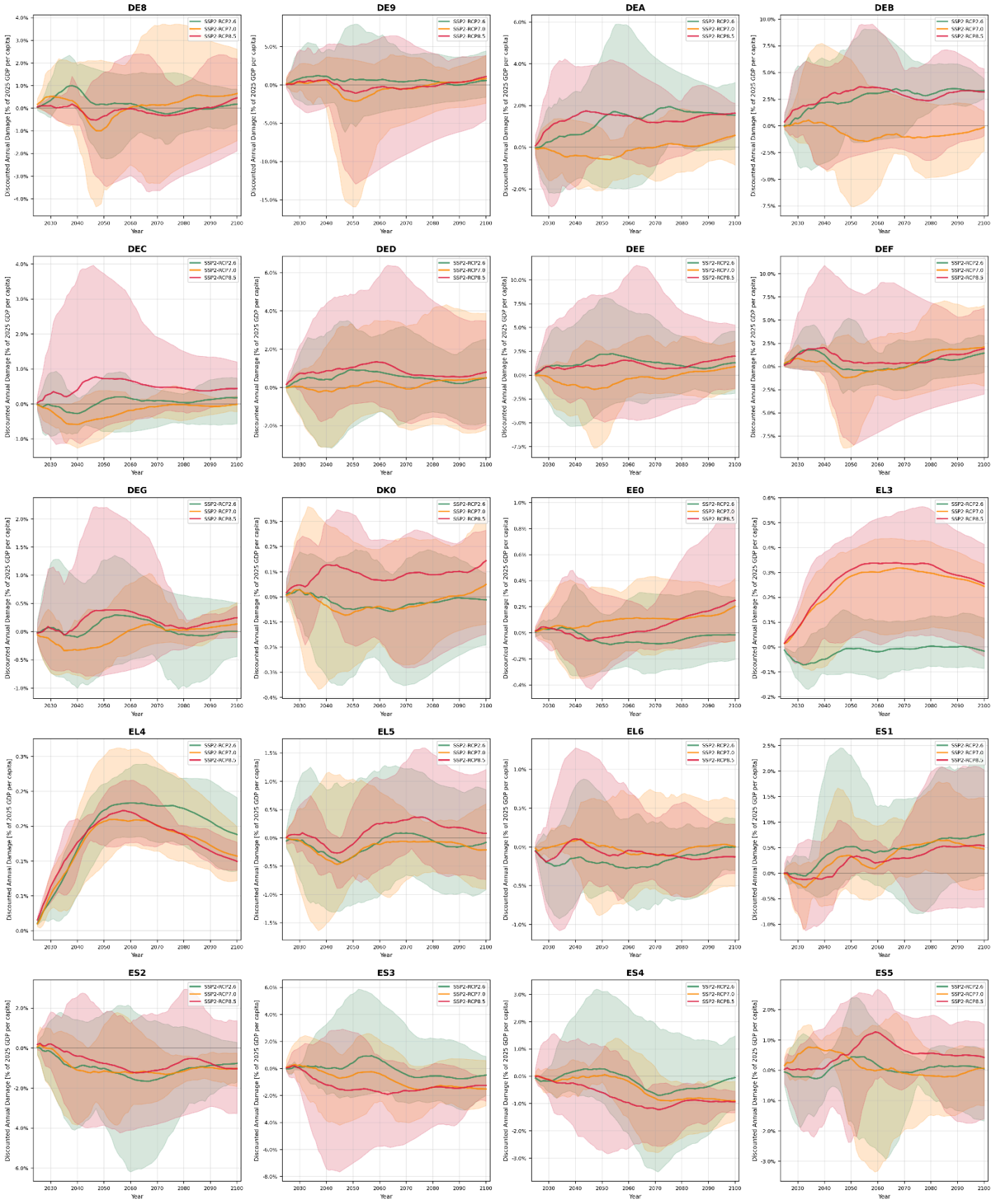

Discounted Annual Damage as percentage of 2025 GDP per capita - Nordhaus DICE model discounting - NUTS1 (Page 3/6)

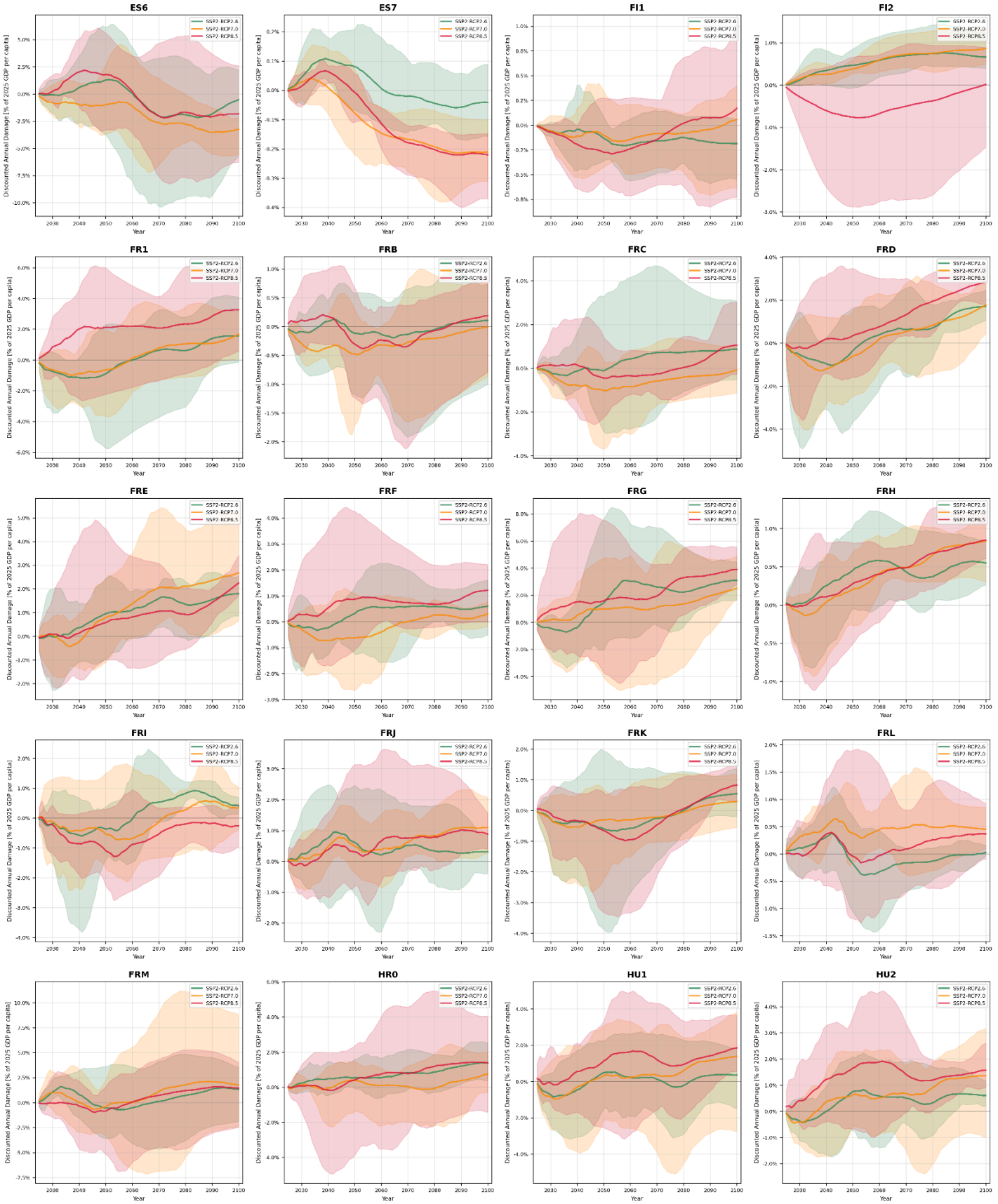

Discounted Annual Damage as percentage of 2025 GDP per capita - Nordhaus DICE model discounting - NUTS1 (Page 4/6)

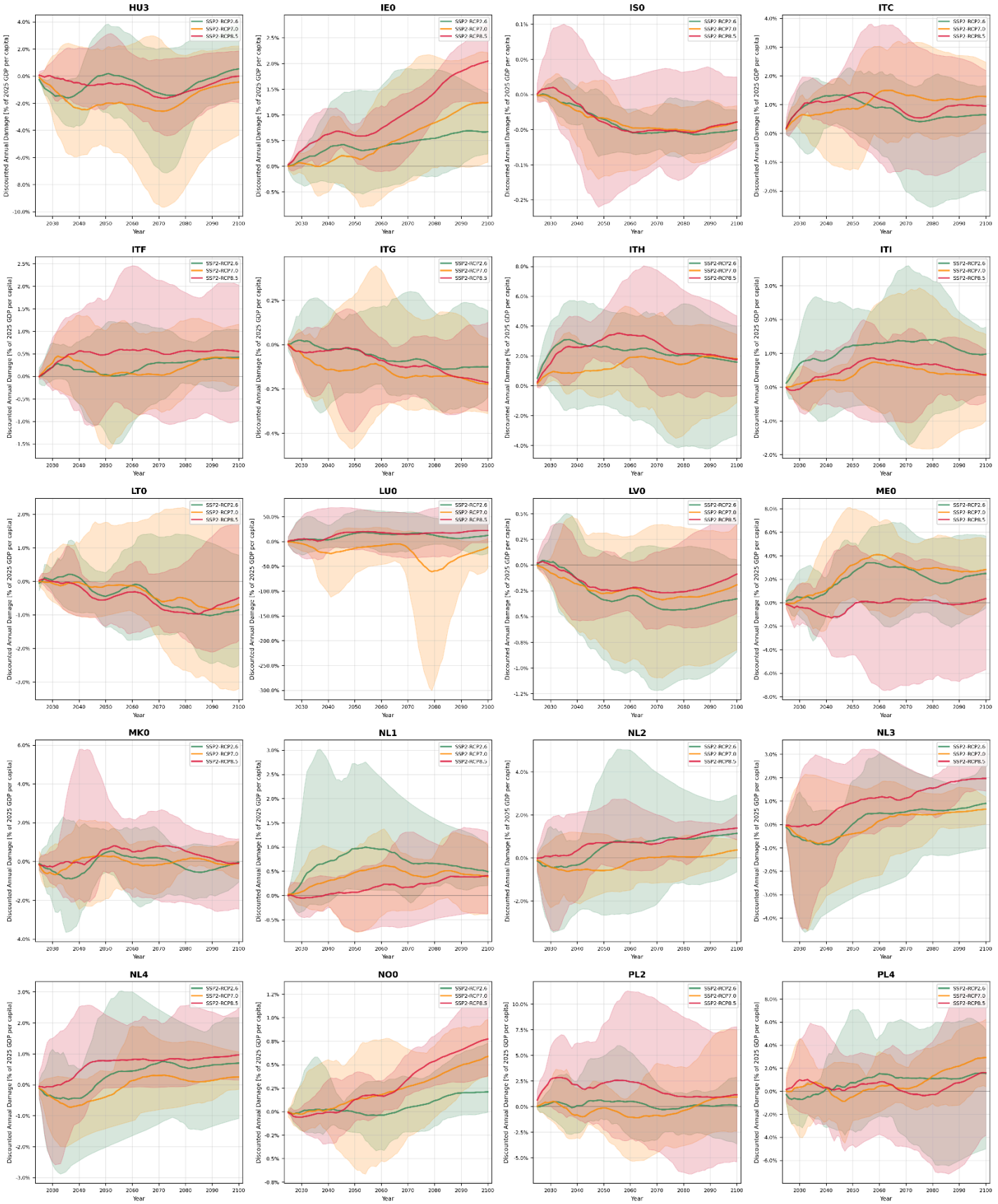

Discounted Annual Damage as percentage of 2025 GDP per capita - Nordhaus DICE model discounting - NUTS1 (Page 5/6)

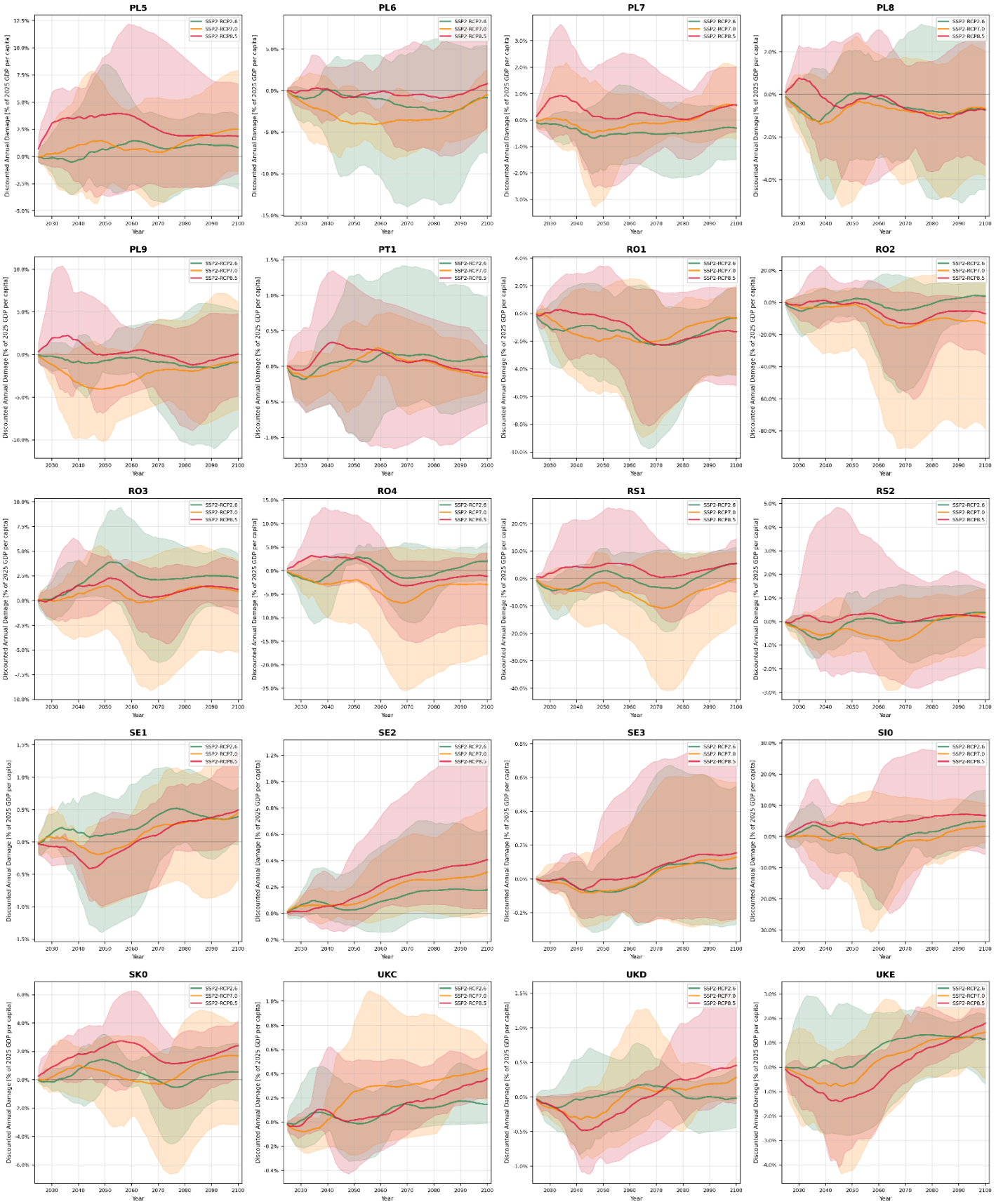

Discounted Annual Damage as percentage of 2025 GDP per capita - Nordhaus DICE model discounting - NUTS1 (Page 6/6)

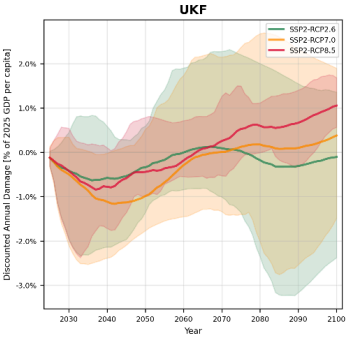

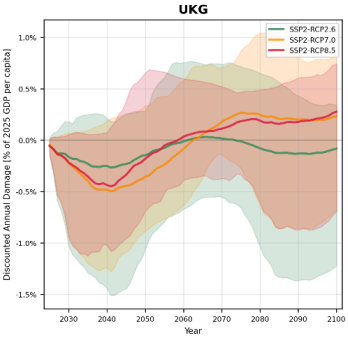

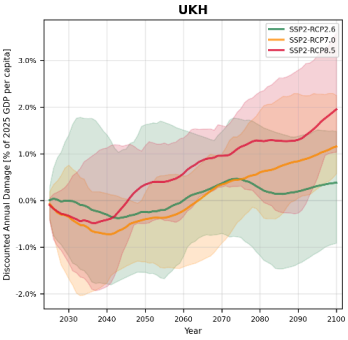

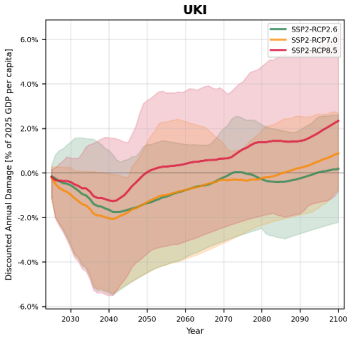

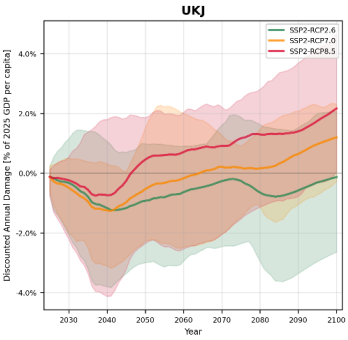

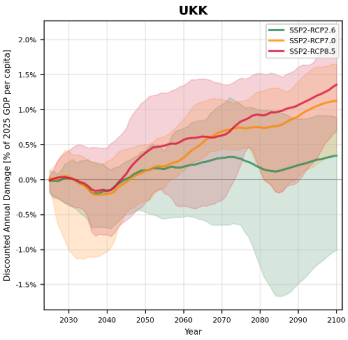

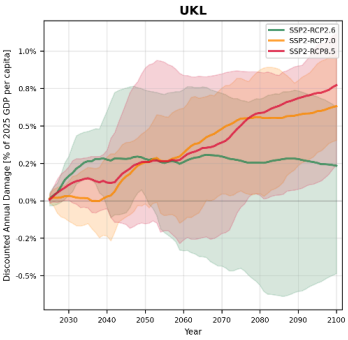

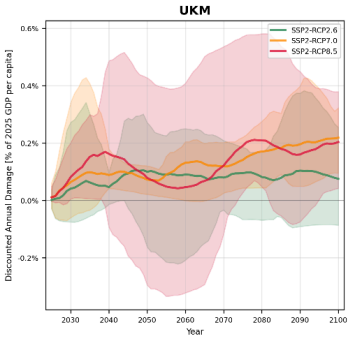

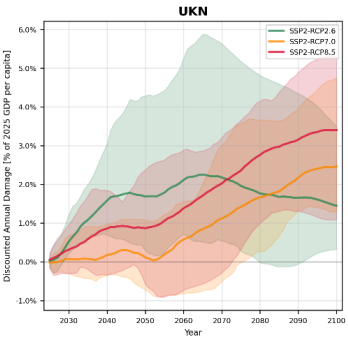

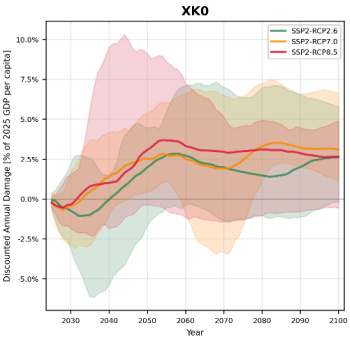

Discounted Annual Damage as percentage of 2025 GDP per capita - Stern Review discounting - NUTS1 (Page 1/6)

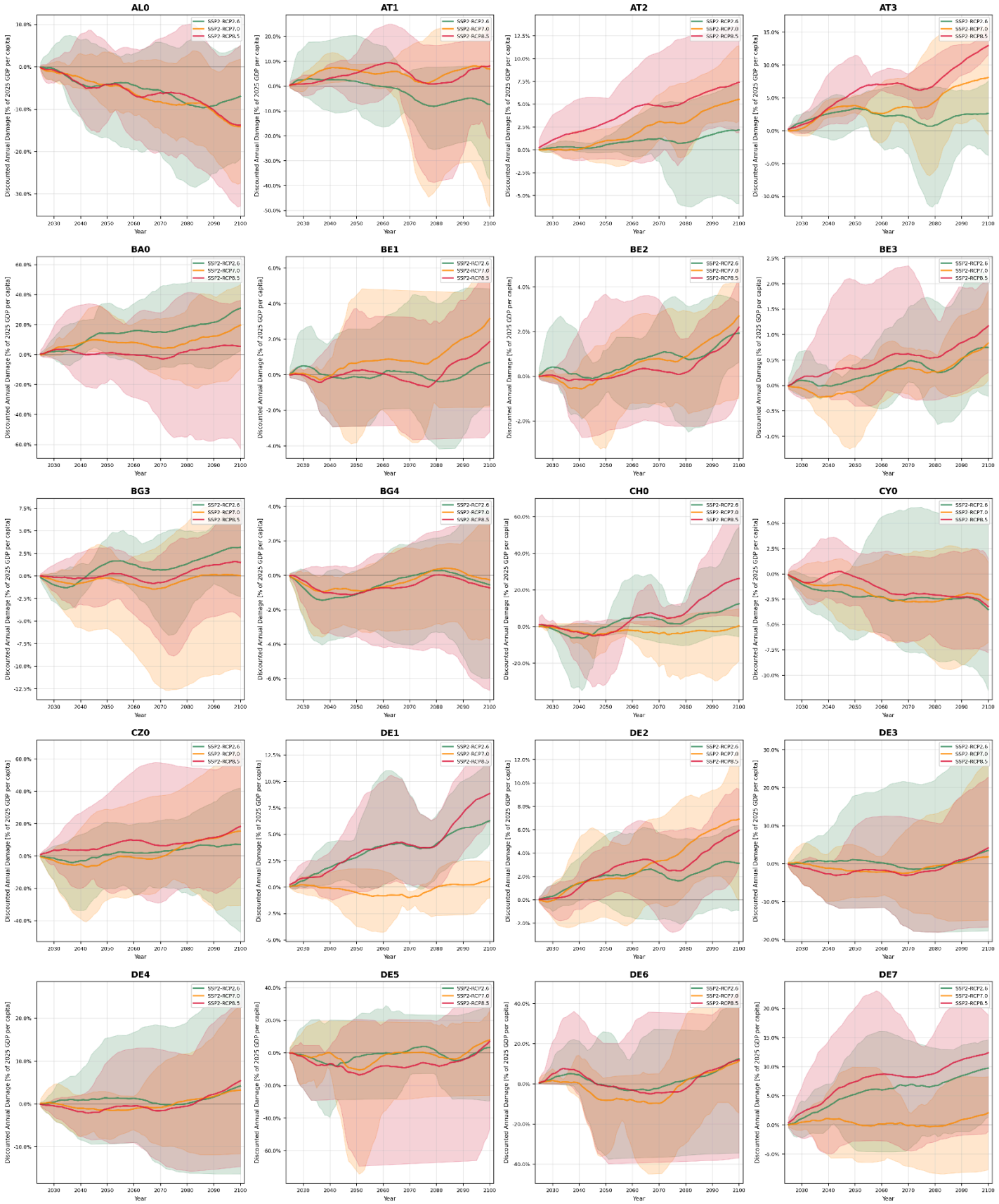

Discounted Annual Damage as percentage of 2025 GDP per capita - Stern Review discounting - NUTS1 (Page 2/6)

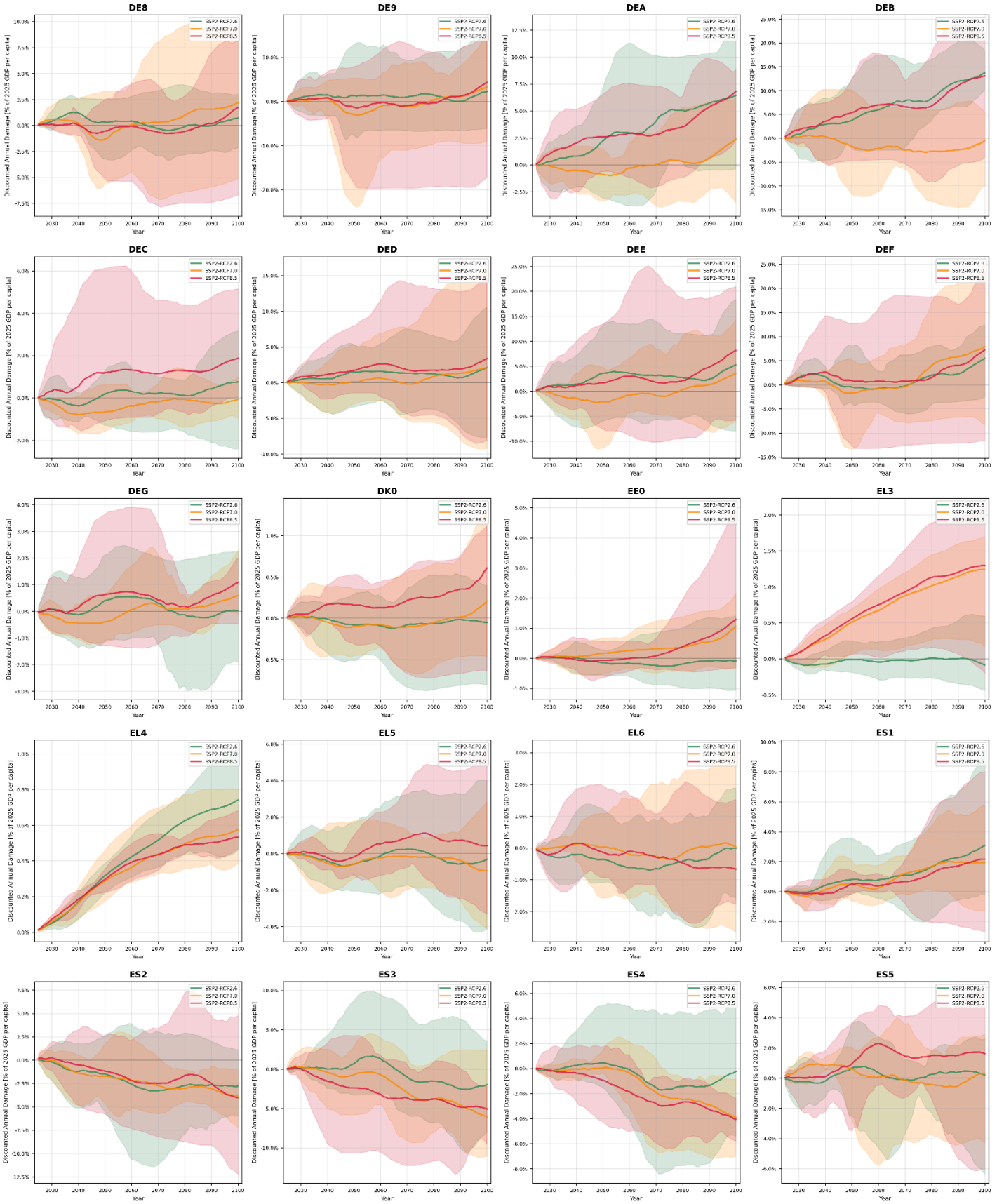

Discounted Annual Damage as percentage of 2025 GDP per capita - Stern Review discounting - NUTS1 (Page 3/6)

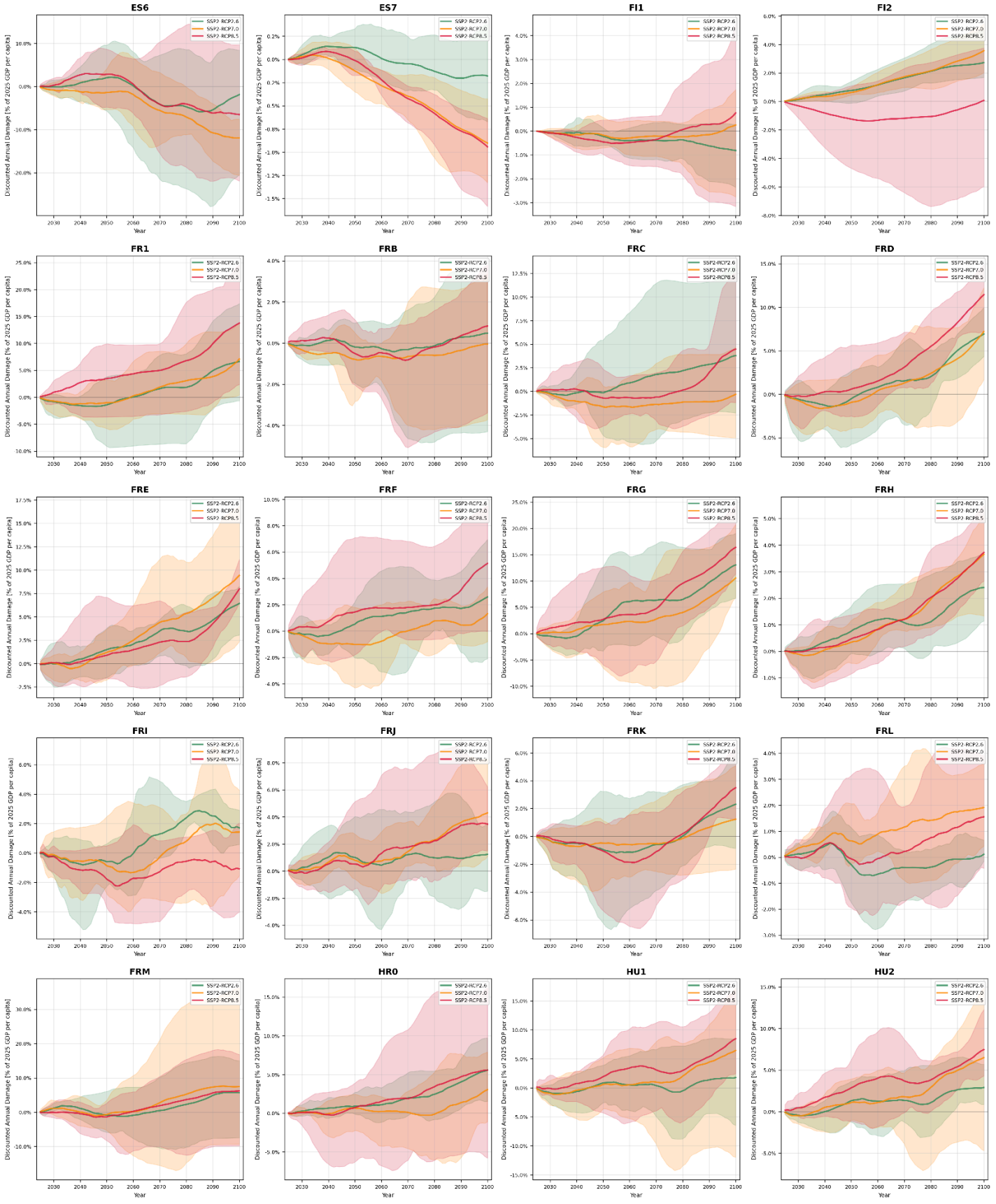

Discounted Annual Damage as percentage of 2025 GDP per capita - Stern Review discounting - NUTS1 (Page 4/6)

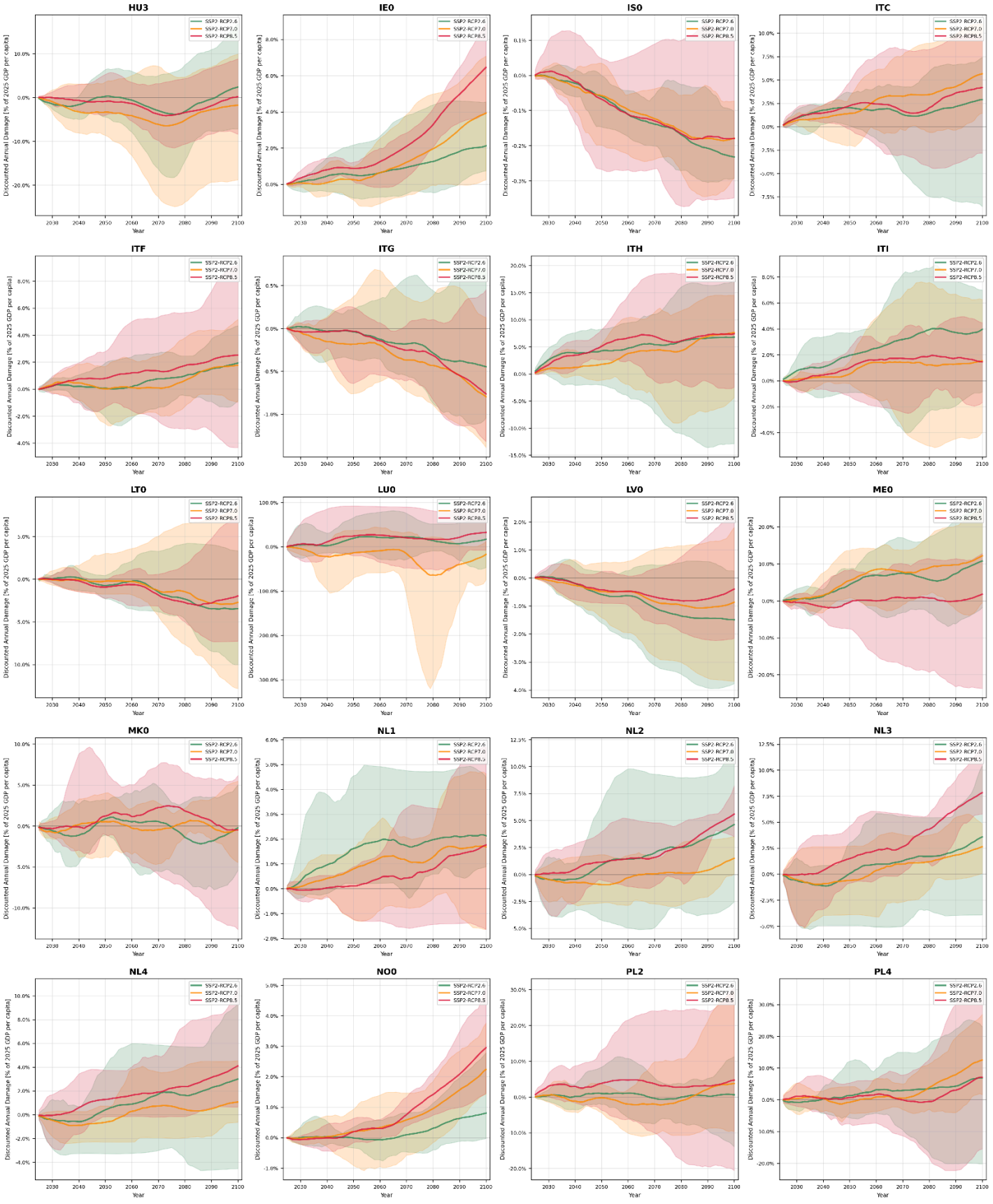

Discounted Annual Damage as percentage of 2025 GDP per capita - Stern Review discounting - NUTS1 (Page 5/6)

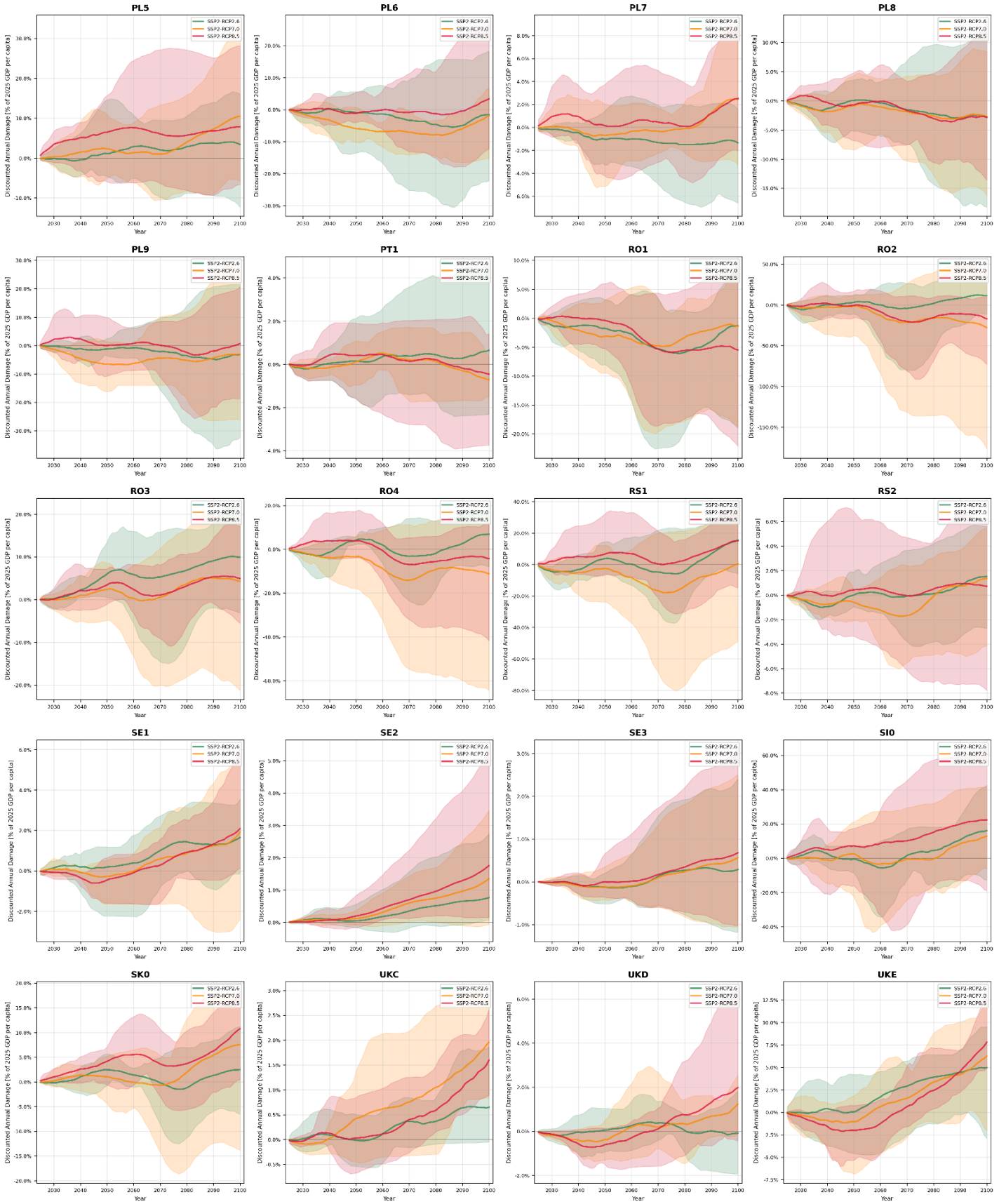

Discounted Annual Damage as percentage of 2025 GDP per capita - Stern Review discounting - NUTS1 (Page 6/6)

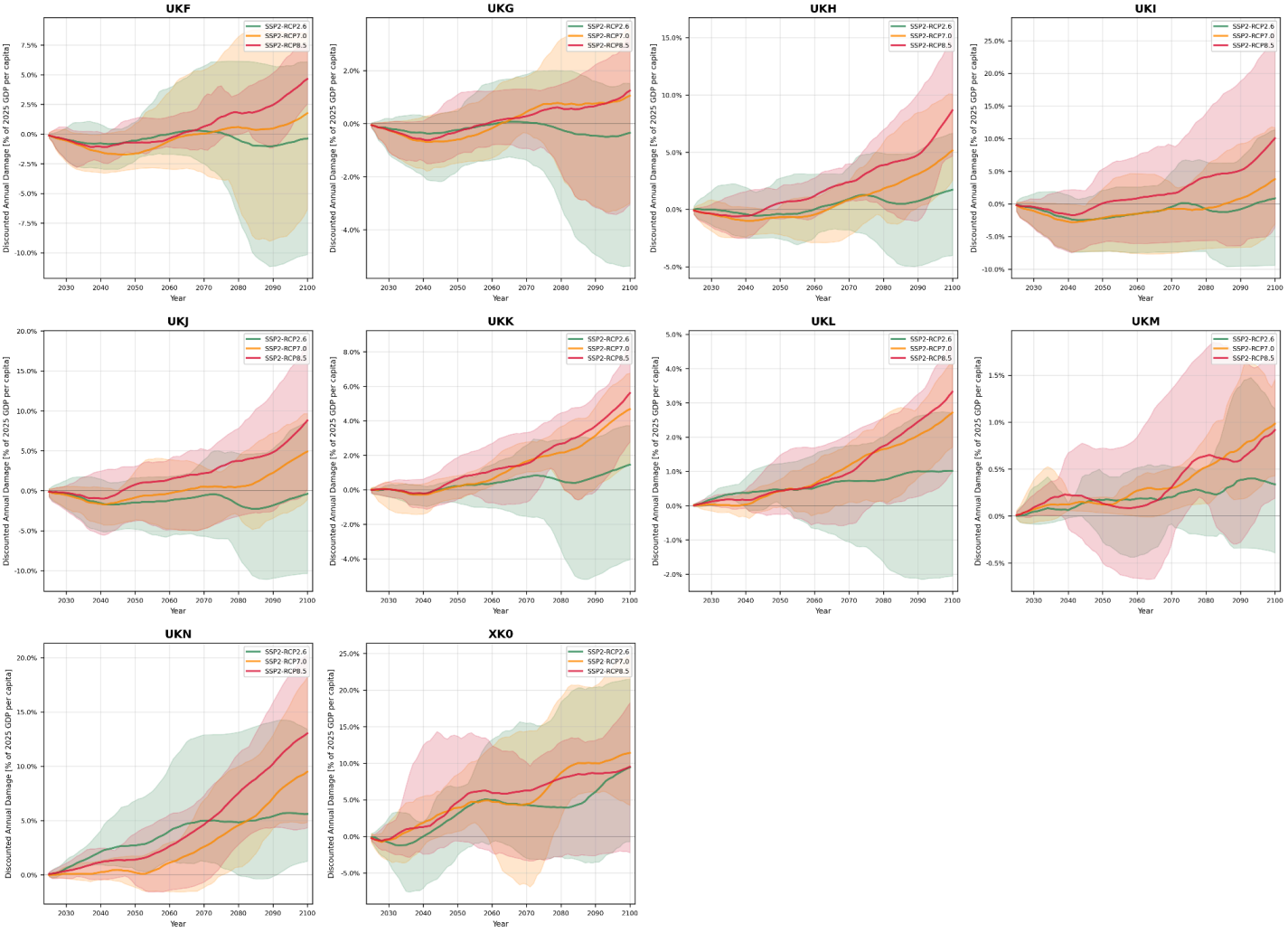

D.3 Map of mean projected Discounted Annual Damage for alternative discounting choices

Maps of the multi-year mean of projected Discounted Annual Damage per NUTS1 region for SSP2 and RCP2.6 , 7.0 and 8.5 for the alternative discounting choices from Nordhaus's DICE model (Nordhaus, 2011; ρ=1.5%, η=1.45) and the Stern Review (Stern, 2008; ρ=0.1%, η=1.01). The values are expressed as a percentage of 2025 GDP per capita.. The original time series data represents the multi-model ensemble mean (across five GCM forcings) per year.

Multi-year mean of Discounted Annual Damage as percentage of 2025 GDP per capita (SSP226 - Nordhaus DICE model discounting)

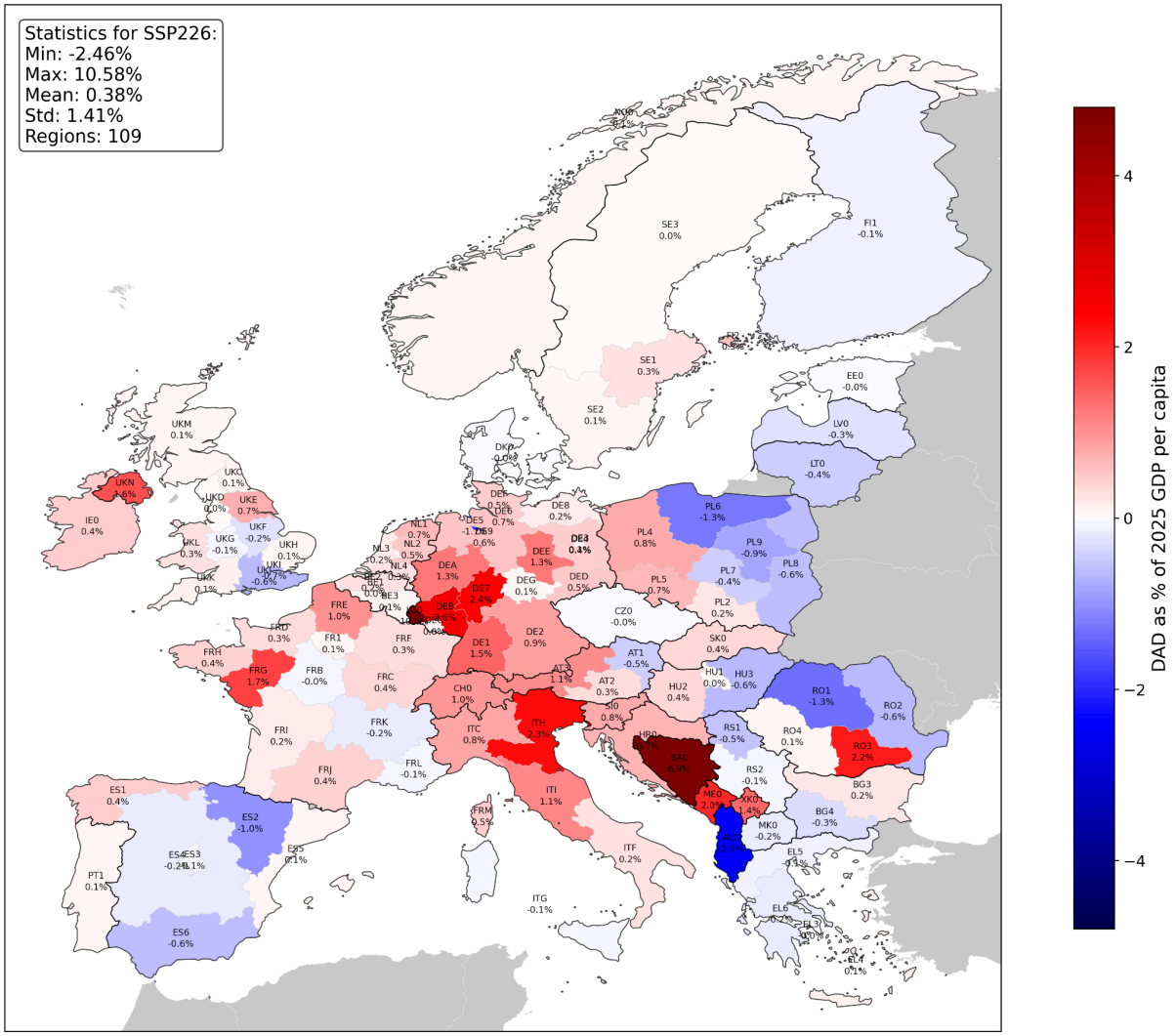

Multi-year mean of Discounted Annual Damage as percentage of 2025 GDP per capita (SSP270 - Nordhaus DICE model discounting)

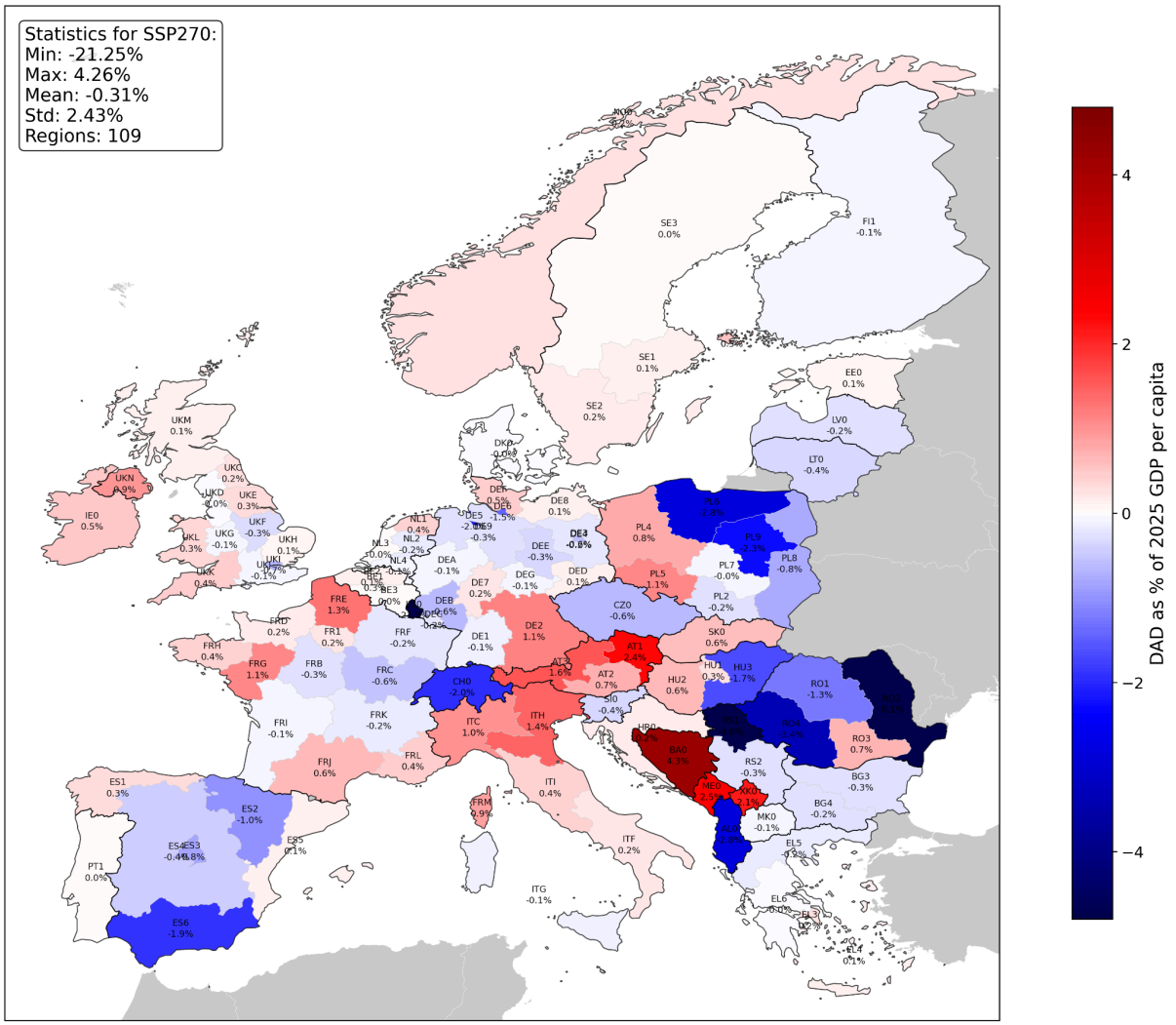

Multi-year mean of Discounted Annual Damage as percentage of 2025 GDP per capita (SSP285 - Nordhaus DICE model discounting)

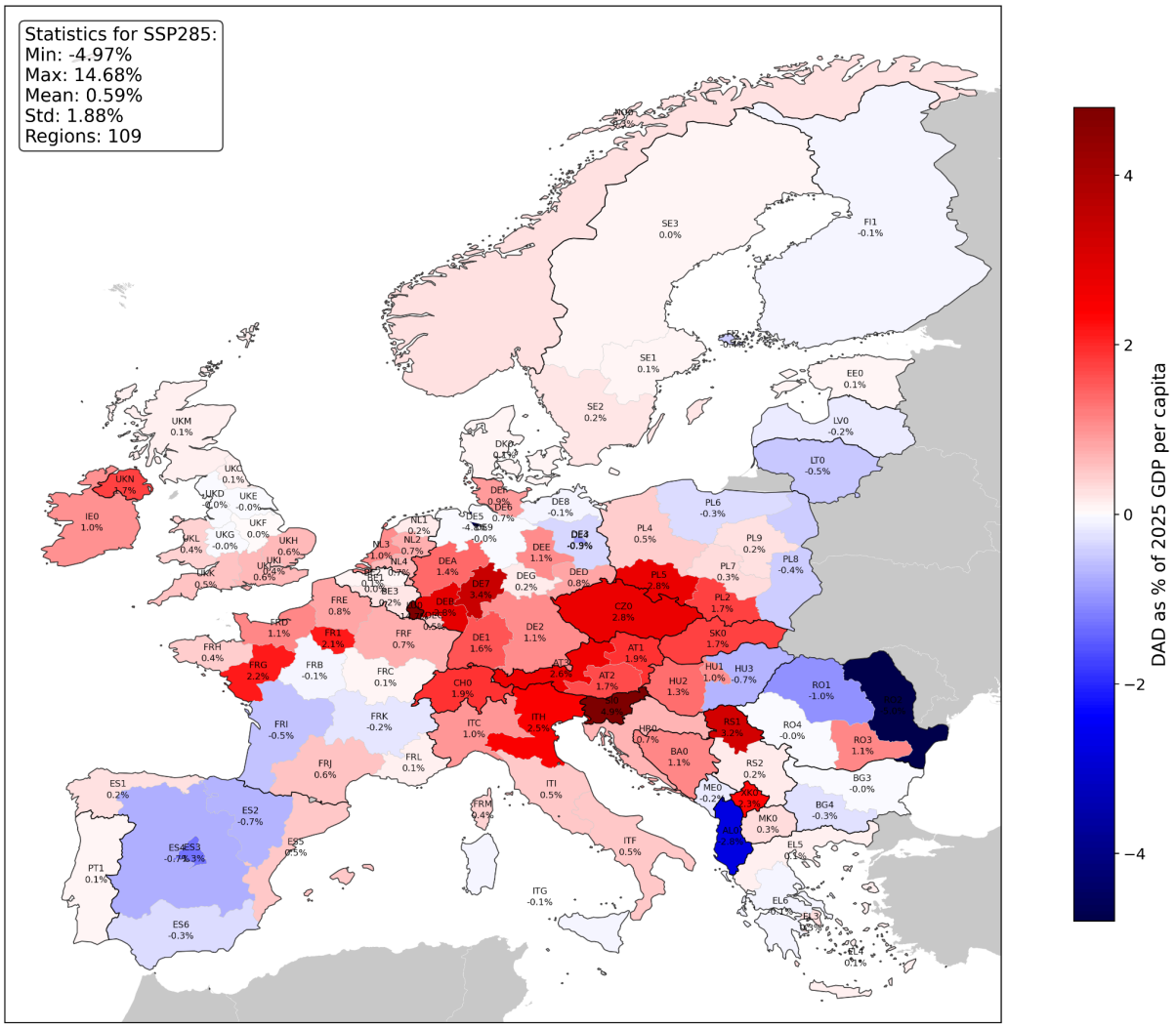

Multi-year mean of Discounted Annual Damage as percentage of 2025 GDP per capita (SSP226 - Stern Review discounting)

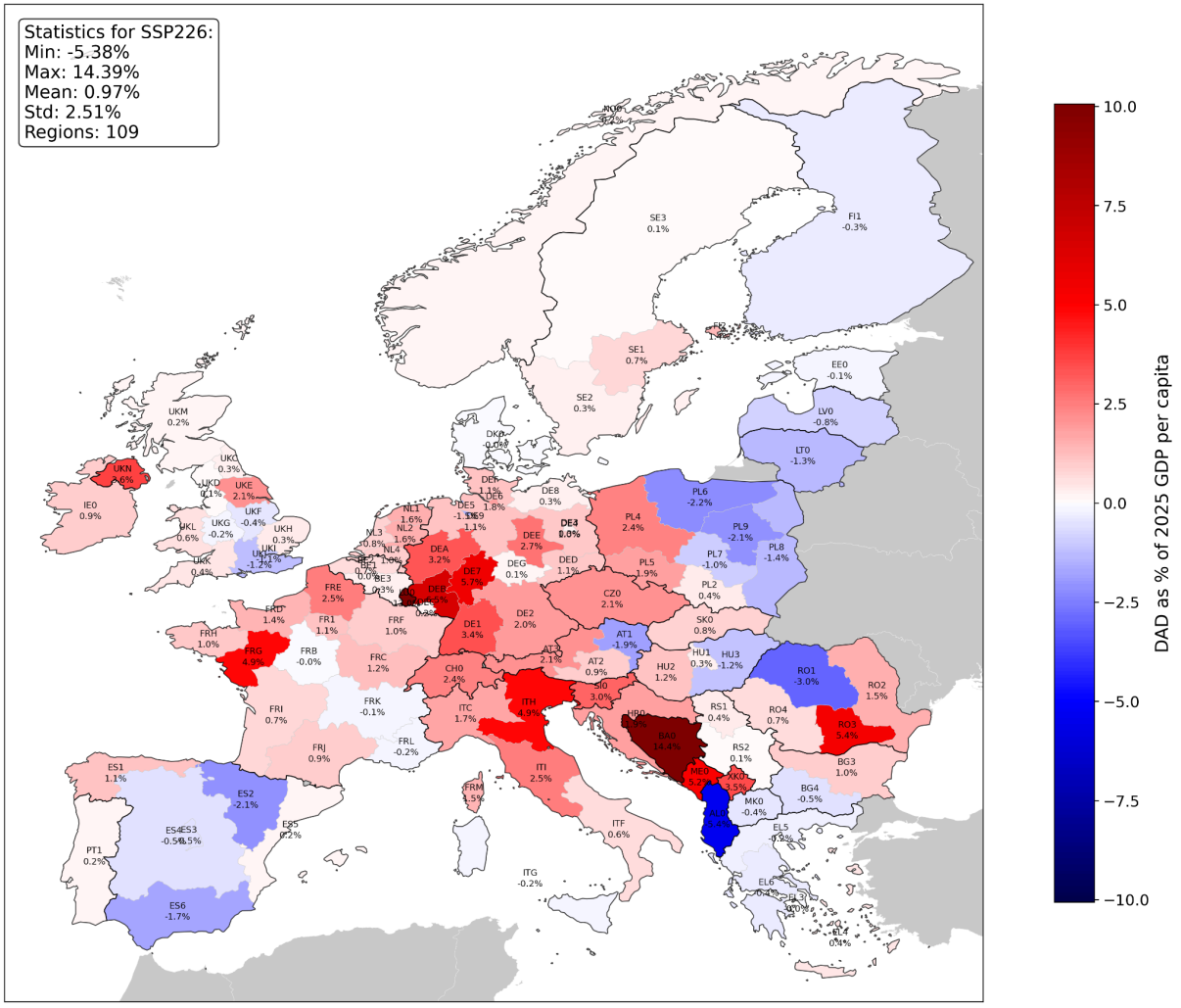

Multi-year mean of Discounted Annual Damage as percentage of 2025 GDP per capita (SSP270 - Stern Review discounting)

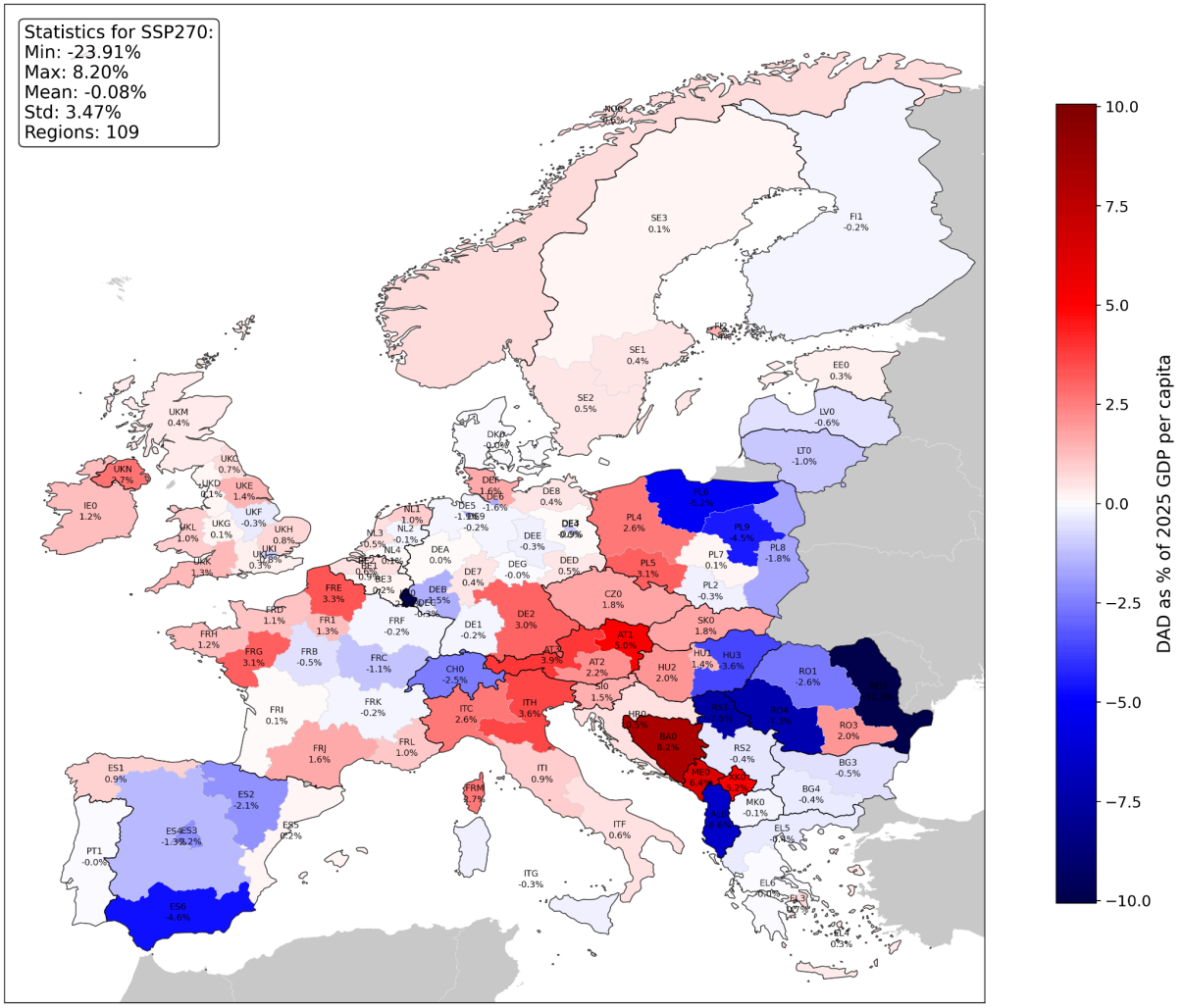

Multi-year mean of Discounted Annual Damage as percentage of 2025 GDP per capita (SSP285 - Stern Review discounting)

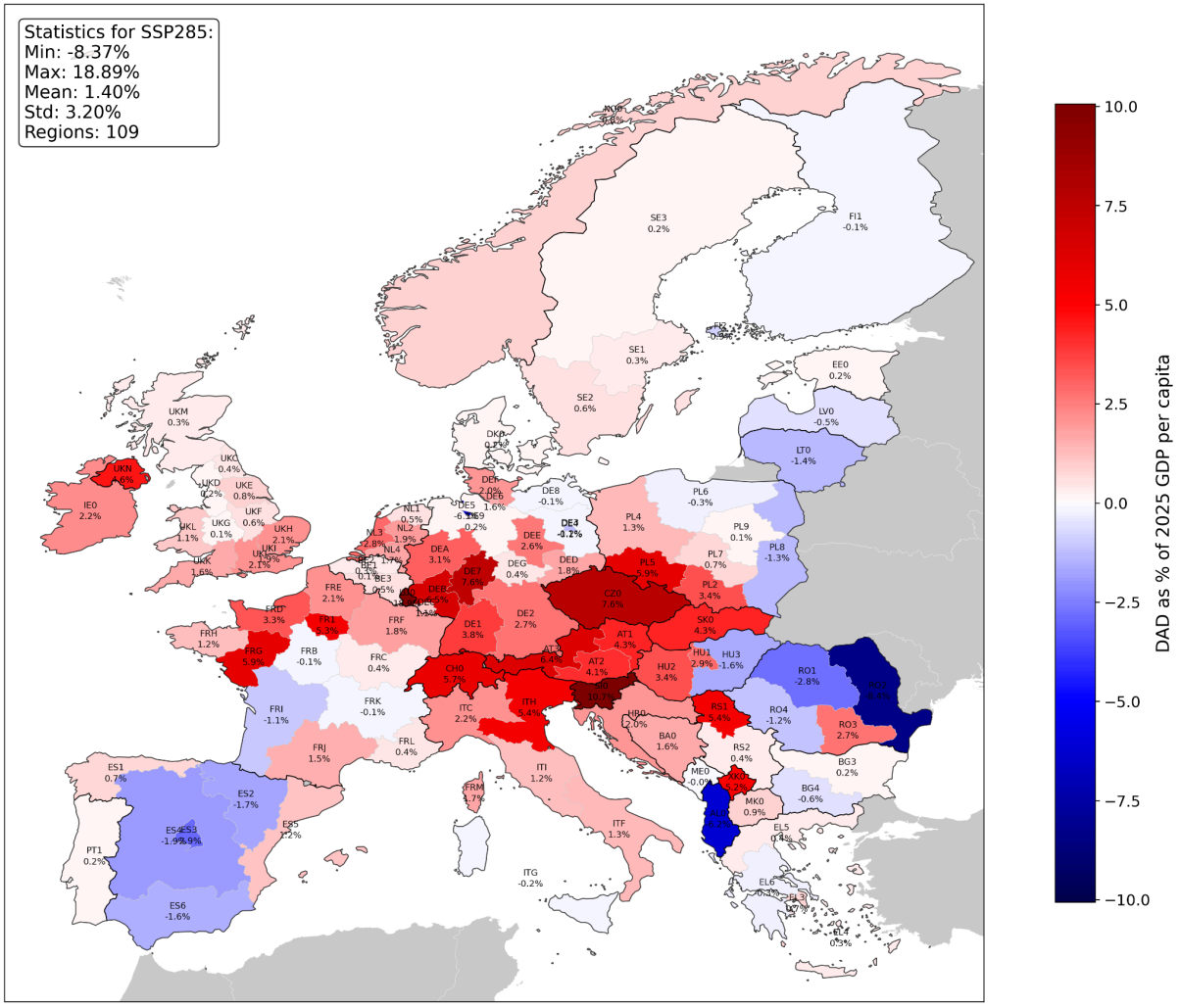

D.4 Table of mean projected Discounted Annual Damage for all discounting choices

Table of the multi-year mean of projected Discounted Annual Damage per NUTS1 region for SSP2 and RCP2.6, 7.0 and 8.5 based on the discounting choices from Ricke et al. (2018; ρ = 2%, η = 1.5), Nordhaus's DICE model (Nordhaus, 2011; ρ=1.5%, η=1.45) and the Stern Review (Stern, 2008; ρ=0.1%, η=1.01). The values are expressed as a percentage of 2025 GDP per capita. The original time series data represents the multi-model ensemble mean (across five GCM forcings) per year.

	Ricke et al. (2018) discounting ρ = 2%, η = 1.5			**Nordhaus's DICE model discounting ρ=1.5%, η=1.45**			**Stern Review discounting ρ=0.1%, η=1.01**		
NUTS1 region	**RCP2.6**	**RCP7.0**	**RCP8.5**	**RCP2.6**	**RCP7.0**	**RCP8.5**	**RCP2.6**	**RCP7.0**	**RCP8.5**
AL0	-1.97	-2.24	-2.22	-2.46	-2.84	-2.78	-5.38	-6.56	-6.15
AT1	-0.22	1.99	1.57	-0.45	2.36	1.91	-1.87	5.05	4.3
AT2	0.26	0.54	1.31	0.33	0.73	1.65	0.89	2.15	4.09
AT3	0.89	1.27	2.1	1.05	1.59	2.64	2.1	3.87	6.37
BA0	5.51	3.48	0.93	6.92	4.26	1.1	14.39	8.2	1.64
BE1	0.02	0.22	-0.01	0.02	0.29	0.0	0.03	0.88	0.13
BE2	0.19	0.09	0.05	0.24	0.14	0.08	0.67	0.59	0.33
BE3	0.08	0.02	0.16	0.1	0.03	0.2	0.28	0.17	0.5
BG3	0.14	-0.24	-0.02	0.22	-0.29	-0.01	0.98	-0.53	0.16
BG4	-0.28	-0.2	-0.25	-0.31	-0.23	-0.29	-0.51	-0.37	-0.59

CH0	0.58	-1.68	1.23	0.95	-1.98	1.89	2.39	-2.51	5.7
CY0	-0.9	-0.75	-0.48	-1.09	-0.92	-0.6	-2.13	-1.88	-1.37
CZ0	-0.2	-0.8	2.17	-0.02	-0.61	2.76	2.1	1.78	7.64
DE1	1.16	-0.1	1.23	1.45	-0.12	1.56	3.45	-0.22	3.85
DE2	0.7	0.89	0.85	0.86	1.15	1.08	1.96	3.01	2.67
DE3	0.05	-0.5	-0.79	0.06	-0.58	-0.89	0.29	-0.89	-1.2
DE4	0.34	-0.19	-0.33	0.42	-0.19	-0.34	1.03	0.02	-0.12
DE5	-1.62	-1.85	-4.17	-1.74	-2.04	-4.8	-1.54	-1.88	-6.45
DE6	0.54	-1.28	0.62	0.67	-1.45	0.68	1.84	-1.63	1.57
DE7	1.95	0.17	2.72	2.43	0.2	3.36	5.66	0.43	7.62
DE8	0.16	0.1	-0.07	0.18	0.14	-0.08	0.27	0.45	-0.12
DE9	0.47	-0.24	-0.04	0.55	-0.27	-0.03	1.12	-0.19	0.22
DEA	0.99	-0.1	1.09	1.27	-0.1	1.36	3.23	0.02	3.14
DEB	2.05	-0.49	2.24	2.61	-0.63	2.8	6.46	-1.51	6.49
DEC	0.02	-0.18	0.39	0.04	-0.2	0.48	0.17	-0.34	1.08
DED	0.42	0.09	0.66	0.51	0.13	0.81	1.1	0.46	1.75
DEE	1.02	-0.32	0.85	1.25	-0.34	1.07	2.7	-0.29	2.6

DEF	0.4	0.34	0.76	0.48	0.49	0.93	1.11	1.63	2.01
DEG	0.05	-0.06	0.15	0.06	-0.06	0.18	0.11	-0.02	0.43
DK0	-0.02	-0.02	0.07	-0.02	-0.02	0.09	-0.05	-0.03	0.21
EE0	-0.03	0.07	0.03	-0.04	0.09	0.05	-0.11	0.3	0.23
EL3	-0.02	0.19	0.21	-0.02	0.25	0.27	-0.03	0.69	0.75
EL4	0.11	0.1	0.1	0.14	0.12	0.13	0.42	0.35	0.35
EL5	-0.11	-0.13	0.08	-0.13	-0.16	0.11	-0.25	-0.36	0.39
EL6	-0.14	-0.01	-0.07	-0.17	-0.02	-0.09	-0.37	-0.05	-0.27
ES1	0.34	0.22	0.18	0.44	0.3	0.25	1.12	0.86	0.72
ES2	-0.82	-0.79	-0.54	-1.01	-0.99	-0.69	-2.08	-2.14	-1.66
ES3	-0.06	-0.6	-1.03	-0.11	-0.8	-1.3	-0.53	-2.15	-2.94
ES4	-0.13	-0.32	-0.57	-0.18	-0.44	-0.74	-0.54	-1.31	-1.89
ES5	0.04	0.15	0.41	0.06	0.15	0.52	0.18	0.16	1.17
ES6	-0.39	-1.47	-0.16	-0.56	-1.91	-0.34	-1.66	-4.65	-1.55
FI1	-0.1	-0.07	-0.09	-0.13	-0.08	-0.1	-0.34	-0.15	-0.13
FI2	0.42	0.42	-0.37	0.54	0.54	-0.44	1.35	1.43	-0.86
FR1	-0.0	0.09	1.65	0.1	0.21	2.11	1.1	1.25	5.31

FRB	-0.03	-0.23	-0.05	-0.04	-0.27	-0.06	-0.04	-0.51	-0.11
FRC	0.26	-0.47	0.02	0.37	-0.56	0.05	1.23	-1.13	0.37
FRD	0.17	0.04	0.79	0.31	0.15	1.09	1.42	1.12	3.3
FRE	0.79	0.97	0.61	1.03	1.29	0.8	2.51	3.3	2.06
FRF	0.24	-0.19	0.57	0.33	-0.2	0.72	0.99	-0.16	1.83
FRG	1.3	0.84	1.67	1.74	1.11	2.17	4.94	3.13	5.87
FRH	0.3	0.28	0.31	0.39	0.38	0.42	1.03	1.19	1.24
FRI	0.09	-0.11	-0.46	0.16	-0.1	-0.55	0.74	0.07	-1.06
FRJ	0.34	0.47	0.42	0.41	0.61	0.56	0.87	1.58	1.5
FRK	-0.17	-0.16	-0.19	-0.18	-0.18	-0.2	-0.11	-0.19	-0.11
FRL	-0.03	0.35	0.11	-0.05	0.44	0.15	-0.16	1.05	0.43
FRM	0.37	0.64	0.26	0.48	0.87	0.41	1.48	2.65	1.71
HR0	0.55	0.12	0.51	0.71	0.16	0.69	1.88	0.49	2.01
HU1	-0.03	0.17	0.78	0.0	0.29	1.02	0.29	1.38	2.89
HU2	0.27	0.45	1.04	0.37	0.61	1.31	1.16	2.02	3.42
HU3	-0.53	-1.38	-0.55	-0.62	-1.68	-0.69	-1.15	-3.55	-1.63
IE0	0.34	0.39	0.79	0.43	0.51	1.01	0.9	1.23	2.25

IS0	-0.03	-0.03	-0.03	-0.04	-0.04	-0.04	-0.11	-0.1	-0.1
ITC	0.68	0.82	0.79	0.81	1.04	0.97	1.71	2.63	2.2
ITF	0.17	0.17	0.4	0.23	0.21	0.5	0.65	0.55	1.26
ITG	-0.04	-0.09	-0.06	-0.06	-0.12	-0.08	-0.17	-0.31	-0.23
ITH	1.86	1.12	2.01	2.26	1.42	2.47	4.86	3.57	5.4
ITI	0.88	0.31	0.41	1.1	0.39	0.52	2.52	0.93	1.22
LT0	-0.32	-0.27	-0.38	-0.44	-0.36	-0.51	-1.31	-1.05	-1.36
LU0	8.98	-17.91	12.23	10.58	-21.25	14.68	13.0	-23.91	18.89
LV0	-0.22	-0.18	-0.14	-0.28	-0.24	-0.18	-0.8	-0.62	-0.47
ME0	1.58	1.93	-0.18	2.02	2.48	-0.18	5.16	6.39	-0.04
MK0	-0.14	-0.06	0.23	-0.17	-0.06	0.31	-0.44	-0.09	0.85
NL1	0.54	0.31	0.13	0.67	0.4	0.18	1.56	1.0	0.55
NL2	0.37	-0.17	0.55	0.52	-0.18	0.72	1.56	-0.14	1.91
NL3	0.1	-0.02	0.79	0.19	0.04	1.05	0.84	0.48	2.85
NL4	0.2	-0.09	0.51	0.29	-0.08	0.66	0.99	0.07	1.71
NO0	0.04	0.17	0.21	0.06	0.23	0.29	0.18	0.63	0.82
PL2	0.17	-0.2	1.46	0.19	-0.23	1.74	0.39	-0.25	3.43

PL4	0.56	0.54	0.36	0.77	0.76	0.45	2.42	2.61	1.32
PL5	0.48	0.84	2.29	0.65	1.1	2.77	1.88	3.07	5.94
PL6	-1.01	-2.32	-0.27	-1.26	-2.82	-0.32	-2.21	-5.24	-0.29
PL7	-0.34	-0.05	0.27	-0.42	-0.04	0.32	-1.0	0.11	0.71
PL8	-0.46	-0.63	-0.29	-0.58	-0.78	-0.41	-1.36	-1.76	-1.28
PL9	-0.67	-1.89	0.25	-0.86	-2.28	0.23	-2.06	-4.52	0.09
PT1	0.05	0.0	0.08	0.07	0.0	0.1	0.23	-0.0	0.15
RO1	-1.08	-1.02	-0.74	-1.34	-1.25	-0.99	-3.01	-2.65	-2.79
RO2	-0.72	-6.55	-3.95	-0.6	-8.07	-4.97	1.51	-12.02	-8.37
RO3	1.7	0.53	0.87	2.16	0.69	1.09	5.41	2.02	2.67
RO4	0.0	-2.7	0.14	0.07	-3.38	-0.02	0.68	-7.29	-1.16
RS1	-0.61	-3.96	2.7	-0.54	-4.79	3.21	0.36	-7.53	5.36
RS2	-0.07	-0.26	0.13	-0.06	-0.3	0.16	0.06	-0.42	0.37
SE1	0.21	0.09	0.02	0.27	0.12	0.06	0.72	0.44	0.34
SE2	0.08	0.13	0.16	0.11	0.17	0.21	0.3	0.47	0.6
SE3	0.0	0.0	0.03	0.01	0.01	0.05	0.07	0.09	0.17
SI0	0.52	-0.42	3.88	0.77	-0.35	4.89	3.03	1.51	10.71

SK0	0.31	0.43	1.39	0.37	0.57	1.74	0.81	1.76	4.28
UKC	0.06	0.17	0.09	0.08	0.23	0.13	0.25	0.68	0.4
UKD	0.01	-0.02	-0.04	0.02	-0.01	-0.02	0.06	0.14	0.21
UKE	0.53	0.19	-0.11	0.72	0.32	-0.03	2.12	1.43	0.83
UKF	-0.2	-0.3	-0.02	-0.24	-0.32	0.03	-0.43	-0.32	0.61
UKG	-0.09	-0.07	-0.04	-0.11	-0.05	-0.02	-0.22	0.11	0.14
UKH	0.03	0.02	0.44	0.06	0.09	0.62	0.33	0.77	2.15
UKI	-0.58	-0.6	0.27	-0.66	-0.66	0.45	-1.07	-0.83	1.94
UKJ	-0.51	-0.14	0.45	-0.61	-0.11	0.65	-1.19	0.31	2.13
UKK	0.1	0.3	0.4	0.13	0.42	0.55	0.41	1.32	1.63
UKL	0.2	0.25	0.28	0.25	0.34	0.38	0.61	0.98	1.08
UKM	0.06	0.1	0.1	0.08	0.13	0.13	0.2	0.35	0.34
UKN	1.29	0.69	1.32	1.61	0.94	1.74	3.64	2.73	4.59
XK0	1.07	1.65	1.82	1.41	2.14	2.32	3.49	5.2	5.23

D.5 Regression results for dataset filtered with respect to macroeconomic outliers.

Regression results for a trimmed dataset which excludes growth values smaller than the 1st or greater than the 99th percentile. Cumulative response of GDP, total GVA and sector GVA per capita growth to the population exposed to floods in terms of the cumulative coefficient for different NUTS levels. Shaded areas represent the confidence intervals at the 90% level, with clustered standard errors at the region-year level.

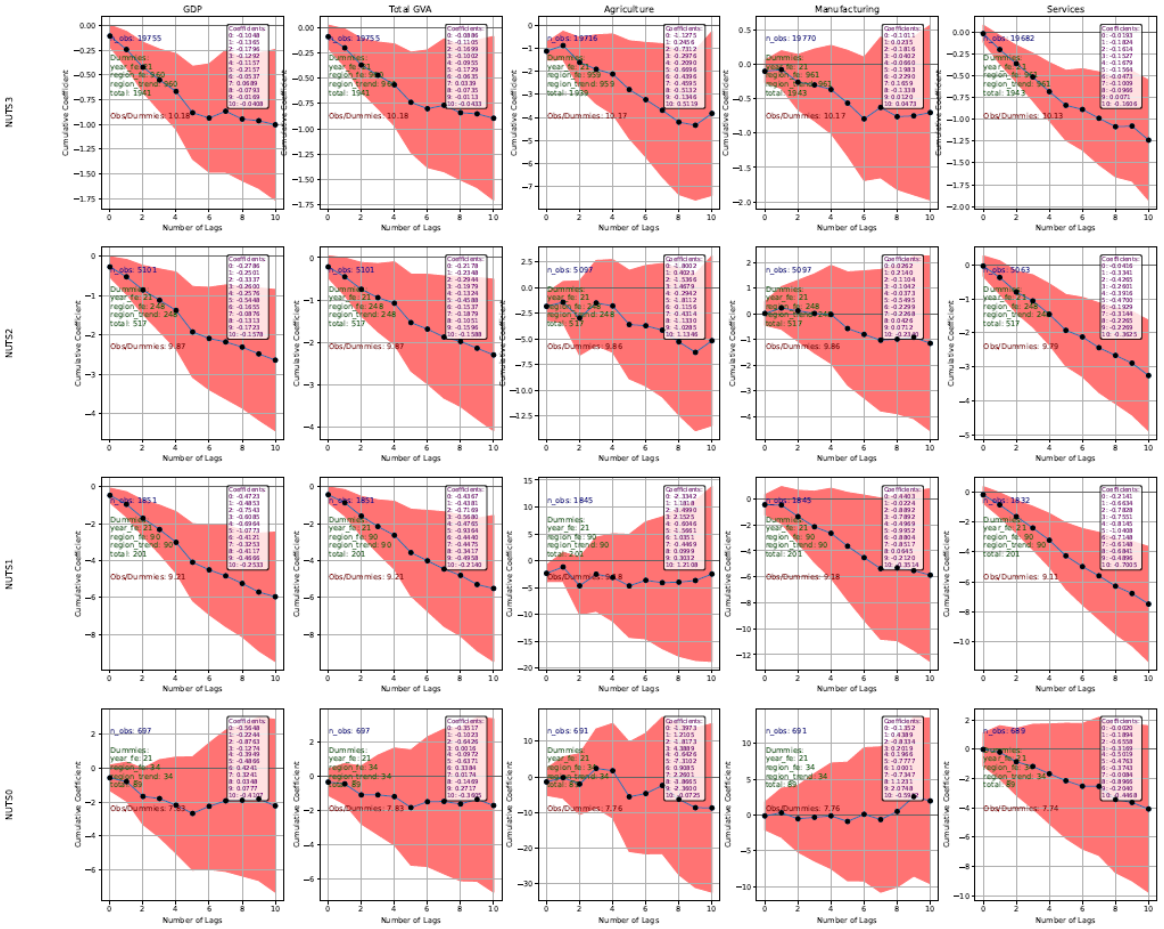

Annex E: Supply Chain Spillovers Intensify the Economic Impact of Local Climate Anomalies

E.1 Geographical coverage: subnational gross value added

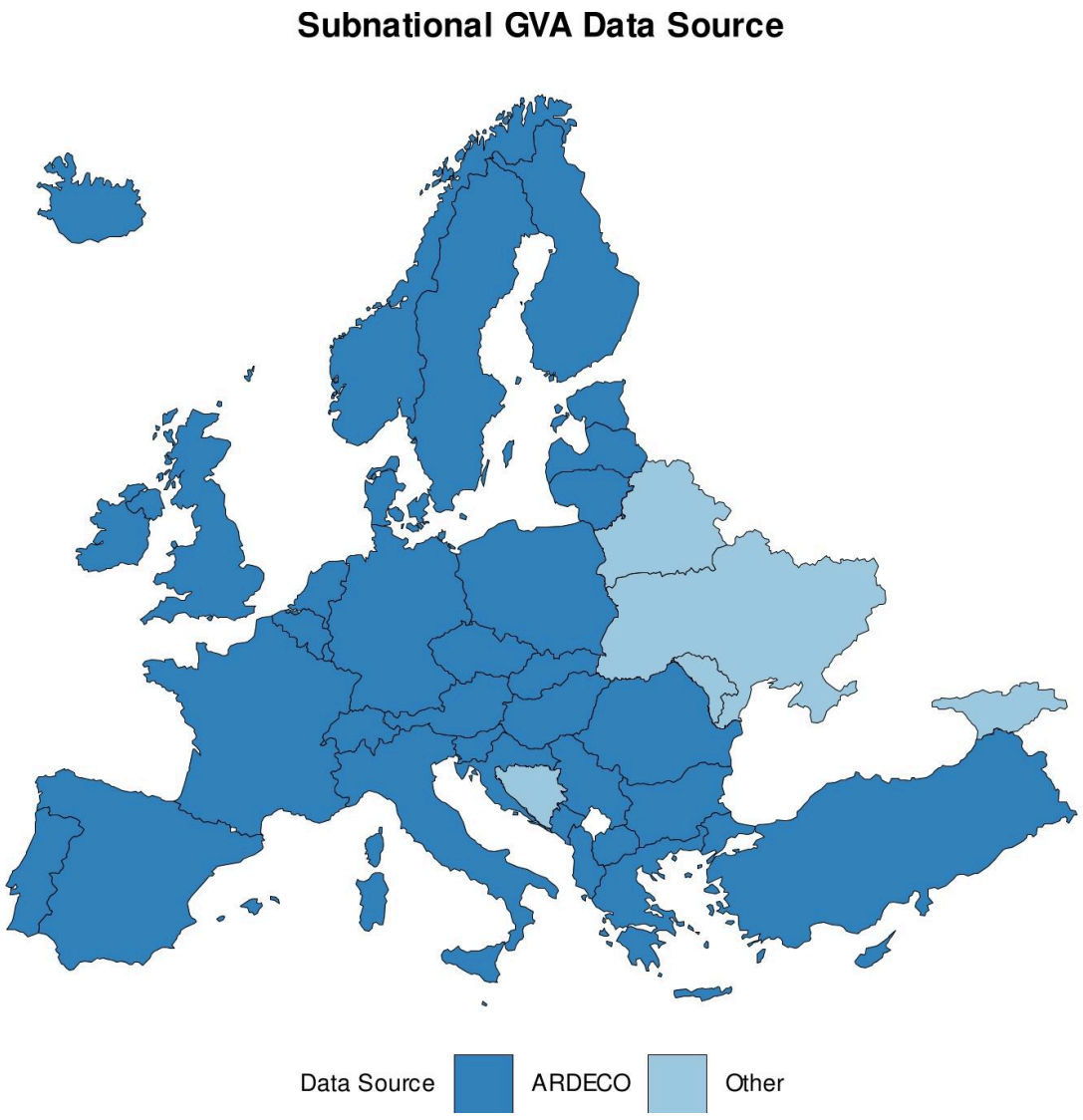

E.2 Direct and indirect bilateral supply chain connections: Illustration for 2003

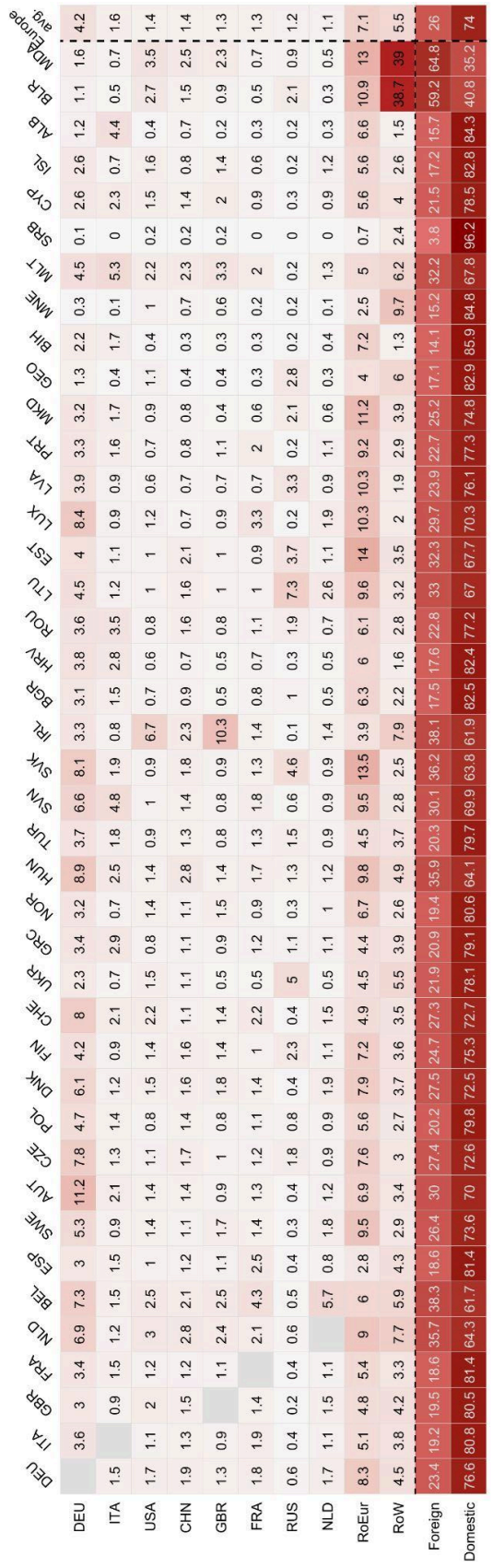

E.3 Water availability shocks in 2003: Grid cell, national, and supply chain adjusted shocks

A Grid cell-level shocks

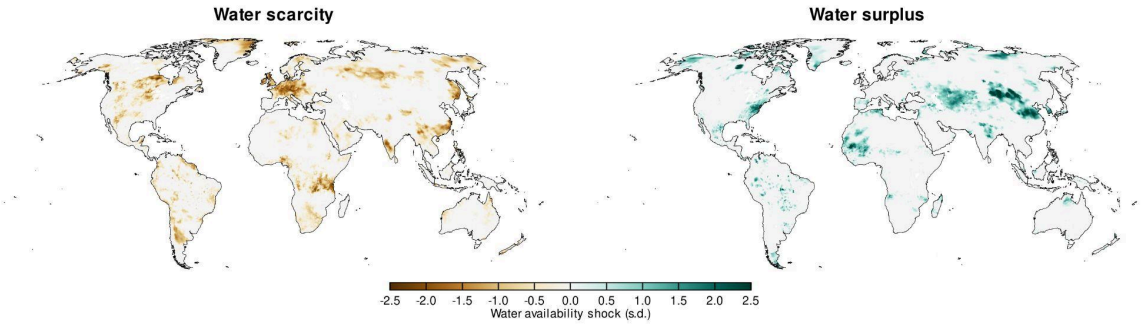

B National-level shocks

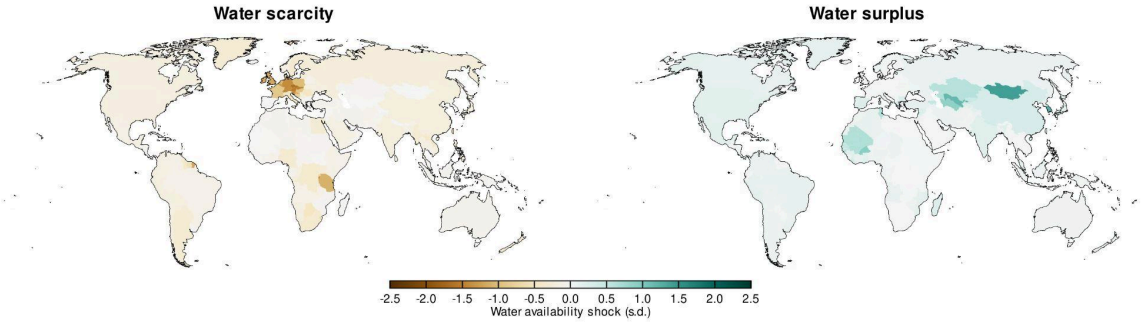

C Supply chain-adjusted shocks

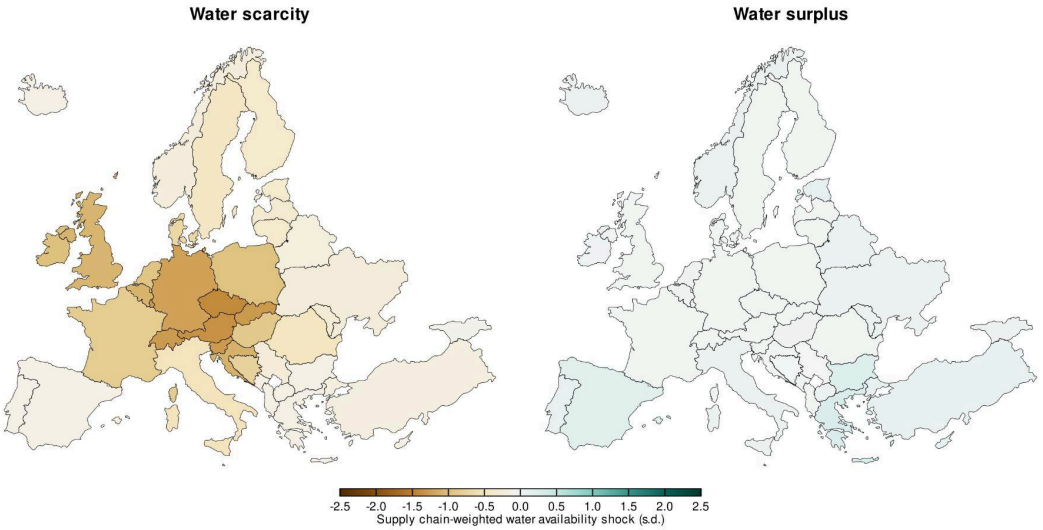

E.4 Robustness: Local Projections with longer horizons (h = 9)

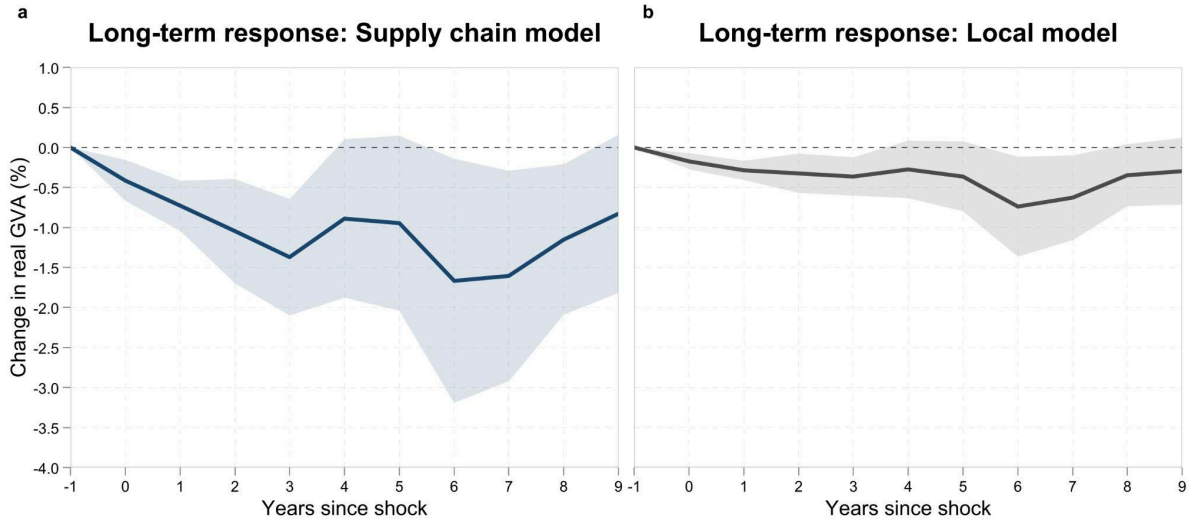

E.5 Robustness: Common pre-trends

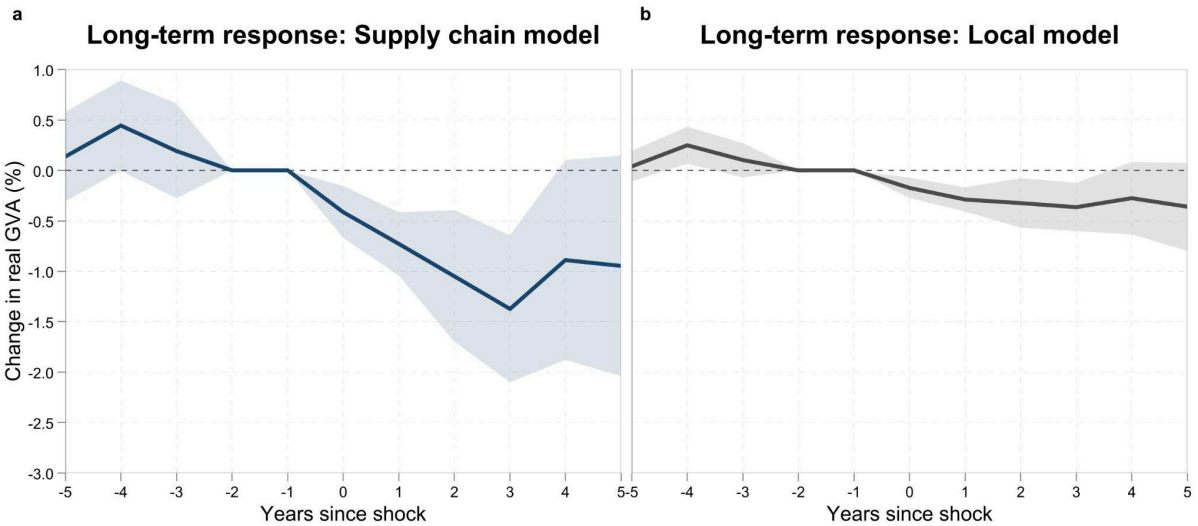

E.6 Heterogeneous impulse responses for local model

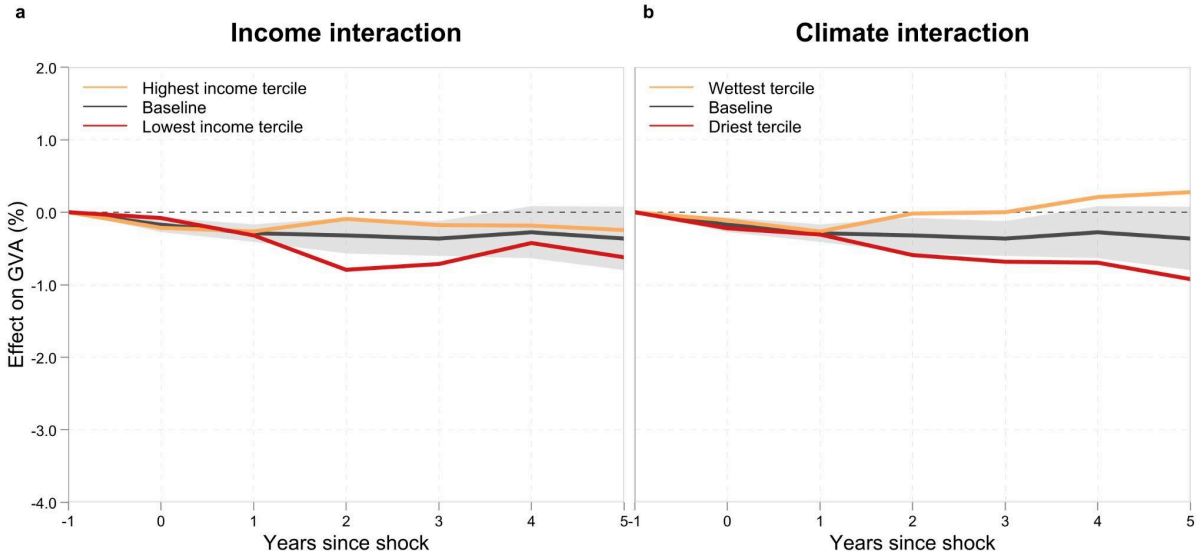

E.7 Country-specific impulse responses based on supply chain-adjusted climate interaction model

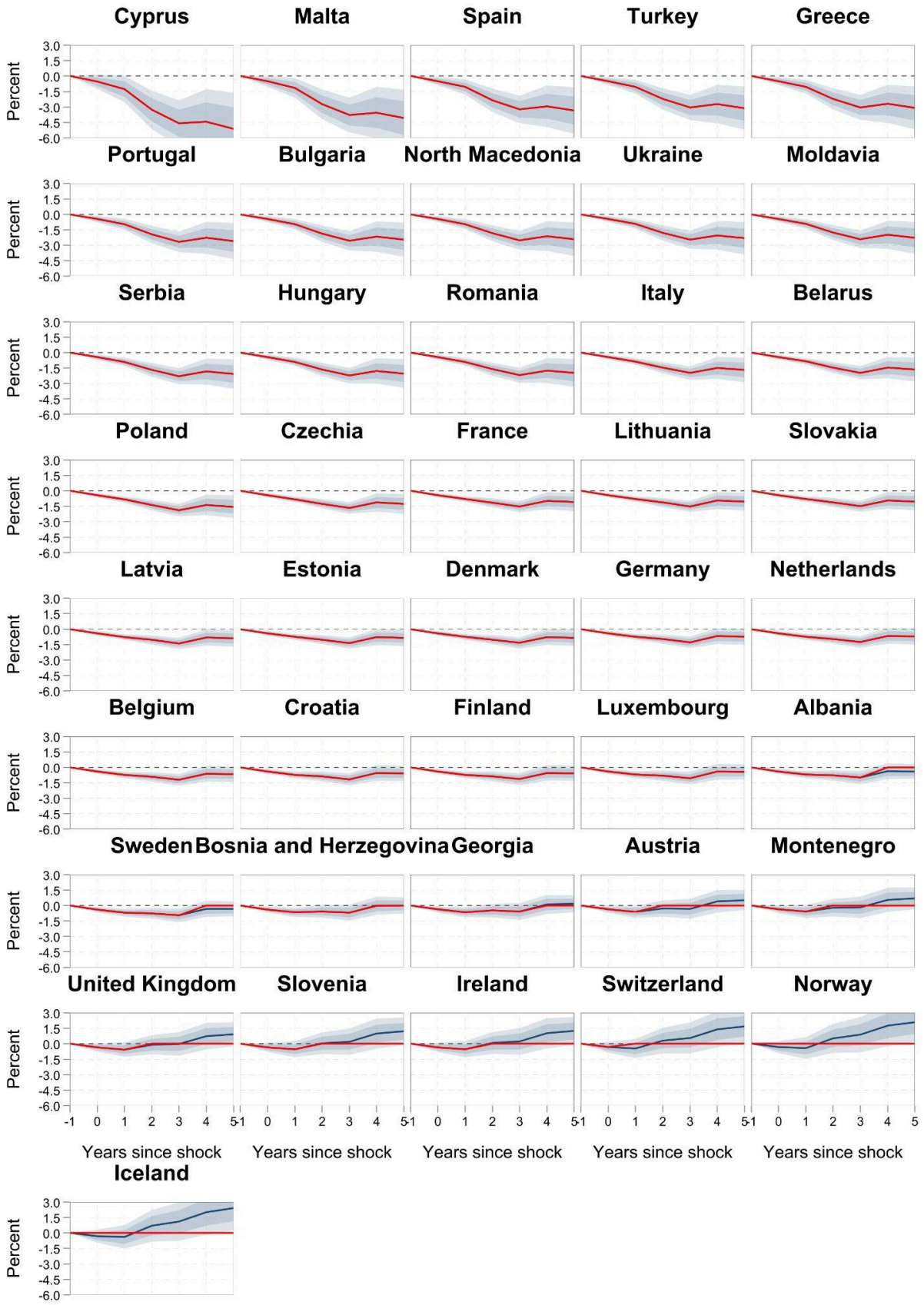

E.8 Country-specific impulse responses based on local climate interaction model

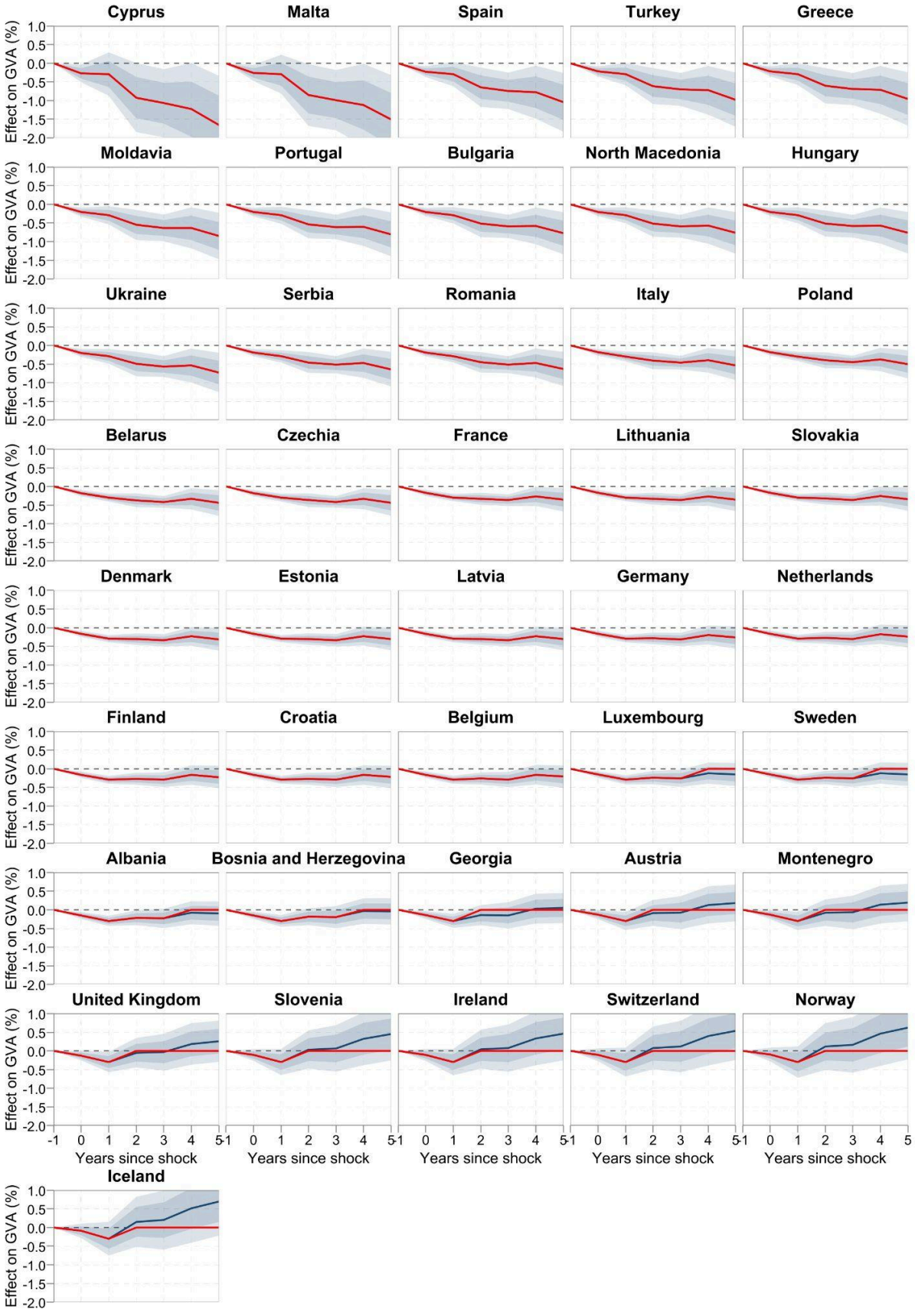

Annex F: Impacts of compound wildfires

[to-do DTU]

F.1 Item

References

Nordhaus, William D. 2011. Estimates of the Social Cost of Carbon: Background and Results from the RICE-2011 Model. National Bureau of Economic Research. https://doi.org/10.3386/w17540

Ricke, Katharine, Laurent Drouet, Ken Caldeira, and Massimo Tavoni. 2018. Country-level social cost of carbon. *Nature Climate Change* 8 (10): 895–900. https://doi.org/10.1038/s41558-018-0282-y

Stern, Nicholas. 2008. The Economics of Climate Change. *American Economic Review* 98 (2): 1–37. https://doi.org/10.1257/aer.98.2.1